Secretory Overexpression of PET Hydrolases for Scale Up Applications

Master Thesis

Biotechnology M.Sc. in Engineering

Maren Rickert

Supervisors
Cristiano Varrone & Virender Kumar

June 2024

Abstract

The petroleum-derived polyethylene terephthalate (PET) is one of the most widely produced thermoplastics, extensively processed in packaging materials and clothing, however, its continuous production contributes significantly to environmental pollution and plastic waste accumulation. Up to date, several enzymes have been reported to show PET-hydrolyzing activity, an ability that can be exploited for bioremediation of PET waste. Two engineered PET hydrolases, namely LCC_{ICCG}, a mutant of the cutinase derived from leaf-branch compost metagenome, and FastPETase, a mutant of the wild type *Is*PETase derived from *Ideonella sakaiensis*, proved to be promising candidates as they exhibited highest PET degradation rates at their respective optimal temperatures and are therefore focus of this project.

For recombinant expression of these enzymes at industrial scales, establishing a platform for extracellular overexpression is beneficial. This has the advantage of minimizing downstream processes and costs as well as avoiding intracellular degradation and solubility problems. To achieve this, two approaches were employed in this project. First, secretion efficiency of the PET hydrolases via the type 1 α-hemolysin (HlyA) secretion system was evaluated, which requires the fusion of the target protein to C-terminal HlyA signal peptide and the co-expression of two membrane complex proteins HlyB and HlyD, and comparing it to the established SecB-dependant pathway for PET hydrolases via the PelB signal peptide in *E. coli* BL21 (DE3). Besides the challenges of expressing FastPETase during the course of this project, for LCC_{ICCG} extracellular localization was observed even without the mediation of a signal peptide. Protein analytic methods indicated that the use of a signal peptide resulted in partial intracellular or periplasmic accumulation, reducing the overall yield.

In a second approach, extracellular expression was evaluated using the host organism *B. subtilis* RIK 1285. For this purpose, a library of Sec-dependant signal peptides was screened for their potential to secrete the PET hydrolases via the endogenous secretion machinery. Plasmid libraries were successfully constructed for both, FastPETase and LCC_{ICCG}. The subsequent screening for target protein expression and extracellular activity was conducted solely for LCC_{ICCG} so far. The signal peptide *yqgA* was proven to be most effective for the secretion of LCC_{ICCG}, achieving yields of 3.7 mg/L of culture supernatant. However, to compete with expression rates in *E. coli* and for industrial requirements, the level of extracellular expression needs to be improved considerably.

Preface

This Master's thesis was written by Maren Rickert as part of the Master of Science (MSc) in Engineering (Biotechnology) at the Faculty of Engineering and Science at Aalborg University (AAU). First, I would like to thank my supervisor Cristiano Varrone, Associate Professor at the Section for Bioscience and Engineering (Sustainable Bioresource Technology) at AAU, and Virender Kumar, Postdoc at the Section for Bioscience and Engineering (Sustainable Bioresource Technology) at AAU, for their inspiration and guidance throughout my whole thesis. Additionally, I would also like to thank Peter Kristensen, Professor at the Section for Bioscience and Engineering (Medical Biotechnology) at AAU, for providing me with a workstation in his laboratory and other laboratory necessities. Furthermore, thanks to all employees and PhD's at the Laboratory 4 and 5 North at the Institute of Chemistry and Bioscience at AAU, for their support and constant exchange.

In this Master's thesis, abbreviations used are written out the first time they are mentioned, followed by the abbreviation written in parenthesis. Common abbreviations, e.g. DNA, amino acids and growth media are not written out. The IEEE citation style was used, listing the cited sources in the bibliography in order of use. If a figure was inspired by a source, it will be mentioned in the captions. Figures were generated with BioRender and PowerPoint (Version 2404, Microsoft Office) and graphs were plotted using Excel (Version 2404, Microsoft Office). The molecular structures were made with ChemDraw Professional (Version 15.0).

Maren Rickert

Abbreviations

2-HE(MHET)$_2$	2-hydroxyl-(MHET)$_2$
HlyA	α-hemolysin
AB	Antibody
BHET	Bis-(2-hydroxyethyl)-terephtalate
BSA	Bovine Serum Albumin
DMT	Dimethyl terephthalic acid
EG	Ethylene glycol
EU27+3	Eu Member State, Norway, Switzerland and the United Kingdom
GRAS	Generally Recognized as Safe
HPLC	High performance liquid chromatography
IMAC	Immobilized metal ion affinity chromatography
IPTG	Isopropyl-β-D-thiogalactopyranosid
***Is*PETase**	PET hydrolase derived from *Ideonella sakaiensis*
ε	Molecular extinction coefficient
LCC	Cutinase derived from leaf-branch compost metagenome
MCS	Multiple cloning site
MHET	Mono(2-hydroxyethyl) terephthalate
(MHET)$_2$	Dimeric MHET
MHETase	MHET hydrolyzing enzyme derived from *Ideonella sakaiensis*
Mt	Million metric tons
MW	Molecular weight
NK	Negative control
OD$_{600}$	Optical density at 600 nm
OD$_{660}$	Optical density at 660 nm
OPEX	Operational expenses
oN	Over night
pNPB	p-Nitrophenylbutyrate
PCR	Polymerase chain reaction
PET	Polyethylene terephthalate
PK	Positive control
RTX	Repeat-in-toxin
RE	Restriction enzyme
RT	Room temperature
SDS-PAGE	Sodium dodecyl sulfate polyacrylamide gel electrophoresis
SP	Signal peptide
T_G	Glass transition temperature
T_m	Melting temperature
TPA	Terephthalic acid
TPA$_{eq}$	Equivalent TPA (including TPA and MHET)
T1SS	Type I secretion system

Contents

Introduction 1

1.1 The Plastic Waste Issue

Plastic is a material that has become an everyday part of our lives. Its versatility and durability allows it to be used in all kinds of fields, from food packaging, household devices, medical equipment to the automotive industry. However, its extensive implementation is leading to vast accumulation of plastic waste in landfill and contributes increasingly to the pollution of the environment calling for a transition towards a "Circular Economy for Plastics" (See Figure 1.1 A)[1].

Whereas some products such as pipes or car components can have a lifespan of several decades, many plastic products are discarded within less than a year or even days, especially when its comes to single use products like food packaging and drinking bottles. In 2022, global plastic production amounted to 400,3 million metric tons (Mt), with 90,6 % being manufactured from fossil-based raw materials [2]. The EU27+3, which comprises the 27 EU members as well as the United Kingdom, Norway and Switzerland, accounted for approx. 14 % of the total production corresponding to 58,8 Mt (See Figure 1.1 B). In the same year, 32,3 Mt of post-consumer plastic waste was collected in the EU27+3, referring to waste that is discarded by the end consumer after its use unlike e.g. production leftovers which are considered as pre-consumer waste (See Figure 1.1 C). Around 26,9 % of post-consumer plastic waste was sent to recycling in 2022 displaying an increase of 22,5 % compared to 2018. At the same time, landfill disposal decreased by 6,1 % to 23,5 %, however, a large percentage (49,6 %) was still processed via incineration for energy recovery with an increase of 15,1 % since 2018 [3]. Apart from the negative impact on the environment and human health, landfill and incineration also display a loss of valuable resources which is why the EU set the goal to reuse or recycle 60 % of everyday waste collected by municipalities by 2030 [4].

Currently, plastic waste originating from the packaging sector reaches the highest recycling rate, although this rate still needs to improve in order to reach the 2018 Packaging and Packaging Waste Directive's target of 50 % by 2025 [5]. This will require extended producer responsibility to increase separate waste collection and the sorting of mixed waste. Recycling rates of the total post-consumer plastic waste have been shown to be 13x higher when collected separately compared to mixed waste collection, as other types of waste like different polymers or organics can contaminate the plastics preventing a part from reaching the recycling process. In 2022, 19,2 % of the manufactured plastic products and components in the EU27+3 have been circular, with 18,1 % originating from mechanical recycling (pre- and post-consumer), while only 0.2 % were recycled by chemical processes and 1 % was attributable to bio-based feedstock (See Figure 1.1 B) [3, 6].

Thus, the expansion of chemical recycling and biorecycling as a complement to mechanical recycling must be given greater priority, as this could make a decisive contribution to the reuse of resources from plastic waste that would otherwise be lost through landfilling or incineration.

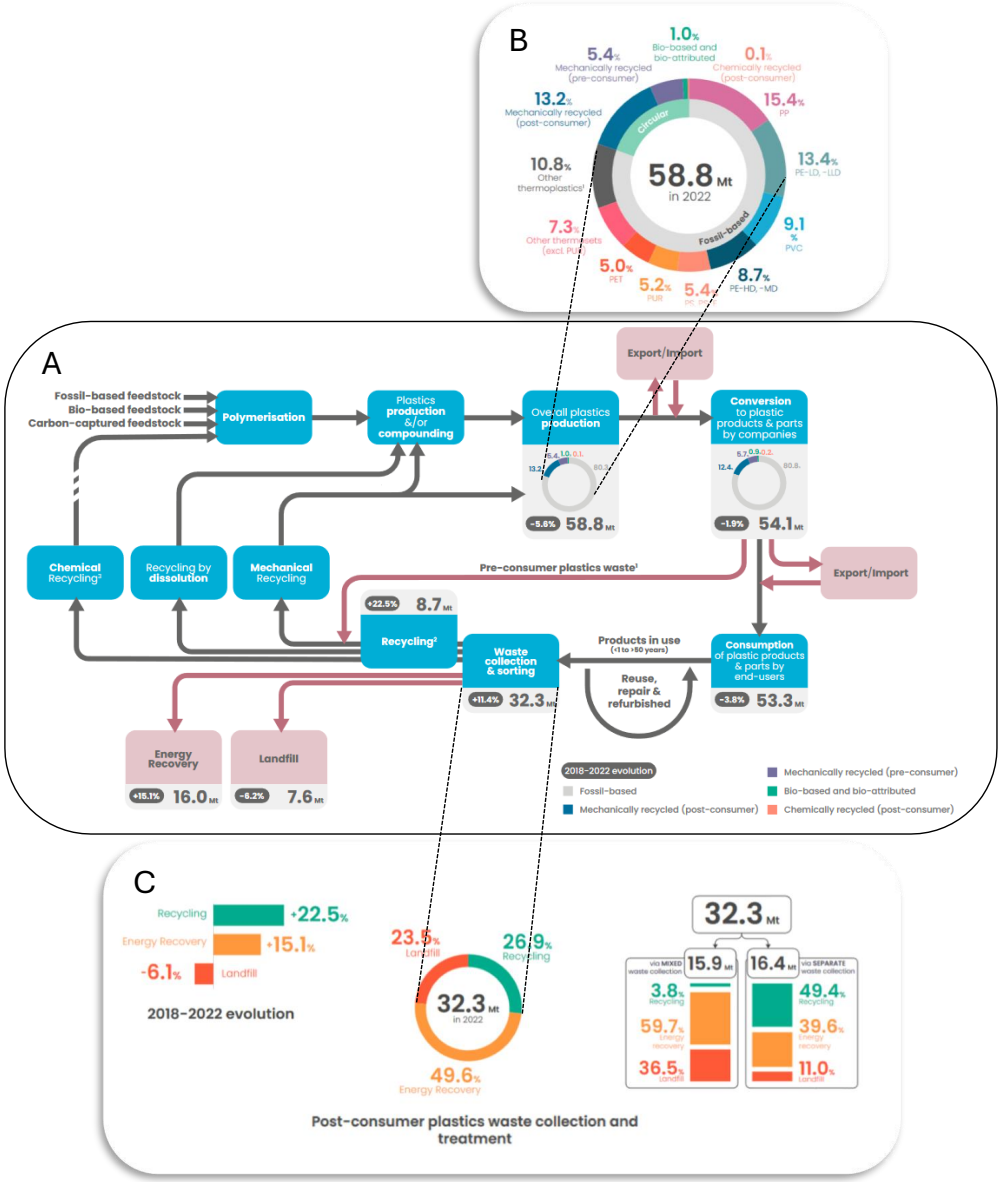

Figure 1.1. European circular plastic production and waste management. **(A)** Schematic overview of the model of the circular plastic economy showing the pathways of plastic, from its production and processing, to its disposal or recycling, closing the circle. Focus is on the changes between 2018 and 2022. **(B)** Overall plastic production in EU27+3 in 2022, displaying the contribution of different types of plastic, as well as the origin of their raw materials. **(C)** Statistics of developments in post-consumer plastic waste collection and treatment between 2018 and 2022. Derived from [3]

Current research efforts and developments in the industry are mainly focusing on PET [7]. A polymer that accounts for 5 % of the European plastic production and is mainly used for beverage bottles and food packaging, i.e. single use plastic and textiles. The percentage of recycled PET is marginal as it is a food contact material and the quality can no longer be guaranteed after mechanical recycling, especially if colorants have been added [3, 8, 9].

1.2 PET

Since its market launch by the English chemist John R. Whinfield in 1941 and its later adaptation by the DuPont Company, polyethylene terephthalate (PET) has grown to one of the most widely used polymers [10]. PET belongs to the family of thermoplastic polyesters, referring to a class of polymers which are known to contain ester groups in there polymer backbone, generally formed by the condensation of a diacid and a diol [11]. The unsaturated ester linkages in PET provide its semi-rigid to rigid structure and ensure its impact strength as well as chemical resistance. Furthermore, its thermoplastic nature allows the polyester to be easily molded and processed when exposed to high temperatures [12].

The conventional process of manufacturing PET involves the utilization of ethylene glycol (EG) and terephthalic acid (TPA) or its dimethyl ester called dimethyl terephthalic acid (DMT), respectively. As of present, the predominant source for obtaining the monomers relies on fossil-based raw materials, nevertheless, efforts are ongoing to develop more sustainable production processes, e.g. using bio-based feedstocks [10]. Depending on the monomers deployed, the polymerzation reaction is initiated either by the esterification of EG and TPA or by the transesterification of EG and DMT. Both reactions result in the intermediate polymer bis-(2-hydroxyethyl)-terephthalate (BHET) with either water or methanol as by-product (See Figure 1.2). The implementation of DMT was preferred for a long time since the high insolubility of TPA made it difficult to obtain the pure monomer. However, after optimization of the production process of TPA in the early 1970s making the pure product available in large quantities, direct esterfication was favoured, not least because the by-product of the transesterification, methanol, must be constantly removed by distillation [11, 12]. In the second stage, the polycondensation of BHET yields PET as the final product. The reaction conditions employed in this step determine the degree of polymerization and therefore its molecular weight (MW). Subsequently, solid state polycondensation is commonly conducted to further elevate the degree of polymerization, rendering it for moulding applications [13, 14].

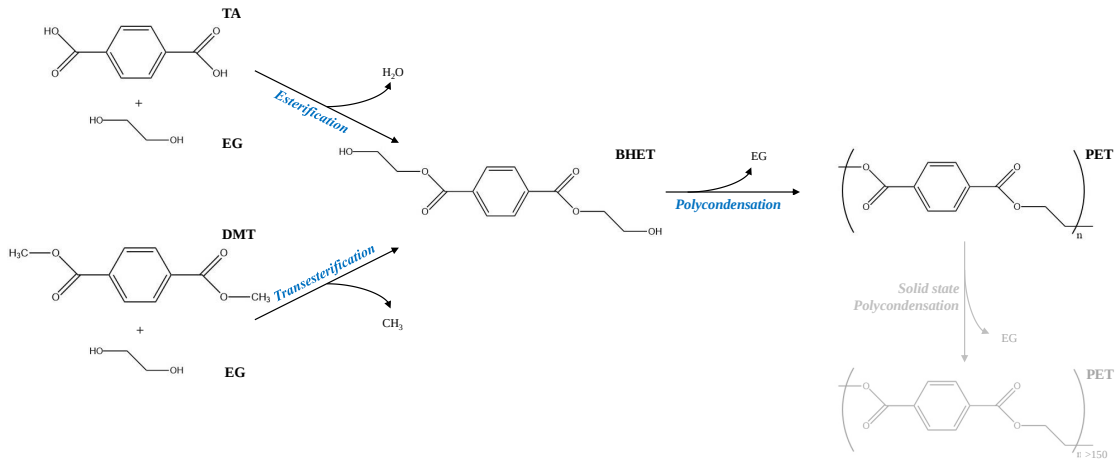

Figure 1.2. PET synthesis. PET polymerisation is initiated by either esterification (substrates: TPA and EG) or transesterification (substrates: DMT and EG) yielding BHET. In a subsequent step, the polyconcensation of BHET results in the final product. PET required for moulding applications can further be processed by solid state polycondensation to a degree of polymerization of over 150. Inspired by [10, 14]

Polymers exist either in a crystalline, partially ordered or amorphous state depending on the regularity of their backbone structure and interchain interactions. Generally, PET occurs in two different states, amorphous and semi-crystalline. Its properties are significantly influenced by the degree of crystallinity, as the polymer chains in crystalline areas are aligning and packed more tightly than in amorphous (see Figure 1.3). Therefore, semi-crystalline PET exhibits a high density resulting in greater thermal and mechanical stability, while amorphous PET is characterized by a better ductility, easier processing and optical clarity [15, 16, 17].

In the molten state of PET, the individual polymer chains are flexible and occur to some extent in the more energy-rich *gauche* conformation. Rapid cooling to a temperature below the so-called glass transition temperature (T_G), where the transition of a rigid to an elastic material takes place, allows these partially twisted and disordered conformations to be retained, resulting in amorphous PET. Conversely, semi-crystalline PET can be obtained by slowly cooling down the amorphous PET, allowing the chains to revert to the more stable *trans* conformation. The emerging elongated structure thus enables the formation of ordered crystalline regions within the polymer. Maximum crystallization rate was found to occur between 150 and 180°C [12, 16, 18]. As the degree of order within the polymeric structure increases, an impact on the T_G can be observed as well. While amorphous PET already displays increased molecular mobility at temperatures around 67°C, for semi-crystalline PET an elevated temperature of 80 up to 125°C is needed to reach the transition state [10].

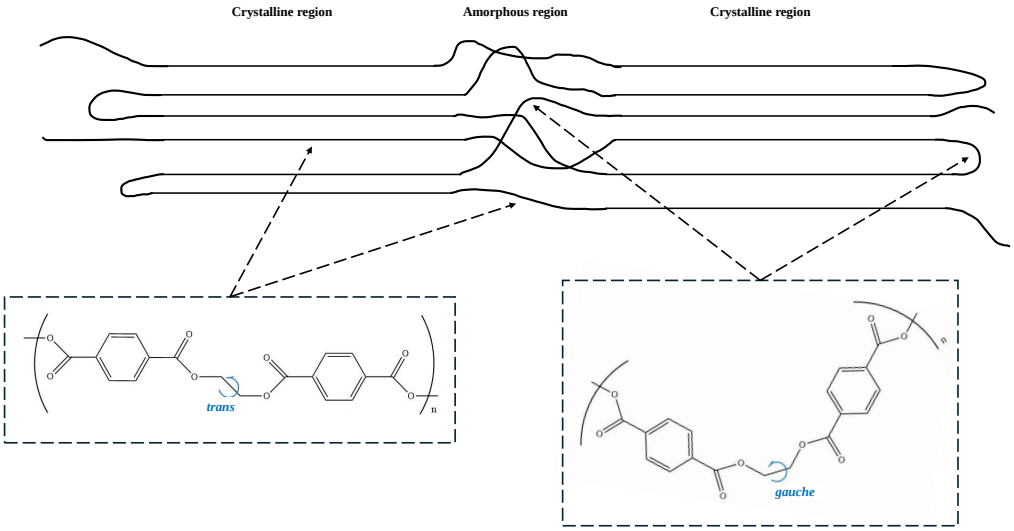

Figure 1.3. Semi-crystalline PET. The structure consists of both amorphous, disordered and crystalline, ordered regions. While amorphous parts provide flexibility, the crystalline lattice contributes stability and strength. Twists in the polymeric backbone are introduced by *gauche* conformation in the ehtylene glycol moiety of the chain. *Trans* conformation, however, stretch the chain favoring interchain interactions. Inspired by [19, 20].

Due to their large molecules and complex polymeric structure, PET is not readily degradable under normal conditions and their natural decomposition takes years as plastic waste continues to pile up in landfills and the environment, such as marine waters [21, 22]. Growing concerns about environmental pollution and preservation of resources are thus driving factors for the continuous development and advancement of recycling technologies.

1.2.1 Recycling of PET

Most commonly applied method remains mechanical recycling, as it can be carried out with minimal effort compared to other existing treatments. During mechanical recycling, the plastic waste is shredded and melted into pellets ready to be converted into a new product, a process that merely alters the physical form of the polymer, but not the chemical structure. However, the recovery rate of PET depends on the sufficient separation of possible contaminates such as other types of plastics, organic compounds and coloured polymers. Moreover, gradually degradation during reprocessing leads to a decreasing MW, resulting in downcycling of the polymer [23, 24].

In contrast, chemical recycling is based on depolymerization of PET into oligomers and monomer building blocks. This process exploits the fact that PET is sensitive to strong acids and bases and generally more susceptible to hydrolysis above its T_G [10, 12]. Thus, standard methods involve, for example, acidic or basic hydrolysis or degradation of PET by methanol at high temperatures (methanolysis). Another approach applied is glycolysis, where PET is mainly degraded to BHET in the presence of glycols such as EG and transesterification catalysts. The resulting products of chemically recycled PET can either be introduced as substrate for synthesis of new PET and other polymers or upcycled to higher value chemicals, like vanillin, catechol, muconic acid or glycolic acid. However, the main downside of chemical recycling remains the high energy costs, making the process less economically feasible[22, 25, 26, 27].

With regard to the circular economy of polyesters, in recent years research and development have focused on microbial and enzymatic degradation to complement mechanical recycling. Although synthetic polymers such as PET were long considered non-biodegradable, more and more microorganisms are identified to produce hydrolytic enzymes that can decompose these complex and inert structures [23]. Biodegradation involves either entire microbial communities that can fully degrade PET and use the degradation products as a carbon source and assimilate them into CO_2 and H_2O, or individual enzymes, whereas the degradation products can be reused in a similar way as after chemical recycling [28, 29].

1.3 PET Degrading Enzymes

Since the discovery of the first PET hydrolyse, a cutinase extracted from the bacterium *Thermobifida fusca*, several other enzymes, originating from different phyla of bacteria and fungi, have been biochemically characterized [30, 23]. Most of these enzymes belong to the classes of cutinases (EC 3.1.1.74), lipases (EC 3.1.1.3) or esterases (EC 3.1.1.1 and EC 3.1.1.2) and show typical characteristics of a serine hydrolases. Highly conserved between all of them is the α/β hydrolyse fold and the catalytic triad consisting of a serine, histidine and aspartate amino acid residue [23, 31]. Furthermore, many PET hydrolytic enzymes share conserved disulfide bridge(s) in the C-terminal region which provides them with significant kinetic and thermodynamic stability [32, 33].

PET hydrolytic enzymes typically possess a hydrophobic binding pocket which helps them recognizing the hydrophobic regions of the polymer chain. Their common mechanism involves the nucleophilic attack of a water molecule on the carbonyl carbon of the ester linkage resulting in cleavage products of PET like BHET, TPA, EG, mono(2-hydroxyethyl) terephthalate (MHET), dimeric MHET ($(MHET)_2$) and 2-hydroxyl-$(MHET)_2$ (2-HE$(MHET)_2$) which are finally all degrade into the benign monomers TPA and EG (See Figure 1.4). However, among these enzymes differences exists in their activity and substrate specificity. For instance, lipases are mainly known to break down ester bonds at hydrophobic surfaces, while esterases tend to prefer soluble esters. On the other hand, cutinases display a broad specificity showing hydrolytic activity for both soluble and long-chain esters [23, 35, 34].

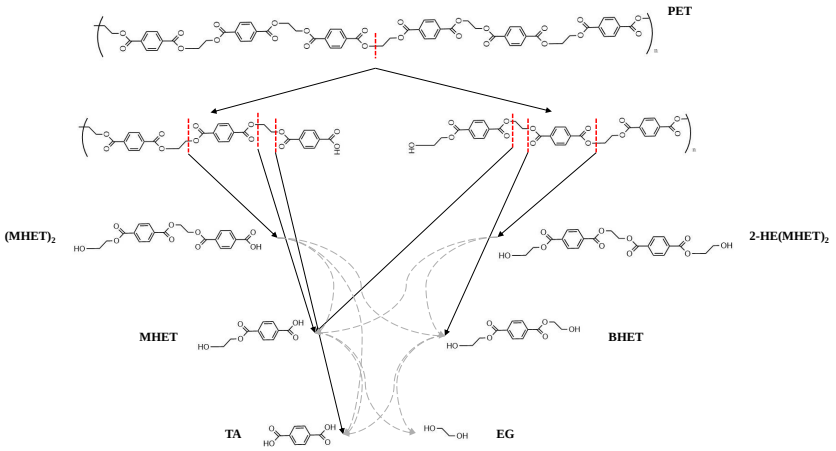

Figure 1.4. PET degradation process by PET hyrolytic enzymes PET hydrolytic enzymes are able to hydrolyze the ester bonds in the polymer chain of PET. In an initial step, intermediate molecules such as BHET, MHET, $(MHET)_2$ and 2-HE$(MHET)_2$ are released, which are ultimately all degraded to TPA and EG. One exception displays *Is*PETase, which is unable to hydrolyze MHET and therefore generates three final products (MHET, TPA and EG). Inspired by [34]

In 2016, a PET degrading bacterium called *Ideonella sakaiensis* was isolated from a microbial consortium growing on a PET bottle and the secreted PET hydrolase (*Is*PETase, EC 3.1.1.101) demonstrated superior specificity and activity toward PET when compared to all other enzymes [35, 36]. *Is*PETase has been characterized to work best at ambient temperatures (20-40°C) but appears to be heat-labile at higher temperatures, where other PET hydrolyzing enzymes reach their maximum activity. The sequence of *Is*PETase shares 51 % identity with the cutinase from *Thermobifida fusca* revealing the main difference to be in the substrate binding site, whereas other important features like the catalytic triad and disulfide bonds seem to be highly conserved [34]. The main products released after PET degradation are MHET, TPA and BHET, however, *Is*PETase cannot decomposed MHET further to TPA and EG. A distinguishing feature of the PET metabolic pathway of *I. sakaiensis* is the presence of a MHET hydrolyzing enzyme (MHETase, EC 3.1.1.102) localized at the outer cell membrane. It is solely responsible for hydrolyzing MHET into TPA and EG which are subsequently transported into the cytoplasm and metabolized in the tricarboxylic acid cycle [37].

PET hydrolitic enzymes are expected to be the future in bioremediation and recycling of our plastic waste, but the enzymes assessed to date have insufficient robustness, struggle with highly crystalline PET and do not achieve a turnover rate high enough to keep up with the continuously mounting post-consumer plastic waste. To address this, protein engineering was implemented to redesign existing enzymes and obtain mutants more appealing for industrial applications [23]. Recently, a variant of *Is*PETase has been developed via machine learning-aided engineering featuring five mutations (N233K/R224Q/S121E/D186H/R280A). The so-called FastPETase

displayed an improved catalytic activity and stability to pH and temperature ranges. Analysis on an untreated commercial water bottle at 50°C showed high release of products on sections that had crystallinity rates of up to 11,7 % and closed-loop enzymatic recycling was achieved by recovering the monomers and repolymerizing into virgin PET [38]. Synergystic effects could also be observed for a chimeric protein fusing *Is*PETase to MHETase via a Glycine-Serine linker. The close proximity of the enzymes resulted in a higher turnover rate and prevented potential feedback inhibition of the product MHET [39].

On average, the bulk of a PET bottle contains a degree of ca. 25 % crystallinity. To overcome the negative effect of high crystallinity, it was proposed to work at temperatures close to the T_G to make the structure more susceptible [38]. In 2014, a cutinase homolog derived from leaf-branch compost metagenome (LCC) was discovered that exhibits optimal functionality at elevated temperatures. Presumably originating from a thermophilic bacterium, the enzyme displayed a melting temperature (T_m) of 86,2°C and optimal PET degradation was identified to be around 70°C [33]. A variant of LCC optimized by Tournier et al. (2020) represents one of the most efficient PET hydrolytic enzyme to date and is referred to as ICCG (F243I/D238C/S283C/Y127G) [40, 41]. By adding two cysteine residues, a new disulfide bridge was introduced, which further improved the thermostability, while substituting isoleucine in the hydrophobic binding groove improved the enzyme contact-surface to the substrate. When employing an enzyme concentration of 3 mg per g of PET, LCC_{ICCG} accomplished at least 90 % PET depolymerization and an average production of 16,7 g/L/h of TPA over 10 h [40]. Moreover, it has been reported that LCC_{ICCG} still showed activity at crystallinity level of 24,4 %, although the product formation rate decreased by a factor of approx. 3 compared to a crystallinity of 10,8 % [42].

Both, FastPETase and LCC_{ICCG} are subject of this project as they outperformed all other currently assessed PET hydrolyzed at their respective temperature optimum [38, 40].

1.3.1 Industrial Deployment

In general, many factors have to be considered, when intending to upscale the enzymatic PET depolymerization for industrial purposes. Arnal et al. (2023) highlighted some of the key parameters to be (1) PET crystallinity and potentially required pretreatment, (2) maximization of the reaction surface, (3) temperatures close to T_G of PET, (4) the efficiency of the enzyme competing with the recrystallization of PET at elevated temperatures, (5) optimal PET concentration for maximal productivity, (6) yield of depolymerization, (7) complete hydrolysis to TPA and EG, and (8) availability of the enzyme in large quantities [41].

Recently, Singh et al. (2021) have published a process model for a scale of 150 tons of PET flakes per day and techno-economic analysis to identify the key factors influencing the feasibility of scaling up enzymatic PET recycling [43]. In their model, the PET feedstock was subjected to extrusion and cryo-grinding in an initial step to transform semi-crystalline post-consumer waste to amorphous powder. For the enzymatic depolymerization, they implemented the conditions previously demonstrated by Tournier et al. (2020). Particularly important here is the addition of a base like NaOH not only to maintain the pH during the continuous product release of acids such as TPA and MHET, but also to increase their solubility. Taking into considerations the Operational expenses (OPEX), the process requires a PET conversion of at least 90 %

to exclusively TPA and EG and an enzyme expressability of more than 20 g/L [41, 44]. In the subsequent steps, the recovered monomers were retrieved through downstream procedures involving crystallization of the recycled TPA at low pH, precipitation of the sodium sulfate by-product and distillation for extraction of EG. Their life cycle assessment predicted a minimum selling price of the recycled TPA of 1,93 $/kg, primarily driven by the costs of the feedstock estimated to be 0,66 $/kg of PET flakes. By comparison, the selling price of virgin TPA in 2020 amounted to 0,98 $/kg [43]. However, results from this scenario demonstrated that enzymatic hydrolysis could lead to significant reduction in energy consumption of up to 83 % and greenhouse gas emissions of up to 43 % compared to virgin TPA production [45].

1.4 Recombinant Extracellular Expression

In most of the studies that assessed and evaluated the properties of PET hydrolizing enzymes, the recombinant genes have been expressed intracellular in the selected productions host. Yet extracellular expression of protein offers several advantages especially regarding the intended large-scale production for industrial applications. Not only would it reduce downstream operations, but additionally lower overall production costs, making the process more economically viable. Furthermore, it can prevent the formation of inclusion bodies and improve the solubility and stability, particularly for proteins containing disulfied bonds, as they are not exposed to the reducing cytoplasmic environment [46, 47].

1.4.1 Protein Secretion Systems in *E. coli*

E. coli is a popular host for recombinant protein expression in the laboratory and on an industrial scale, as it is one of the best studied organisms and its manipulation for fine-tuning of expression levels is relatively simple [46]. For Gram-negative bacteria like *E. coli*, the secretion mechanisms are conventionally assigned to one of five pathways, type I, II, III, IV or V. Most commonly applied for recombinant proteins is the SecB-dependant type II pathway, which involves two steps: the translocation of the protein to the periplasmic space (1), where it is processed, folded and secreted across the outer membrane (2) [48]. The translocation is generally mediated by an N-terminal signal peptide (SP) consisting of 18-30 amino acids with a characteristic positively charged region at the beginning, a hydrophobic core region and a polar region at the end accessible for cleavage. Examples for SP that have already been established for the secretion of recombinant proteins are PelB, LamB and OmpC [49, 50]. In the SecB-dependent pathway, the protein exits the ribosome and is immediately bound by SecB to prevent premature folding and direct it to the membrane-bound SecA. Upon binding the pre-protein is guided to the translocation complex (SecY, SecE and SecG) under ATP hydrolysis. After removal of the SP, the protein is folded into its active form and released over a multi-protein complex, called secreton, to culture medium (See Figure 1.5) [48, 49].

However, the complexity of this two-step process can also cause partial accumulation in the periplasmatic space, reducing the overall yield [51]. In contrast, the type 1 secretion system (T1SS) is able to secrete the unfolded protein of interest in a single step across the double membrane [52]. *In vivo*, *E. coli* uses this pathway to secrete high-molecular-weight toxins and exoenzymes [53]. The best-characterized T1SS is the α-hemolysin (HlyA) secretion system, which

has already been tested for the extracellular overexpression of recombinant *Thermobifida fusca* cutinase in *E. coli* BL21 (DE3) displaying a 2,5 fold higher secretion compared type II secretion pathway [54]. The system was discovered in uropathogenic *E. coli* and is responsible for the secretion of HlyA, which belongs to the family of repeat-in-toxin (RTX) proteins. HlyA contains a SP located at the C-terminus consisting of the terminal 60 amino acid residues, which can be exploited to to secrete heterologous proteins. However, the SP remains attached to the protein after secretion, thus requiring evaluation of its impact on the protein's activity. The secretory machinery of this pathway involves three membrane proteins forming the transmembrane channel (See Figure 1.5). The ATP-binding cassette transporter HlyB located in the inner membrane associated with the membrane fusion protein HlyD are both essential for the translocation of HlyA, while the outer membrane protein TolC is important for the final secretion [47, 55]. While TolC is known to be part of many transmembrane system and therefore already present in commonly employed *E. coli* strains, HlyB and HlyD have been identified as strain specific [54]. Consequently, co-expression of these membrane components is necessary for successful translocation.

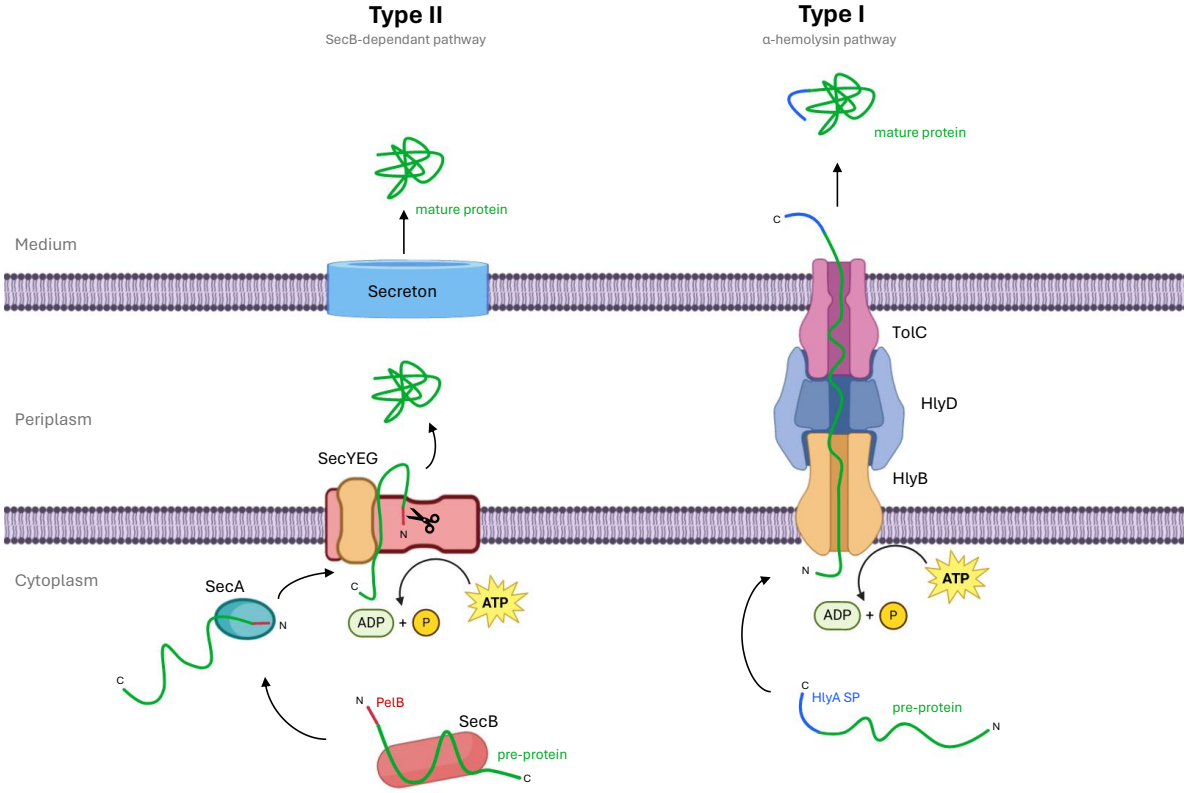

Figure 1.5. Schematic overview of the SecB-dependant secretion pathway (type II) vs. the α-hemolysin secretion pathway in *E. coli* In the SecB-dependant pathway **(type II)**, the pre-protein emerging the ribosome is bound by SecB to prevent folding. SecA recognized the N-terminal SP, here PelB, and guides the pre-protein to the SecYEG transporter channel. The translocation takes place under ATP hydrolysis and the SP is cleaved off before the fully folded protein is released into the periplasm. The final secretion of the folded protein is carried out by the secreton located in the outer membrane. In the α-hemolysin secretion pathway **(type I)**, the pre-protein containing a C-terminal HlyA signal peptide binds to the ABC transporter HlyB. ATP hydrolysis initiates the transport through the membrane fusion protein HlyD and the outer membrane protein TolC in a single step. Folding of the protein with the SP still attached occurs after secretion into the cultural medium. Inspired by [50, 55]

1.4.2 Protein Secretion Systems in *B. subtilis*

One drawback concerning the implementation of *E. coli* as an industrial organism is that the outer cell membrane contains liposaccharides, which can turn into endotoxins upon cleavage and can trigger allergic reactions in the human body. As a result, the production of proteins by *E. coli* must always be evaluated to be "Generally Recognized as Safe" (GRAS) [46].

Bacillus subtilis is generally possessing the GRAS status and is one of the best studied Gram-positive organisms. It is robust, grows in similar cell-densities as *E. coli* and known to secrete homologous proteins in concentrations up to 25 g/L [56]. In order to use the model bacterium for heterologous protein secretion in industrial biotechnology, the protein secretion machinery and the secreted proteins were examined in more detail. Similar to other bacterial systems, these proteins are synthesized with an N-terminal SP, which is cleaved after translocation. The structural composition of the SP is highly conserved, consisting of arginine or lysine residues in the positively charged N-region, the hydrophobic core, referred to as H-region, and the C-region containing a recognition and cleavage site for a SP cleaving peptidase [57]. The majority of the proteins in *B. subtilis* are secreted by the Sec-dependant pathway and also for the bioproduction only Sec-type signal peptides have been implemented so far. The Sec-dependant pathway in *B. subtilis* is comparable with the SecB-dependant pathwas in *E. coli*. The main difference is that *B. subtilis* is lacking the SecB protein, whose function is presumably covered by another chaperone protein. Both the ATP-dependant motor protein SecA and the SecYEG translocon are present, as well as a heterotrimeric complex, named SecDF-YrbF [58]. Since Gram-positive bacteria lack the outer cell membrane, further translocation is not necessary and accumulation in the periplasmic space cannot occur. However, there are two other factors that can limit successful secretion in *B. subtilis*. After the export *trans* of the cytoplasmic membrane, the proteins enter a microenvironment at the periphery of the cell wall that has a high density of negative charges. These are mainly caused by anionic polymers, balanced by cationic metal ions, like Mg^{2+} or Ca^{2+}. The high charge density can influence the post-translocational folding and stability of the protein. In addition, many proteases are located in the cell wall that serve as quality control, but can also degrade sensitive proteins. To prevent this, several strains have already been developed that lack various proteases [57, 59].

The biggest bottleneck in the secretion of heterologous proteins by *B. subtilis* is that no SP has been identified yet that can be applied for all desired proteins. Therefore, Brockmeier et al. (2006) has developed a systematic screening approach to test all Sec-dependant SP (no-lipoprotein) naturally occurring in *B. subtilis* for their efficiency to secrete a protein of interest. In their study, they succeeded, amongst others, to identify a SP that was able to secrete cutinase from *Fusarium solani pisi* in a concentration of 35 mg/L [60]. Based on this, Takara Bio Inc. has designed the "*B. subtilis* Secretory Protein Expression System" allowing the preparation of a vector library of 173 different SPs fused to the protein of interest. Subsequently, extracellular expression by *B. subtilis* and activity can be evaluated. The system was also used in the course of this project.

Problem Statement 2

The current deployment of biorecycling of PET is hindered by economic feasibility, mainly due to high process costs and the complexity of downstream processing. A key step that simplifies the process includes the secretion of PET hydrolases by the expressing host, which avoids labor-intensive procedures such as cell lysis, the separation of cell debris and the solubilized fraction and more. However, one of the main challenges remains the efficient recombinant protein secretion limiting their industrial implementation.

Existing secretion pathways, such as SecB-dependant secretion in *E. coli*, suffer from enzyme expressability and partial accumulation in the periplasm, which reduces the overall yield. To address this, this thesis aims to overcome the issue through two distinct approaches:

1. Introduction of an alternative secretion system for operating in *E. coli*. The so-called T1SS HlyA secretion pathway has demonstrated successful secretion of *Thermobifida fusca* cutinase and benefits from its low complexity.
2. Exploration of an alternative host organism, *B. subtilis*, which has been recognized for its ability to secrete large amounts of proteins. By testing a library of different SP, this approach seeks to identify the most efficient one for secreting the PET hydrolases via the endogenous Sec-machinery.

With these focused approaches, this thesis aims to overcome current obstacles that are preventing the large scale implementation of PET hydrolases for the depolymerization of PET and thus contribute to recycling solutions that are more commercially viable and environmentally sustainable.

Materials and methods 3

3.1 Overview of the Experimental Procedure

The methods and materials applied for the experimental work in this study are described in the following section. The workflow is visualized in the accompanying flowcharts.

3.1.1 Secretory Overexpression of PET Hydrolases in *E. coli* BL21 (DE3)

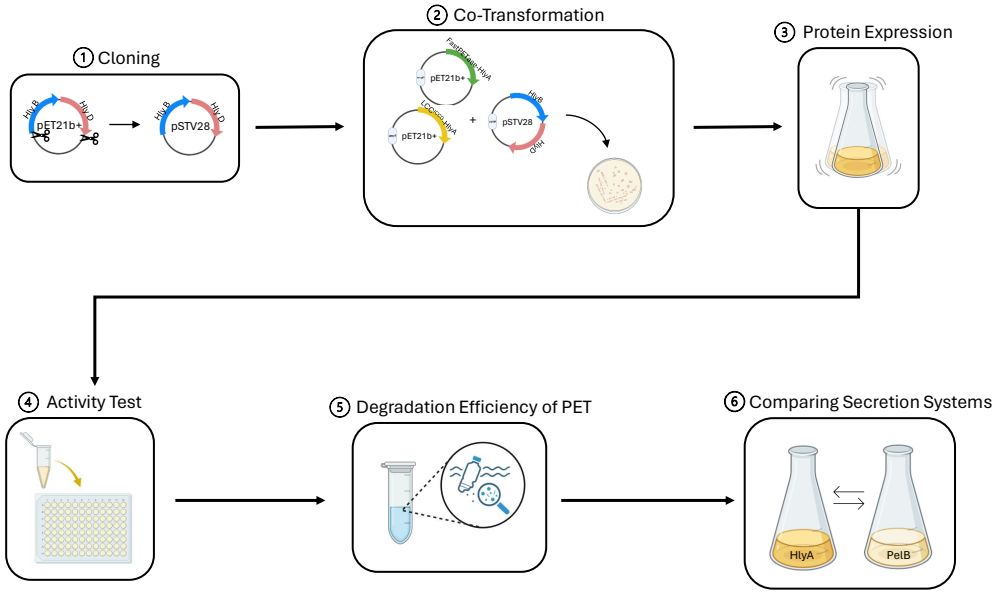

Figure 3.1. Workflow for the Secretory Overexpression of PET Hydrolases via α-hemolysin Secretion Pathway in *E. coli* BL21 (DE3). **(1)** Cloning of the plasmid containing the two membrane proteins HlyB and HlyD (HlyBD) of the translocation complex **(2)** Co-transformation of the plasmid carrying LCC_{ICCG} or FastPETase, respectively, fused to the C-terminal SP of HlyA and the plasmid containing HlyBD **(3)** Protein expression via IPTG induction and evaluation of the secretion via SDS-PAGE **(4)** Assessment of the activity in the supernatant **(5)** Testing PET degradation efficiency of the secreted PET hydrolases **(6)** Comparing the secretion efficiency to the SecB-dependant pathway using PelB and the expression using no SP

3.1.2 Secretory Expression of PET Hydrolases in *B. subtilis* RIK 1285

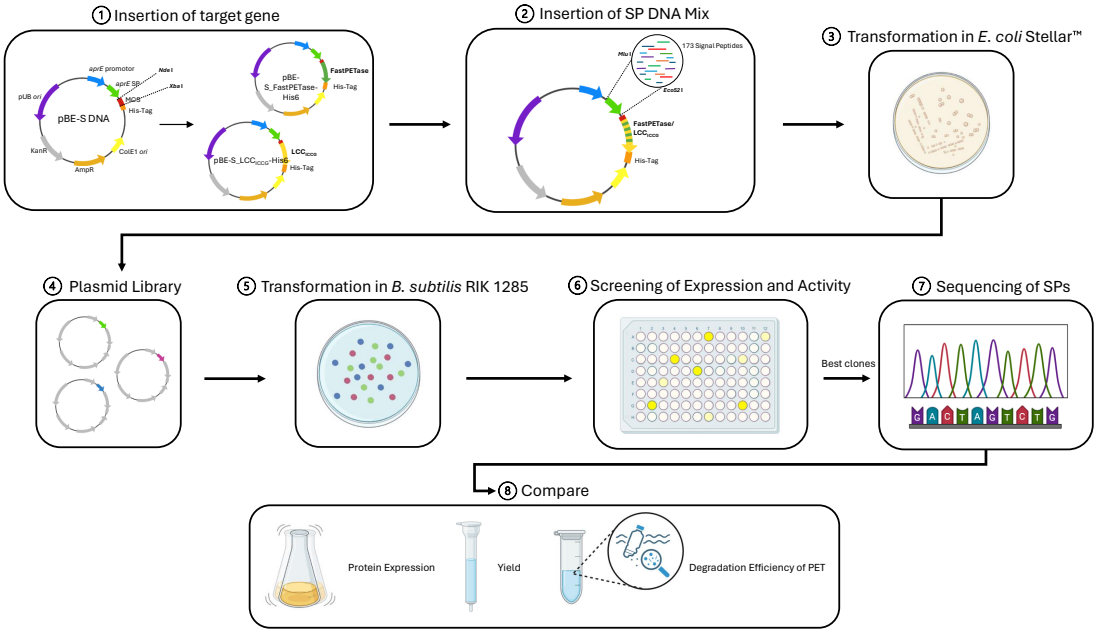

Figure 3.2. Workflow for the Secretory Protein Expression of PET Hydrolases in *B. subtilis* RIK 1285. **(1)** Insertion of codon-optimized LCC_{ICCG} or FastPETase into the multipe cloning site (MSC) of the shuttle vector pBE-S DNA **(2)** Insertion of the Sp mixture containing 173 different SP via In-Fusion cloning **(3)** Transformation of the plasmids into *E. coli* Stellar™ **(4)** Preparation of the plasmid library **(5)** Transformation of the library into *B. subtilis* RIK 1285 **(6)** Initial screening of all the resulting clones for esterase activity in the supernatant **(7)** Selection of possible candidates and identification of their SP **(8)** Expression of the final candidates in a larger culture volume and comparison of their secretion efficiency, yield, PET degradation efficiency

3.2 Materials

3.2.1 Bacterial strains

Table 3.1. Used bacterial strains, their genotype and purpose

Bacterial Strain	Genotype	Purpose
E. coli BL21 (DE3)	F^-, ompT, $hsdS_B$ (r_B^-, m_B^-), gal, dcm, $\lambda(DE3)$	Amplification of plasmid DNA, cloning and secretory protein expression of heterologous genes
E. coli HST08 Stellar	F^-, endA1, supE44, thi-1, recA1, relA1, gyrA96, phoA, $\Phi 80dlacZ\Delta M15, \Delta(lacZYA-argF)U169, \Delta(mrr-hsdRMS-mcrBC), \Delta mcrA, \lambda-$	Preparation of expression Plasmid library
B. subtilis RIK 1285	Marburg 168 derivative: trpC2, ys1, aprEdelta3, nprR2, nprE18	Secretory protein expression of heterologous genes

3.2.2 Plasmids

Table 3.2. Plasmids used or constructed within the scope of this project and their purpose

Plasmid	Purpose	Source
pET21b+-LCC_{ICCG}-His6-HlyA	Secretory expression of LCC_{ICCG}-His6-HlyA (together with pSTV28-HlyBD)	Gene Universal
pET21b+-FastPETase-His6-HlyA	Secretory expression of FastPETase-His6-HlyA (together with pSTV28-HlyBD)	Gene Universal
pSTV28	Cloning of pSTV28-HlyBD	Takara Bio Inc.
pSTV28-HlyBD	Expression of the α-hemolysin secretory machinery proteins HlyB and HlyD	This study
pET21b+-HlyBD	PCR amplification of hlyB and hlyD	Gene Universal
pET26b-LCC_{ICCG}-His6-PelB	Secretory expression of LCC_{ICCG}-His6 through SecB-dependent type II pathway	This study
pET21b+-LCC_{ICCG}-His6	Expression of LCC_{ICCG}-His6 with no SP	This study
pBE-S DNA	*B. subtilis*/ *E. coli* shuttle vector for the preparation of a Plasmid library of secretory signals of *B subtilis* to express extracellular LCC_{ICCG}-His6 and FastPETase-His6	Takara Bio Inc.
pBE-S-LCC_{ICCG}-His6-bac	Insertion of the secretory signal peptide library to screen for efficient secretion of LCC_{ICCG}-His6-bac	This study
pBE-S-FastPETase-His6-bac	Insertion of the secretory signal peptide library to screen for efficient secretion of FastPETase-His6-bac	This study
pET32a+-LCC_{ICCG}-His6-bac	PCR amplification of LCC_{ICCG}-bac (codon optimised for *B. subtilis*)	Gene Universal
pET28a+-FastPETase-His6-bac	PCR amplification of FastPETase-bac (codon optimised for *B. subtilis*)	Gene Universal

Plasmid	Purpose	Source
pBE-S-LCC_{ICCG}-His6-NS	Expression of LCC_{ICCG}-His6-bac with no SP (codon optimised for *B. subtilis*)	This study
pEt28a+-LCC_{ICCG}-Epr	Cloning of pBE-S-LCC_{ICCG}-His6-Epr	Gene Universal
pET28a+-LCC_{ICCG}-YjfA	Cloning of pBE-S-LCC_{ICCG}-His6-YjfA	Gene Universal
pBE-S-LCC_{ICCG}-His6-Epr	Expression of LCC_{ICCG}-His6-bac with the SP *Epr* (codon optimised for *B. subtilis*)	This study
pBE-S-LCC_{ICCG}-His6-YjfA	Expression of LCC_{ICCG}-His6-bac with the SP *YjfA* (codon optimised for *B. subtilis*)	This study

3.2.3 DNA-Oligonucleotides

Table 3.3. DNA Oligonucleotides, their Sequence (5'-3') and purpose

Name	Sequence (5'-3')	Purpose
T7	taatacgactcactataggg	Forward primer for plasmids containing a T7 promoter
T7-term	ctagttattgctcagcggt	Reversed primer for plasmids containing a T7 terminator
HlyBD-F	cggcgagctcggattcttgtcataaa attg	Forward primer for PCR amplification of HlyBD containing a *Sac*I restriction site
HlyBD-R	ccacggatccttaacgctcatgtaaac	Reversed primer for PCR amplification of HlyBD containing a *BamH*I restriction site
M13rev-29	caggaaacagctatgacc	Forward sequencing primer for plasmids with the backbone pSTV28
M13uni-21	tgtaaaacgacggccagt	Reversed sequencing primer for plasmids with the backbone pSTV28
LCC-His6-BamHI	gtcgggatccgatgagcaatccgt	Forward primer for PCR amplification of LCC_{ICCG}-His6 containing a *BamH*I restriction site
LCC-His6-XhoI	ggtgctcgagttaatggtgatgatga	Reversed primer for PCR amplification of LCC_{ICCG}-His6 containing a *Xho*I restriction site

Name	**Sequence** (5'-3')	**Purpose**
pBE-S-FW	agtaagtctactctgaacttaagca	Forward sequencing primer for plasmids with the backbone pBE-S DNA
pBE-S-RV	actgcgttagcaatttaactgtgat	Reversed sequencing primer for plasmids with the backbone pBE-S DNA
pBE-LCC-SP-RV	gactaactgtataggttttaacgc	Reversed sequencing primer for identifing the SP upstream of LCC_{ICCG} in pBE-S DNA
LCC-FW-NdeI	ggaattccatatgatgagcaatccgtat	Forward primer for PCR amplification of LCC_{ICCG}-bac (codon optimized for *B. subtilis*) containing a *Nde*I restriction site
LCC-RV-XbaI	tgctctagactgacaatgacgattatt	Reversed primer for PCR amplification of LCC_{ICCG}-bac (codon optimized for *B. subtilis*) containing a *Xba*I restriction site
LCC-FW-MluI	tagacgcgtatgagcaatccgtatcag	Forward primer for PCR amplification of LCC_{ICCG}-bac (codon optimized for *B. subtilis*) containing a *Mlu*I restriction site
FastPETase-FW-NdeI	ggaattccatatgatgcaaacaaatc cttacg	Forward primer for PCR amplification of FastPETase-bac (codon optimized for *B. subtilis*) containing a *Nde*I restriction site
FastPETase-RV-XbaI	tgctctagattcaaggctgcaattcg	Reversed primer for PCR amplification of FastPETase-bac (codon optimized for *B. subtilis*) containing a *Xba*I restriction site

3.2.4 Restriction Enzymes

Table 3.4. Restriction Enzymes used for the construction of plasmids mentioned in Table 3.2

Name	Company
*Mlu*I	Takara Bio Inc.
*Eco*52 I	Takara Bio Inc.
*Xho*I	NEB
*BamH*I-HF	NEB
*Xba*I	NEB
*Nde*I	NEB
*Sac*I	NEB

3.3 Molecular Genetic Methods

3.3.1 Agarose Gel Electrophoresis

For the preparation of the agarose gel, 1 % (w/v) SeaKem LE Agarose (Lonza) was dissolved in 1x TAE buffer (Bio-Rad) by boiling the solution in the microwave. After cooling down to around 60 °C, 0.0017 % (v/v) SYBR Safe DNA gel stain (Invitrogen) was added and the solution was cast into a gel slide (Bio-Rad) together with a comb for the wells. After solidifying, the gel was placed into the electrophoresis chamber (Mini-Sub® Cell GT, Bio-Rad) filled with 1x TAE buffer. The samples were prepared with 20 % (v/v) Gel Loading Dye, Purple (6x) (NEB) and added to the wells. For sizing of the DNA, 2 µL GeneRuler 1 kb DNA Ladder (Thermo Fisher Scientific) was used. The gel electrophoresis was performed at a voltage 80 V for 45 min and for visualisation of the results the ChemiDoc MP imaging system (Bio-Rad) and Image Lab Software (4.0.1., Bio-Rad) was used.

3.3.2 Restriction Digestion

Enzymatic restriction hydrolysis was carried out according to the manufacturer's instructions for the restriction enzyme (RE) to be used (3.4). All reactions contained 0.5-1 µg DNA, 0.5-1 µL of the corresponding restriction enzyme(s), 5 µL of the specified buffer (concentration: 10x), were filled up with nuclease free water (Omega) to a total volume of 50 µL and incubated at 37 °C for 1 h. Afterwards, the restriction enzyme was either heat-inactivated according to manufacturer's instructions or the DNA was purified with the DNA Clean & Concentrator-5 Kit (Zymo Research). If a step wise digestion was necessary due to two restriction enzymes requiring different reaction buffers, the DNA was purified after every digestion step with the DNA Clean & Concentrator-5 Kit before performing the next digestion.

3.3.3 Ligation

The required volumes of vector DNA and insert DNA for ligation were calculated using the online tool "Ligation Calculator" (version 1.15.5, NEB). A molecular ratio of 1:3 was selected (vector

DNA:insert DNA). In addition to the calculated volumes, 1 µL T4 DNA ligase (NEB), 2 µL T4 ligase buffer (concentration: 10x, NEB) were added and filled up with nuclease free water to a total volume of 20 µL. As a control, one solution containing only vector DNA was prepared. The ligation was incubated for 1 h at RT and then heat inactivated at 65 °C for 10 min. If the ligation was to be subsequently transformed via electroporation, the solution was diluted in a ratio of 1:10 beforehand.

3.3.4 In-Fusion Cloning

In-Fusion Cloning was only used for construction of the expression plasmid library for Secretory Protein Expression in *B. subtilis* RIK 1285. The gene of interest was previously inserted into the multiple cloning site downstream of the secretory signal peptide and upstream of the His6-tag of pBE-S DNA (Table 3.2) and the plasmid was linearized using *Mlu*I and *Eco*52 I (Table 3.3). The In-Fusion reaction was performed in a total volume of 10 µL containing 5x In-Fusion HD Enzyme Premix (Takara Bio Inc.), nuclease free water, 100 ng of the linearized plasmid and the SP DNA mixture (0.032 pmol/µL) with a 2 molar excess. To check the background, the same reaction was performed without the addition of the SP DNA mixture. The reaction mixture was incubated for 15 min at 50°C and kept on ice until transformation into competent *E. coli* HST08 Stellar 3.3.6.

3.3.5 Preparation of Competent Cells

E. coli BL21(DE3)

For generating electrocompetent *E. coli* BL21 (DE3), a frozen glycerol stock of the strain was streaked onto LB plates (1% (w/v) tryptone (Fluka), 1% (w/v) NaCl (VWR), 0.5% (w/v) yeast extract (Thermo Fisher Scientific), 2% (w/v) agar (Fluka)) and grown over night (oN) at 37 °C. A single colony was selected to inoculate a pre-culture of 10 mL LB media (1% (w/v) tryptone (Fluka), 1% (w/v) NaCl (VWR), 0.5% (w/v) yeast extract (Thermo Fisher Scientific)) and shake oN at 37°C. 2 mL of the pre-culture was used to inoculate 200 mL of LB media and incubate at 37°C. The optical density (OD_{600}) of the culture was measured at 600 nm every hour until it reached 0.35-0.4 and then immediately chilled for 30 min on ice. Afterwards, the cells were transferred into pre-cooled 50 mL Falcon tubes (Thermo Fisher Scientific) and centrifuged for 20 min at 4°C at 1000 xg (11133 Swing-out rotor, 13104 Buckets, Sigma). The supernatant was discarded and the pellet resuspended in 50 mL ice cold and sterile ddH_2O. The cells were harvested under the same conditions as mentioned before and the pellet resuspended in 25 mL ice cold ddH_2O. Two of the resuspended cell pellets were combined in one tube and harvested under the mentioned conditions. After discarding the supernatant, the pellet was resuspended with 8 mL ice cold and steril 10 % glycerol (VWR) and transferred to a cooled 15 mL Falcon tube (Thermo Fisher Scientific). The cells were harvested as aforementioned and the supernatant was removed with a sterile Pasteur pipette (Thermo Fisher Scientific). The pellet was carefully resuspended with 200 µL of 10 % glycerol, 60 µL aliquots were distributed into 1.5 mL Eppendorf tubes, the tubes snap frozen with liquid nitrogen and stored at -80°C until transformation via electroporation (3.3.6).

B. subtilis RIK 1285

For preparing of *B. subtilis* RIK 1285 competent cells, the protocol described in the product manual "*B. subtilis* Secretory Protein Expression System" by Takara Bio Inc. was followed. One vial of the glycerol stock of *B. subtilis* RIK 1285 was spread on a LB plate and incubated oN at 37°C. One of the colonies was used to inoculate 2 mL of LB medium and grow the pre-culture oN at 28°C at 170 rpm. 50 µL of the pre-culture were added to 5 mL of SP I medium (0.2% (w/v) $(NH_4)_2SO_4$ (VWR), 1.4% (w/v) K_2HPO_4 (VWR), 0.6% (w/v) KH_2PO_4 (VWR), 0.0877% (w/v) Na-Citrate (Sigma-Aldrich), 0.02% (w/v) $MgSO_4$*H_2O (Sigma-Aldrich), 0.49% (w/v) glucose (VWR), 0.02% (w/v) Casamino Acids (VWR), 0.098% (w/v) Yeast Extract (Merck)) and incubated at 37°C at 170 rpm. The optical density (OD_{660}) for *B. subtilis* RIK 1285 was measured at 660 nm every 30 min after the first hour of incubation to identify the plateau phase of the culture. When the phase was reached, 0.5 mL of the culture were added to 4.5 mL of SP II medium and incubated at 37°C for 90 min at 100 rpm. Afterwards, 50 µL of 100 mM EGTA (Sigma-Aldrich) were added and the culture incubated under the same conditions as before for 5 min. The culture was divided into 1.5 mL Eppendorf tubes with aliquots of each 300 µL and transformation was performed immediately (3.3.6).

3.3.6 Transformation of Plasmids

E. coli BL21(DE3)

Before transformation of the electrocompetent *E. coli* BL21 (DE3) generated in 3.3.5, the electrocuvettes had to be rinsed with 70 % ethanol (VWR) and placed upside down on a paper tissue until all the ethanol was evaporated. Afterwards, the electrocuvettes was placed on ice and one aliquot containing 60 µL of the electrocompetent *E. coli* BL21 (DE3) was transferred. If a ligated plasmid was to be transformed, 2.5 µL was added to the cells, otherwise 1 µL of plasmid DNA was sufficient. Electroporation was carried out in the Electroporator 2510 (Eppendorf) applying a voltage of 2.5 kV to the cells (time constant: 5,8-6.2). 1 mL of LB medium was added immediately and the cell suspension was incubated for 1 h at 37°C at 190 rpm. 100 µL was plated on a LB plate with the corresponding antibiotic(s) and incubated oN at 37°C. If a low transformation efficiency was expected, e.g. after ligation of a plasmid, the cell suspension was centrifuged first at 6000 xg, the supernatant was removed up to 100 µL, the cell pellet was resuspended in the remaining liquid and then spreaded on the LB plate.

E. coli HST08 Stellar

Competent *E. coli* HST08 Stellar were used to transform the plasmids generated via In-Fusion Cloning 3.3.4. For each In-Fusion reaction, 100 µL of *E. coli* HST08 Stellar, previously thawed on ice, was transferred to a 1.5 mL Eppendorf tube and mixed with 2 µL of the In-Fusion reaction solution. The cells were incubated on ice for 30 min, given a heat shock at 42°C for 45 sec and immediately placed back on ice for 2 min. Afterwards, 900 µL of LB medium was added and the transformed cells were incubated at 37°C for 1 h at 190 rpm. The whole cell suspension was plated on 150mmx15mm LB plates containing 100 µg/mL ampicillin (Sigma-Aldrich) and incubated oN at 37°C.

B. subtilis RIK 1285

1 µg of DNA was added per 300 µL of competent cells as prepared in 3.3.5 and incubated at 37°C for 90 min at 100 rpm. The culture was streaked onto LB plates with 10 µg/mL kanamycin (Sigma-Aldrich) and incubated oN at 37°C.

3.3.7 Plasmid Preparation

E. coli BL21(DE3)

Depending on whether the plasmid to be isolated was a high copy or low copy plasmid (plasmids with the backbone pST28), 5 mL or 10 mL of LB medium containing the required antibiotic was inoculated with a previously transformed single colony (3.3.6) and incubated oN at 37°C at 190 rpm. Afterwards, the plasmid DNA was isolated with the NucleoSpin Plasmid Kit (Macherey-Nagel) following either the protocol for high copy or low copy plasmids. For both protocols the additional washing step with Buffer AW was carried out.

B. subtilis RIK 1285

One colony was used to inoculate 5 mL LB medium containing 10 µg/mL kanamycin and incubated oN at 37°C. The culture was harvested for 30 sec at 11000 xg in a 1.5 mL Eppendorf tube and the supernatant discarded. Afterwards, the cell pellet was resuspended with 250 µL of buffer A1 of the Nucleo Spin Plasmid Kit (3.3.7) containing 10 mg/mL additional lysozyme (Sigma-Aldrich). The resuspended pellet was incubated for 30 min at 37°C and the subsequent steps were carried out as described in the protocol of the NucleoSpin Plasmid Kit.

3.3.8 Library Preparation

E. coli HST08 Stellar

After transformation of the plasmid library in *E. coli* HST08 Stellar 3.3.6, the colonies on the LB plate were suspended with 5 mL of LB medium using a spreader. The plate was washed two more times with 5 mL of LB medium and the resuspended cells were collected in a 15 mL Falcon tube. The plasmids isolated from the cells using the protocol for high copy plasmids of the NuclepSpin Plasmid Kit. The obtained plasmid library was subsequently used to transform *B. subtilis* RIK 1285 3.3.6.

3.3.9 Determination of DNA Concentration

The concentration of DNA was determined by UV spectroscopy using the NanoDrop-1000 (PeqLab, Software: NanoDrop 1000 3.7.1). For this purpose, an absorption spectrum ranging from 220-340 nm was measured. The DNA concentration was calculated from the absorbance

value at 260 nm using Lambert-Beer's law and possible impurities were detected by checking the ratios at 260/280 nm and 260/230 nm.

3.3.10 DNA Sequencing and Sequence Analysis

For verification of the sequence of the cloned plasmids, the purified plasmid DNA was prepared according to the instruction for Mix2Seq Kit (Eurofins Genomics Germany GmbH). The sequencing was then carried out by Eurofins Genomics and compared with the expected sequence of the plasmid using the online program MultAlin (F.CORPET, 1988).

3.3.11 Polymerase chain reaction (PCR) and Colony PCR

The primers used for the amplification of the different DNA fragments were designed in Benchling (2024) 3.3 and their annealing temperature was determined using the NEB Tm Calculator (version 1.16.5).

A preparative PCR was performed in a total reaction volume of 50 µL containing 25 µL of Q5 High-Fidelity 2x Master Mix (NEB), 2.5 µL Forward Primer (10 µM), 2.5µL Reverse Primer (10 µM), 1 µL of template (concentration: 1 pg-10 ng) and 19 µL of nuclease free water. As negative control (NK), the template was substituted by 1 µL of nuclease free water. The settings used for the ThermoCycler XT^{96} (VWR) are listed in Table 3.5

Analytic PCR was used to verify the presence of a certain plasmid in bacterial colonies. The reaction volume was 25 µL consisting of 12.5 µL 2x DreamTaq Green PCR Master Mix (Thermo Fisher Scientific), 1.25 µL Forward Primer (10 µM), 1.25 µL Reverse Primer (10 µM) and 10 µL of nuclease free water. A bacterial colony was isolated with a pipette tip and added to the reaction as template. For the positive control (PK) or NK, respectively, 1 µL of plasmid DNA containing the gene of interest or 1 µL of nuclease free water was added instead of the template. The settings used for the ThermoCycler XT^{96} (VWR) are listed in Table 3.5. PCR products were purified using the DNA Clean Concentrator-5 Kit (Zymo Research).

Table 3.5. Parameters for PCR reactions using the Q5 Polymerase or DreamTaq Polymerase, respectively

	Q5 Polymerase	**DreamTaq Polymerase**
Initial Denaturation [Temperature/ Time]	98°C/ 30 sec	95°C/ 60 sec
Number of cycles	30	30
Denaturation [Temperature/ Time]	98°C/ 10 sec	95°C/ 30 sec
Annealing [Temperature/ Time]	NEB T_m Calculator/ 30 sec	T_m-5/ 30 sec
Extension [Temperature/ Time]	72°C/ 25 sec/kb	72°C/ 60 sec
Final extension [Temperature/ Time]	72°C/ 5 min	72°C/ 5 min

3.4 Protein Analytic Methods

3.4.1 SDS PAGE

Denaturing sodium dodecyl sulfate polyacrylamide gel electrophoresis (SDS-PAGE) was used to separate protein mixtures in the electric field according to their size. Depending on whether the supernatant or the unlysed cells were to be analysed, the samples were prepared in a different way. For the unlysed cells, the volume taken should equal an OD_{600} (for *E. coli* BL21 (DE3)) or OD_{660} (for *B. subtilis* RIK1285) of 1. respectively. The samples was centrifuged for 1 min at 5834 xg, the supernatant aspirated and the cell pellet resuspended in 57 µL 1x SDS buffer (50 mM Tris-HCl (pH 7.5) (VWR), 2 % (w/v) SDS (Sigma), 10 % (v/v) Glycerol (VWR), 0.015 % (w/v) Bromophenol Blue (Sigma)), and 3 µL DTT (Thermo Fisher Scientific). For the supernatant, 28 µL of the liquid were collected after centrifugation of the cell suspension and prepared with 10 µL 4x SDS (200 mM Tris-HCl (pH 7.5), 8 % (w/v) SDS, 40 % (v/v) Glycerol, 0.06 % (w/v) Bromophenol Blue and 2 µL DTT. Afterwards, all the samples were incubated for 5 min at 95°C (Hettich - MHR 23) and centrifuged for 1 min at 16100 xg. The SurePAGE™, Bis-Tris, 10x8, 4-20 % (GenSkript) gel was placed in Mini-PROTEAN Tetra vertical electrophoresis cell (Bio-Rad) and filled with Tris-MOPS-SDS Running Buffer (GenSkript). For each sample 20 µL was loaded in the wells together with 7 µL of Pierce Protein Marker (Thermo Fisher Scientific 26610). The electrophoresis was carried out for 1 h at 120 V and 400 mA. For Coomassie staining, the gel was first washed in distilled water, covered with a staining solution (45 % (v/v) Ethanol (VWR), 10 % (v/v) acetic acid (VWR), 0.025 % (w/v) Coomassie Brilliant Blue-250 (Sigma)) and heated in the microwave at 800 W for 30 sec. After incubation for 30 min at 200 Mot 1/min on an IKA LABORTECHNIK KS250 basic, the solution was replaced with destaining solution (8 % Ethanol, 5 % Acetic acid) and shaken for at least 3 h or oN. Documentation of the gel was carried out using the ChemiDoc MP imaging system (Bio-Rad) and Image Lab Software (4.0.1., Bio-Rad).

3.4.2 Western Blot (semi dry)

All blots were performed using the semi dry method. Beforehand, the proteins were seperated by SDS PAGE (3.4.1) using 7 µL Precision Plus Protein™ Dual Color Standards and transferred to a TransBlot® Turbo™ Mini-Size Nitrocellulose (Bio-Rad). For each gel, two Trans-Blot Turbo Mini-size Transfer Stacks (Bio-Rad) and one TransBlot® Turbo™ Mini-Size Nitrocellulose were equilibrated in 1x Trans-Blot Turbo Transfer Buffer (Bio-Rad). First, one Trans-Blot Turbo Mini-size Transfer Stacks was placed into the cassette of the Trans-Blot® Turbo™ (Bio-Rad) and the TransBlot® Turbo™ Mini-Size Nitrocellulose was placed on top. The polyacrylamid gel was washed in 1x Trans-Blot Turbo Transfer Buffer, transferred directly onto the membrane, and covered by the second Trans-Blot Turbo Mini-size Transfer Stacks. Surplus buffer was removed by a blot roller before closing the cassette. Blotting was performed with the preinstalled program "MIXED MW" (1.3 A, 25 V, 7 min). Subsequently, the membrane was transferred to a 50 mL Falcon tube and incubated with 5 mL Blocking buffer (1x PBS (Thermo Fisher Scientific), 2 % (w/v) Dried Skimmed Milk Powder (Marvel)) for 2 h at RT on a roller mixer (SRT6, Stuart). The membrane was washed 2x with 5 mL 1x PBS for 5 min and afterwards incubated with 5 mL Antibody (AB) buffer (1x PBS, 2 % (w/v) Dried Skimmed Milk Powder, 1:2500 Anti-

polyHistidinePeroxidase antibody, Mouse monoclonal (A7058, Merck)) for 1 h at RT. After three additional washing steps with 5 mL 1x PBS for each 5 min, the membrane is placed into a weighing tray and covered with 2 mL Amersham ECL Prime Western Blotting Detection Reagent (1:1 ratio of solution A (luminol) and B (peroxide), Cytiva). The detection of the chemiluminescence was carried out immediately with the ChemiDoc MP imaging system (Bio-Rad) and Image Lab Software (4.0.1., Bio-Rad). The exposure time for the detection was set manually to 10 sec.

3.4.3 Determination of Protein Concentration

Spectrophotometric Determination

The concentration of the purified protein was determined by UV spectroscopy using the NanoDrop-1000 (PeqLab, Software: NanoDrop 1000 3.7.1). The protein concentration was calculated based on the absorption at 280 nm, the molecular extinction coefficient (ε) and MW. $\varepsilon$and MW were determined using ProtParam [61].

Bradford Assay

For the Bradford Assay, two different standard curves had to be generated. For low protein concentrations, dilutions of 5-25 µg/mL of Bovine Serum Albumin (BSA) (Thermo Fisher Scientific) in 50 mM phosphate buffer (0.04674 M K_2HP_4, 0.003262 M KH_2PO_4, pH 8) were prepared. 100 µL of each dilution was filled into a well of a 96-Well Microplate (Thermo Fisher Scientific) and directly after adding 100 µL of 1x Quick Start™ Bradford Dye Reagent (Bio-Rad) to each well, the samples were incubate for 5 min. The shift in colour was measured by BioTek Cytation 5 Cell Imaging Multimode Reader at 595 nm. All reactions were performed in triplicate and the average absorption at 595 nm was plotted against the protein concentration to obtain a standard curve. For high protein concentrations, dilutions of 200-1600 µg/mL of BSA were prepared in 50 mM phosphate buffer and 4 µL were filled into a well. The reaction was started by adding 196 µL of 1x Quick Start™ Bradford Dye Reagent resulting in a total volume of 200 µL. The following steps were performed the same way as for the low concentration standard. For every measurement, 50 mM phosphate buffer was used as "blank" to zero the microplate reader. To determine the protein amount in a given sample, the volumes for the sample and the Bradford Dye Reagent corresponded either to the low or the high concentration standard, depending on whether the protein amount was within the linear range of the respective standard curve. The measured absorbance and the standard curve were used to determine the protein concentration within the sample [62].

3.5 Protein Biochemical Methods

3.5.1 Secretory Overexpression of PET Hydrolyses in *E. coli* BL21 (DE3)

E.coli BL21 (DE3) were co-transformed with pET21b+-LCC_{ICCG}-His6-HlyA or pET21b+-FastPETase-His6-HlyA, respectively, and pSTV28-HlyBD. To ensure successful transformation of both plasmids, pSTV28-HlyBD was transformed first and the cells containing the plasmid were made electrocompetent as described in section 3.3.5. Afterwards, the second plasmid, either pET21b+-LCC_{ICCG}-His6-HlyA or pET21b+-FastPETase-His6-HlyA, was transformed. To demonstrate the difference in intra- and extracellular expression, pET21b+-LCC_{ICCG}-His6-HlyA and pET21b+-FastPETase-His6-HlyA were also transformed individually. Furthermore, pET26b-LCC_{ICCG}-His6-PelB containing a PelB SP using the SecB-dependent type II pathway for extracellular expression and pET21b+-LCC_{ICCG}-His6 containing no SP were transformed as well. All transformations are shown in Figure 3.3.

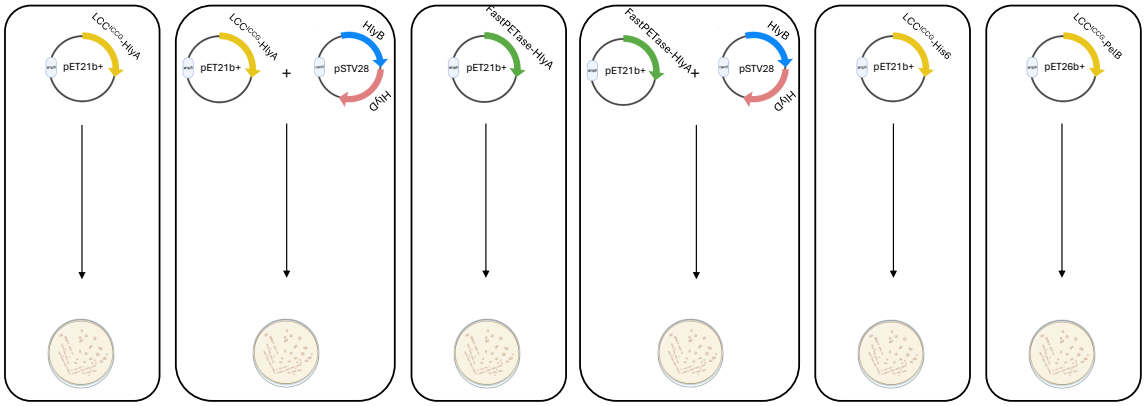

Figure 3.3. Overview of the plasmids transformed into *E. coli* BL21 (DE3).

Transformants were selected from the LB plates to inoculate a pre-culture of 5 mL LB medium containing the required antibiotics and grown oN at 37°C at 190 rpm. 2 mL of the pre-culture were used to inoculate 100 mL of fresh LB medium. The cells were grown at 37°C until an OD_{600} of 0.5-1.0 was reached and expression was induced with 1 mM Isopropyl-β-D-thiogalactopyranosid (IPTG). After induction, cells expressing a variant of LCC_{ICCG} were grown at 170 rpm at 30°C and cells expressing a variant of FastPETase were grown at 25°C. After 24 h, the expression cultures were harvested for 20 min at 4°C at 10000 xg (12310 Fixed-angle rotor, Sigma).

3.5.2 Secretory Expression of PET Hydrolyses in *B. subtilis* RIK 1285

After transformation of the plasmid library as described in 3.3.8 in *B. subtilis* RIK 1285, the resulting transformants were selected to inoculated a 200 µL of LB (10 µg/mL kanamycin) in 96-Well Microplate for an initial screening. The cell cultures were incubated for 24 h at 37°C at 190 rpm and afterwards centrifuged for 20 min at 4°C at 1120 xg (09100 Microplate Centrifuge Rotor, Sigma). The supernatant was collected for activity measurements (See 3.6.1) and based

on the results, 16 different clones were selected for inoculation of a culture volume of 1 mL in a 15 mL Eppendof tube. The cell cultures were inoculated under the same conditions as mentioned above and the supernatant harvested for 20 min at 4°C at 5242 xg (11133 Swing-out rotor, 13104 Buckets, Sigma). After evaluation of the protein content in the supernatant (See 3.4.3) and the activity, finally 5 candidates were selected. Together with the constructs pBE-S-LCC_{ICCG}-His6-NS, pBE-S-LCC_{ICCG}-His6-Epr, pBE-S-LCC_{ICCG}-His6-YjfA, previously transformed into *B. subtilis* RIK 1285, these 8 clones were used to inoculate an expression culture of 100 mL LB medium (10 µg/mL kanamycin). After 48 h, the cells were harvested for 20 min at 4°C at 10000 xg (12310 Fixed-angle rotor, Sigma). The secretion level of the target protein was evaluated via Bradford Assay, SDS-PAGE and Esterase activity assay.

3.5.3 Purification

After verifying the secretion of the enyzme of interest by SDS-Page (3.4.1) and Esterase activity assay (3.6.1), the culture supernatant was prepared for purification via immobilized metal ion affinity chromatography (IMAC). The pH and conductivity were adjusted to 8 and 30 µS/cm, respectively, and imidazol (Sigma-Aldrich) was added to a final concentration of 5 mM. The purification was performed with the liquid chromatography system ÄKTA™and the UNICORN™ software (6.4). The utilized HisTrap™ 5 mL column was first equilibrated with Loading buffer (50 mM phosphate buffer, 300 mM NaCl, 5 mM imidazol, pH 8) and then loaded with the adjusted supernatant at a flow rate of 2 mL/min. The column was washed with Loading buffer and eluted with 70 % of Elution buffer (50 mM phosphate buffer, 300 mM NaCl, 200 mM, pH 8). The peak fractions were pooled and dialyzed against 1 L of Dialysis buffer (50 mM phosphate buffer) for 2 h and afterwards against 2 L of Dialysis buffer oN with a Standard RC Tubing Dialysis Membrane (MWCO: 6-8 kD, Spectra/Por®). If not used immediately, the purified enzyme was snap frozen with liquid nitrogen and stored at -80°C.

3.6 Protein Activity Studies

3.6.1 Esterase activtiy assay

The Esterase Activity Assay is based on the enzymatic hydrolysis of p-nitrophenylbutyrate (pNPB) to p-nitrophenol, which can be detected at a wavelength of 405 nm (See Figure 3.4. The reaction was carried out in a total volume of 220 µL. Previously, the BioTek Cytation 5 Cell Imaging Multimode Reader was set to 50°C and solutions A (50 mM pNPB (Thermo Fisher Scientific) in 1 mL butanol (VWR)) and Solution B (40 µL Solution A and 1 mL of 50 mM phosphate buffer (pH 8)) were freshly prepared. For determination of the volumetric activity, 1-5 µL of the supernatant or purified enzyme were used and filled up to 20 µL with 50 mM phosphate buffer. For measuring the specific activity, 30 ng of protein (supernatant or purified enzyme) was added to a total volume of 20 µL with 50 mM phosphate buffer. The 20 µL enzyme solution was transferred to a wel of a 96-Well Microplate and the reaction was started by adding 200 µL of Solution B with a multi pipette. 20 µL of 50 mM phosphate buffer with 200 µL of Solution B was used as "blank". After 5 min of incubation, the absorption was measured at 405 nm. Each measurement was performed in triplicate.

Prior to the activity measurement, a standard curve with different concentrations of p-nitrophenol ranging from 0.01-0.25 mM was prepared and the values plotted in a graph. The dilutions were prepared with 50 mM phosphate buffer in a total volume of 20 µL and transferred to a 96-Well Microplate. 200 µL of Solution B (without Solution A) was added and the absorption at 405 nm was measured with the microplate reader. All measurements were performed in triplicate and the average absorption was plotted against concentration to obtain a standard curve which was used to determine the amount of p-nitrophenol generated in a given sample and thus conclude on the activity.

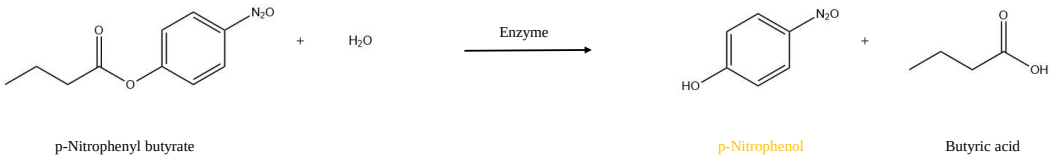

Figure 3.4. Enzymatic hydrolysis of pNPB. The cleavage product p-nitrophenol can be detected spectrophotometrically at 405 nm as a yellow color. Inspired by [47].

3.6.2 PET depolymerization

Initially, the PET film (GoodFellow, amorphous, 0.25 mm) had to be prepared for the depolymerization experiment. The film was cut in 0.5x1.0 cm pieces and washed in a 600 mL beaker containing 5 g/L Triton X100 (VWR) for 30 min at RT at 80 rpm. Afterwards, the PET film was rinsed 2x with 50 mL ddH_2O to remove the detergent. For the second washing step, 200 mL of 0.1 M Na_2CO_3 was added in incubated for 30 min at RT at 80 rpm. After rinsing the film with 2x 50 mL ddH_2O, the third washing step was performed with 200 mL of ddH_2O under the same conditions as mentioned above. The PET film was transferred to a 50 mL Falcon tube, the lid punctured, and the tube frozen at -80°C before lyophilization for 24 h at 0.05 mbar.

For the PET depolymerization experiment, the weight of the prepared PET films and a 2 mL Eppendorf tube was measured, whereas the weight of the PET film added was generally in the range of 14-18 mg. If the supernatant was used directly, 2 mg of protein per gram of PET was added in a total volume of 1 mL and the pH value of the medium was adjusted to 8. The supernatant of the host strain without expression plasmid was run as "blank". In case the purified enzyme was used, three different concentrations were tested, namely 0.2, 1 and 2 mg of protein per gram of PET. The reaction was carried out in a total volume of 1 mL in 50 mM phosphate buffer (pH 8). For the "blank", 1 mL of buffer was run only.

For variants of LCC_{ICCG} the reaction was performed at 72°C at 700 rpm (Hettich), for variants of the FastPETase the reaction was carried out at 50°C. All reactions were performed in duplicate and run for a period of 24 h and 48 h. After the given incubations time, the PET film was removed, washed with ddH_2O and lyophilized for 24 h at 0.05 mbar. Afterwards, the % weight loss of PET was determined.

The residual solution of the reaction was filtered (0.45µm, phenomenex) and prepared for high performance liquid chromatography (HPLC). 10 µL was diluted in 490 µL ultra pure HPLC water (Sigma-Aldrich), 500 µL of ice cold methanol (VWR) was added and the solution transferred to

HPLC vials (VWR).

For the HPLC analysis, the instrument used was Agilent Technologies, 1260 Infinity (Palo Alto, CA, USA) equipped with a reversed phase column C18 (Poroshell 120 EC-C18 2.7 µm 3.0 x 150 mm). Analysis were carried out at 40°C with a gradient of methanol and 0.1 % formic acid (VWR) further described in Table 3.6. A flow rate of 1 mL/min was applied and for each sample a total volume of 2 µL was injected. Detection of the components was performed at 241 nm with a photodiode array detector (Agilent Technologies, 1290 Infinity II, Vienna, Austria). Prior to the analysis, the column was equilibrated for 5 min. Standard curves were prepared for TPA using di-sodium-TPA (TCI) in concentrations ranging from 0.005 to 1 mM and for MHET (Advanced ChemBlocks) ranging from 0.001 to 0.5 mM in the same way as described previously.

Table 3.6. HPLC method applied for detection of TPA and MHET

Time [min]	Methanol [%]	0.1 % Formic Acid [%]
0	30	70
2	50	50
9	100	0
18	100	0
19	30	70
20	30	70

Results & Discussion 4

4.1 HlyA Secretory System for Extracellular Overexpression in *E. coli* BL21 (DE3)

In this section, the secretion efficiency of the HlyA secretion pathway to secrete the PET hydrolases LCC_{ICCG} and FastPETase in *E. coli* BL21 (DE3) was investigated. For this purpose, LCC_{ICCG} and FastPETase were fused to the C-terminal SP of HlyA and co-expressed with a plasmid containing the two membrane components HlyB and HlyD of the translocation complex, as described by Su et al. (2012). The results were compared with the already established SecB-dependant (type II) secretory system for LCC_{ICCG} using the PelB SP and the expression of LCC_{ICCG} with no SP.

4.1.1 Construction of the Plasmids pSTV28-HlyBD and pET21b+-LCC_{ICCG}-His6

The two plasmids pET21b+-LCC_{ICCG}-His6-HlyA and pET21b+-FastPETase-His6-HlyA were ordered from Gene Universal containing the gene for LCC_{ICCG} or FastPETase, a His6-tag and the C-terminal residues (AA 965-1024) of HlyA (See Appendix 6.1). The plasmid pET26b-LCC_{ICCG}-His6-PelB for expression of LCC_{ICCG} via SecB-dependant secretion pathway using a N-terminal PelB SP was provided.

For the construction of the vector containing the two membrane components HlyB and HlyD of the secretory machinery of the HlyA system, the bicistronic gene sequence was derived from the genome of *E. coli* CFT073 (GenBank: AE014075.1) and synthesized and cloned into pET21b+ by Gene Universal (See Appendix 6.2 A). Subsequently, the gene sequence had to be cloned into pSTV28 (CamR) to ensure stable propagation alongside LCC_{ICCG}-His6-HlyA or FastPETase-His6-HlyA in pET21b+ (AmpR). Using the primers HlyBD-F and HlyBD-R (3.3), the sequence was PCR amplified, the PCR product purified and digested with *Sac*I and *BamH*I-HF as well as the expression vector pSTV28. After ligation of the fragment and the vector and transformation into *E. coli* BL21 (DE3), the cells were plated on LB plates containing 34 µg/mL chloramphenicol and the resulting colonies analyzed via Colony PCR (See Appendix 6.2 B). As all clones appeared to contain the sequence of HlyBD, Clone 1 was chosen for DNA sequencing using the primers M13rev29 and M13uni-21 (3.3). The plasmid was isolated following the protocol for low-copy plasmids (3.3.7).

The plasmid pET21b+-LCC_{ICCG}-His6 possessing no SP was constructed using the primers LCC-His6-BamHI and LCC-His6-XhoI (3.3) to amplify the sequence of LCC_{ICCG}-His6 from the

plasmid pET21b+-LCC_{ICCG}-His6-HlyA. Afterwards, both, the PCR product and pET21b+-LCC_{ICCG}-His6-HlyA, were digested with *BamH*I-HF and *Xho*I, ligated, transformed into *E. coli* BL21 (DE3) and plated on LB selection plates (50 µg/mL ampicillin). As there was a high chance of LCC_{ICCG}-His6-HlyA re-ligating into the vector backbone, Colony PCR was conducted using the primers T7 and T7-term (3.3) to identify the plasmid containing LCC_{ICCG}-His6 (See Appendix 6.3). Clone 1 was chosen for DNA sequencing with the primers T7 and T7-term. The plasmid was isolated following the protocol for high-copy plasmids (3.3.7).

4.1.2 Expression of Recombinant LCC_{ICCG} and FastPETase

In order to establish an extracellular expression system using the α-hemolysin secretion pathway, the expression host *E. coli* BL21 (DE3) had to be co-transformed with two plasmids: pSTV28-HlyBD and pET21b+-LCC_{ICCG}-His6-HlyA/ pET21b+-FastPETase-His6-HlyA (See 3.3). To be able to compare intra- and extracellular expression, control groups were included containing only pET21b+-LCC_{ICCG}-His6-HlyA or pET21b+-FastPETase-His6-HlyA, respectively. For comparison with the currently applied secretion system for LCC_{ICCG} involving the SecB-dependant pathway via an N-terminal PelB SP that is spliced upon secretion, pET26b-LCC_{ICCG}-His6-PelB was transformed, as well as a plasmid expressing LCC_{ICCG}-His6 with no SP, pET21b+-LCC_{ICCG}-His6. The successful transformation and presence of the correct plasmid was confirmed by Colony PCR on the resulting colonies (Data not shown).

The 100 mL expression culture were induced each with 1 mM IPTG at an OD_{600} between 0.5-0.6. Note that only plasmids with the pET backbone contain a T7-inducible promoter, while pSTV28 harbors a constitutive promoter. After incubation for 24 h at the respective temperature (3.5.1), the cell growth was evaluated before harvesting of the supernatant (See Figure 4.1 A). When compared to a culture of *E. coli* BL21 (DE3) without any plasmid, cultures expressing a variant of LCC_{ICCG} showed significantly higher OD_{600}. However, cultures containing the plasmid for FastPETase expression displayed cell growth similar to *E. coli* BL21 (DE3). The introduction and expression of foreign DNA often leads to changes in the metabolism of the cells, but these usually constitute a "burden" slowing down cell growth [63]. Thus, the fact that the expression of LCC_{ICCG} appeared to increase the cell count should be investigated further.

Similar observations were made when assessing the protein content in the supernatant (See 4.1 B). Cells containing the plasmid pET21b+-LCC_{ICCG}-His6-HlyA (LCC-HlyA), pET21b+-LCC_{ICCG}-His6-HlyA and pSTV28-HlyBD (LCC-HlyA/HlyBD) or pET21b+-LCC_{ICCG}-His6 (LCC-His6) displayed protein concentrations exceeding fourfold those of *E. coli* BL21 (DE3), and cells harboring pET26b-LCC_{ICCG}-His6-PelB (LCC-PelB) demonstrated a protein content surpassing fivefold. Conversely, the level of secreted protein in cells possessing pET21b+-FastPETase-His6-HlyA (Fast-HlyA) or pET21b+-FastPETase-His6-HlyA and pSTV28-HlyBD (Fast-HlyA/HlyBD) was only about twice as high.

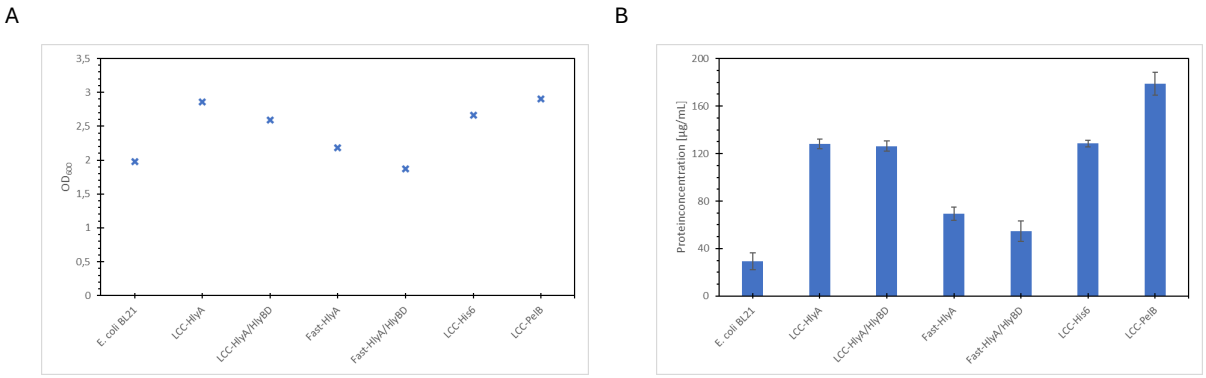

Figure 4.1. (A) Measurement of cell growth and (B) protein concentration in the supernatant. **(A)** Cell growth of the expression cultures was assessed after 24 h.**(B)** Protein concentration was determined using the Bradford Assay (3.4.3). For calculations, the slope of the standard curve derived from high protein concentrations (See Appendix 6.4) and the mean absorbance values at 595 nm from three measurements were employed.

In addition, the protein content in the cell pellets (Pellet) and in the supernatant (SN) was analyzed before (BI) and after induction (AI) of the expression via SDS-PAGE (See Figure 4.2 A and B). The expected MW of the expressed enzymes was previously calculated with Expasy [64] and listed in Figure 4.2 C. To aid the identification of the enzymes, Western Blot analysis was performed alongside due to difficulties in discerning specific bands, especially in the cell pellet.

Examination of cell pellets post-induction revealed a notable accumulation of LCC_{ICCG} in the cells, presumably in the periplasmic space, when expressed with the PelB SP. In contrast, LCC_{ICCG}-His6-HlyA, regardless of the co-expression of HlyBD, and LCC_{ICCG}-His6 showed minimal cellular presence. Interestingly, for LCC_{ICCG}-His6-HlyA, the presence of two distinct bands was detected suggesting potential cleavage of the C-terminal SP although HlyA is expected to remain attached after secretion.

Analysis of the supernatant after induction showed predominant secretion of LCC_{ICCG} in all cases. Unexpectedly, SDS-PAGE indicated that highest secretion occurred when no SP was involved. Western Blot analysis revealed the persistent presence of two distinct bands for LCC_{ICCG}-His6-HlyA. Presumably, the co-expression of HlyBD did not appear to influence the secretion level, as the observed intensity remained unchanged regardless of the presence of pSTV28-HlyBD. Unfortunately, verification if HlyBD was expressed at all was not possible due to unavailability of suitable antibodies. Consequently, for further investigations, it should be considered to provide the terminally expressed HlyD with a His6-tag or a green fluorescent protein (GFP), facilitating detection via commercially available antibodies or fluorescence assays. Recently, Pourhassan et al. (2018) further stated that the secretion carrier not only includes the 60 AA-long C-terminus but also the preceding triple glycine-rich motif (GGxGxDxUx).

Moreover, after induction of LCC_{ICCG} expression with PelB, the supernatant also revealed two bands. The lower, thicker band corresponded to the MW of LCC_{ICCG}-His6 (28.97 kDa), while the higher, thinner band likely represented LCC_{ICCG} with uncleaved PelB (31.99 kDa).

Regarding FastPETase-His6-HlyA, both SDS-PAGE and Western Blot analysis indicated a lack of expression as the enzyme was not detectable in either the cell pellet nor the supernatant. The higher protein concentration that was initially measured in the supernatant for both

compared to *E.coli* BL21 (DE3) might either result from the slightly increased OD_{600}, or potentially the presence of the plasmid(s) and the IPTG-induced overexpression stimulated also the enhanced production of other proteins. For further investigations, a reduction of the expression temperature to e.g. 20°C, as employed by Wu et al. (2023), should be considered. Additionally, the implementation of an *E. coli* strain suited for the expression of toxic proteins, such as *E. coli* BL21-Gold (DE3), may be advantageous [47]. Since the WT *Is*PETase from *Ideonella sakaiensis* naturally occurs as an extracellular protein, its intracellular production might have cytotoxic effects on the host cells.

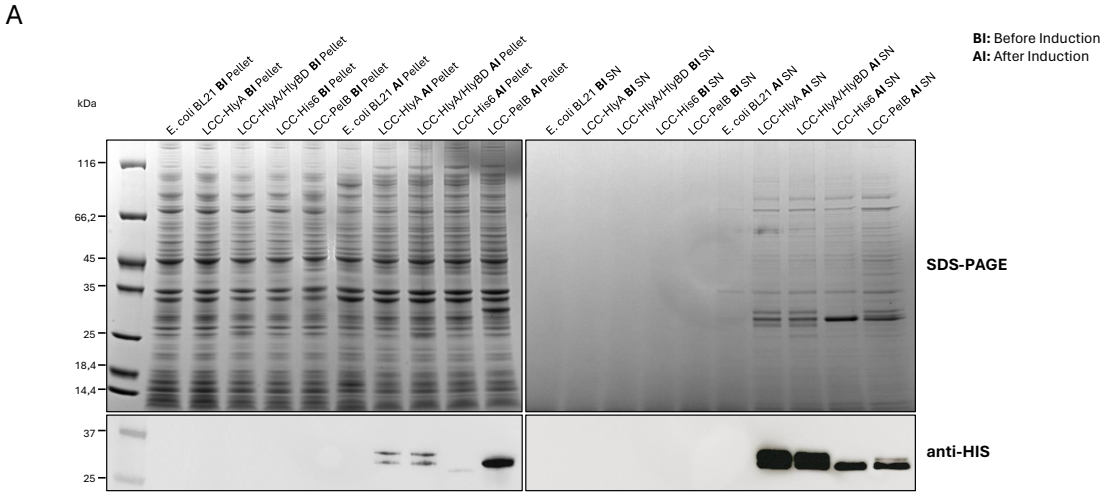

	Predicted MW [kDa]
LCC_{ICCG}-His6	28.97
LCC_{ICCG}-His6-HlyA	35.24
LCC_{ICCG}-His6-PelB	31.99
FastPETase-His6-HlyA	34.99

Figure 4.2. Expression of Recombinant LCC_{ICCG} and FastPETase (A) SDS-PAGE of the expression of LCC_{ICCG}-His6-HlyA, LCC_{ICCG}-His6 and LCC_{ICCG}-PelB analysing the cell pellet (Pellet) and supernatant (SN) before (BI) and after induction (AI) .**(B)** SDS-PAGE of the expression of FastPETase-His6-HlyA analysing Pellet and SN, BI and AI.**(C)** Predicted MW of the expressed enyzmes calculated with Expasy.

4.1.3 Esterase Activity Assay on Culture Supernatant

To evaluate the activity of the expressed and secreted enzymes, an Esterase Activity Assay was conducted on the supernatant (See Figure 4.3 A and B). The assay was conducted at 50 °C based on prior findings indicating that LCC exhibits its peak hydrolytic activity towards fatty acid monomeric substrates, such as pNPB, at this temperature [33]. Assessing both volumetric activity (total activity per unit of volume) and specific (activity per unit of protein) in the supernatant provides complementary insight. While a higher volumetric activity suggest a generally higher amount of secreted proteins per unit of volume of culture, a higher specific activity indicates a higher amount of active enzyme per unit of total proteins secreted. The standard curve of p-nitrophenol and respective calculations of volumetric and specific activity can be found in the Appendix 6.5.

The results of the assay support the observations from SDS-PAGE analysis, exhibiting that LCC_{ICCG} expressed without any SP (LCC-His6) likely possess the highest quantity of secreted enzyme, showing the highest volumetric as well as specific activity. Very similar levels of enzymatic activity can be observed for the variants of LCC_{ICCG} expressed with HlyA or PelB. However, regarding the extracellular activity of LCC_{ICCG} expressed with HlyA, the amount of secreted enzyme does not seem to depend on the prensence of the additional plasmid harbouring the membrane components HlyB and HlyD, as it has been observed in the SDS-PAGE and Western Blot analysis. These findings indicate that the secretion of LCC_{ICCG} is probably not attributed to the secretion system employed. Su et al. (2013) was addressing a similar phenomenon observed during the expression of *Thermobifida fusca* cutinase in *E. coli* BL21 (DE3).They reported that cutinase showed phospholipase activity, indicating its hydrolity activity towards one of the key components of the cell membrane. Consequently, the study also detected heightened permeability of both the inner and outer membranes upon expression of cutinase. However, when an inactive form of cutinase was expressed, it was only localized intracellular [65]. Despite the increased permeability the expression of LCC_{ICCG} seems to cause, in this project there was no evidence that it affects the cell viability (See Figure 4.1 A).

Furthermore, as anticipated based on SDS page analysis, the supernatant of the cells intended to express FastPETase with HlyA exhibited no detectable activity, due to the general issues of expression.

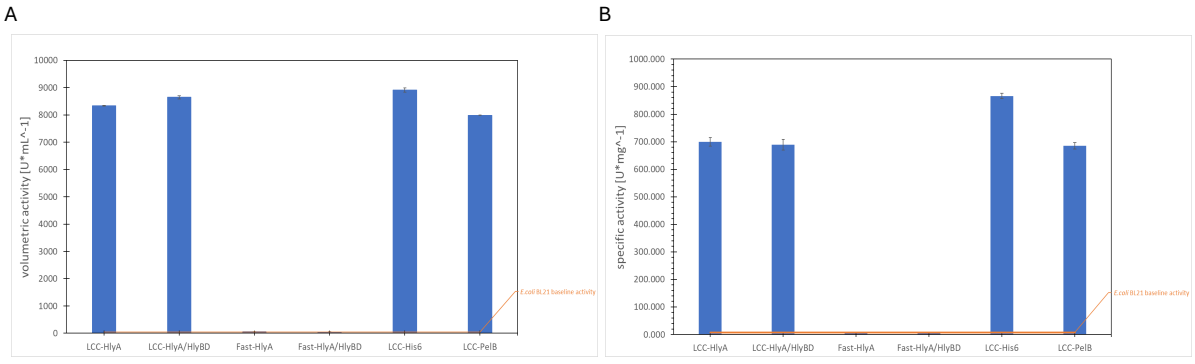

Figure 4.3. (A) Volumetric and (B) specific activity in the supernatant. Enzymatic activity in the supernatant was determined using the Esterase Activity Assay (3.6.1). Formulas for the calculation of the volumetric and specific activity can be found in the Appendix 6.5 B.

4.1.4 Catalytic Activity of Culture Supernatant towards Amorphous PET Films

The efficiency of PET depolymerization was initially evaluated directly in the supernatant. Tournier et al. (2020) determined the optimal PET depolymerization temperature for LCC_{ICCG} to be 72°C and reached highest level at enzyme loadings of 2 and 3 mg per gram of PET, respectively, whereas FastPETase displayed maximal activity at 50°C according to Arnal et al. (2023). In this assay, 2 mg of the total protein measured in the supernatant per gram of PET was utilized, incubated at the corresponding temperatures and weight loss, specific activity as well as the amount of the produced monomers TPA and MHET after 24 and 48 h were assessed (See Figure 4.4 and Appendix 6.7). The specific activity of the enzymes towards PET, measured in mg of equivalent TPA (TPA_{eq}) generated per h per mg of enzyme, was monitored via HPLC at 241 nm, whereby TPA_{eq} refers to the main degradation products TPA and MHET, EG excluded, as it lacks a detectable aromatic component.

However, the results for the PET degradation directly in the supernatant seem to be inconclusive, as it can be concluded from values and standard deviation presented in Figure 4.4 A and B. As anticipated, the supernatant of the cells intended to express FastPETase with HlyA displayed no activity at all, nonetheless, depolymerization in the supernatants containing the secreted variant of LCC_{ICCG} do not correlate with the results of the Esterase Activity Assay. The inconsistency in the data is likely due to the experimental setup, as the reaction was conducted directly in the supernatant i.e. LB medium. Although the pH was initially adjusted to pH 8, the lack of a buffering system in this setup does not ensure optimal conditions for enzyme activity over the course of time. Furthermore, this experiment is typically conducted on a larger scale in a bioreactor, allowing for constant control of all conditions [41, 66, 67]. Especially important during PET degradation is the pH control, as previously stated in 1.3.1. As the PET degradation proceeds, an increasing number of acidic monomers TPA and MHET is produced, constantly decreasing the pH, causing the catalytic activity to drop. Therefore, the experiment was intended to be repeated using the purified enzyme from the supernatant in a stabilizing buffer system. As neither protein analytic methods nor protein activity studies were able to detect expression of FastPETase, the further steps only focused on the variants of LCC_{ICCG}.

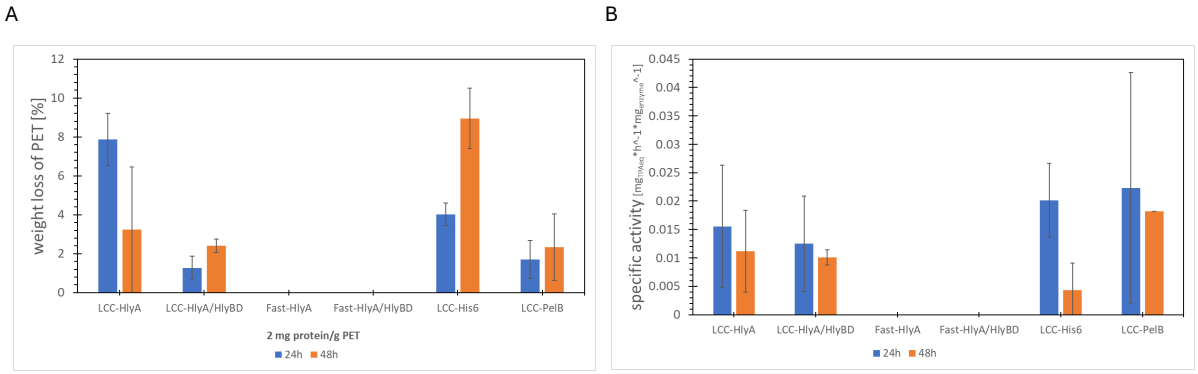

Figure 4.4. (A)Weight loss and (B) specific activity after PET degradtion with the culture supernatant after 24 and 48 h. Variants of LCC_{ICCG} were incubated at 72°C, variants of FastPETase were incubated at 50°C. Calculated values and standard deviation are based on two independent replicates. The specific activity was calculated as followed: specific activity=$(mg_{TPA}+mg_{MHET})*h^{-1}mg_{enzyme}{}^{-1}$.

4.1.5 Purification of LCC_{ICCG}-His6 Expressed with SP PelB/ no SP from Culture Supernatant

For further experiments, the enzymes were purified from the supernatant as indicated in 3.5.3. Unfortunately, the purification of LCC_{ICCG}-His6-HlyA via IMAC was not possible, presumably due to the positioning of the His6-tag between LCC_{ICCG} and the HlyA SP, making it inaccessible for binding to the HisTrap™ column. Consequently, only LCC_{ICCG}-His6 expressed with no SP (LCC-His) and with PelB (LCC-PelB) were obtained, their purification process outlined in Figure 4.5. Both eluates showed predominately the desired enzyme, LCC_{ICCG}-His6, at a MW of 28.97 kDa, and a yield of approx. 3.7 mg per 100 mL of expression culture could be obtained for both (NanoDrop: ε=38.39 $M^{-1}cm^{-1}$). Although the activity assay 4.1.3 initially indicated a higher enzyme concentration per unit volume in the supernatant of LCC-His, the supernatant of LCC-PelB expressed with PelB contained more total protein due to a higher cell count, explaining the similar yield. However, the elution fraction of LCC-PelB additionally showed a weak band that might indicate the co-purification of LCC_{ICCG}-His6-PelB (MW=31.99 kDa), which is possible, because the N-terminal SP does not interfere with the accessibility of the C-terminal His6-tag. Whether the attached PelB SP alters the folding or activity of the enzyme remains to be clarified.

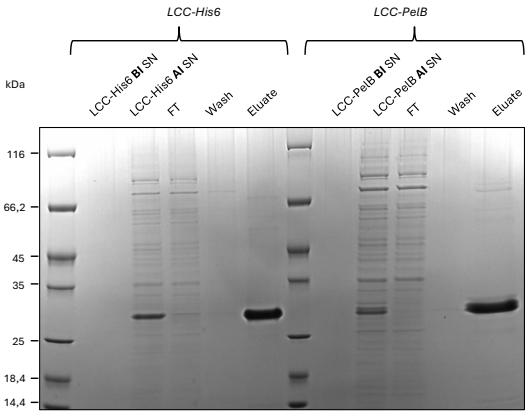

Figure 4.5. Purification of LCC_{ICCG}-His6 expressed with no SP (LCC-His) and with PelB (LCC-PelB) from the culture supernatant. Supernatant (SN), before induction (BI), after induction (AI), flow through (FT). The expected MW of LCC_{ICCG}-His6 is 28.97 kDa.

Overall, the absence of the SP appears to optimize the secretion efficiency of LCC_{ICCG}, not least because this prevents accumulation in the periplasm. Therefore, optimization during expression of LCC_{ICCG}-His6 with no SP, such as adjusting temperature, IPTG concentration, agitation, etc., to increase the cell count and total protein secreted could potentially lead to higher overall yields.

4.1.6 Catalytic Activity of Purified LCC_{ICCG} Expressed with SP PelB/ no SP towards Amorphous PET Films

To assess whether the activity of LCC_{ICCG} was affected by the different secretion pathways or the expression with PelB (LCC-PelB) or no SP (LCC-His), respectively, the PET degradation experiment was carried out with LCC_{ICCG}-His6 purified from the supernatant. Their performance was evaluated applying various enzyme loadings: 0.2, 1 and 2 mg of enzyme per gram of armorphous PET film. These values were selected based on the setups by Arnal et al. (2023) and Tournier et al. (2020) in order to determine the optimal enzyme-to-substrate ratio for maximum performance.

When comparing the weight loss of the added amorphous PET film for LCC-His and LCC-PelB at different enzyme concentrations, it is notable that both show similar levels of depolymerization (See Figure 4.6 A). This observation was expected, given that the enzyme possess the same sequence once the PelB SP has been cleaved off during translocation, verifying that both approaches result in the secretion of active LCC_{ICCG}-His6. LCC-His as well as LCC-PelB displayed a weight loss of just over 5 % at enzyme concentrations of 0.2 mg per gram of PET after 24 h. At 1 mg of enzymes, both variants showed a weight loss of over 40 %, while at 2 mg of enzyme, LCC-His displayed approx. 46 % of PET depolymerization and LCC-PelB approx. 42 %. These values indicated that a point of saturation has been reached at which an increase in enzyme concentration will no longer lead to enhanced PET conversion. As hydrolysis can only occurr at the interface of the aqueous solution and the PET film, the limiting factor is the accessibility of the PET surface [41, 68].

Remarkably, the weight loss observed after 48 h for LCC-His and LCC-PelB for almost all enzyme concentrations appeared to be lower. Apart from the fact that the enzyme activity naturally decreases over the course of time, which would be visible as a plateau, this does not fully explain the lower level of depolymerization. Additionally, decreased PET depolymerization rates after 24 h are also attributable to an effect that has previously been described as "enzyme activity vs PET recrystallization" (See 1.3.1) [41]. This experiment was conducted at 72°C, a temperature close to the T_G of PET (around 75°C), which was initially thought to be beneficial for enhanced chain mobility, however, it was reported that operating at these temperature not only causes recrystallization but also accelerates the physical ageing, converting amorphous PET slowly into more crystalline [42, 66]. Moreover, the T_G was shown to decrease even further when immersed in water [42]. Tournier et al. (2020) reported an increase in the level of crystallinity from around 15 to 40 % when incubating post-consumer waste PET for 15 h at 72°C. Nevertheless, PET recrystallization does not explain the reduced weight loss of the PET films after 48 h, thus this experiment should be repeated with a higher number of replicates to increase the accuracy and rule out the inclusion of random fluctuations.

When comparing the appearance of the PET film after 24 h at the different enzyme concentrations (See Appendix 6.8), it becomes evident that crystallization of some sort occurred, as at lower enzyme concentrations (0.2 mg per gram of PET) the film mostly remains transparent, while a change to an opaque color can be seen for higher enzyme concentrations, a characteristic optical property of higher crystalline PET [10]. With increasing depolymerization, the effect of recrystallization became more apparent, as the ratio of crystalline PET rises the more the preferred amorphous regions were degraded, resulting in the optical change. Therefore, lowering the operating temperature for future experiments to e.g. 68°C, as implemented by Arnal et al. (2023), could decrease the susceptibility for crystallization events, and increase overall PET conversion. Although enzyme activity for LCC_{ICCG} might be slightly reduced at this temperature.

Analysis of the released monomers via HPLC confirmed that LCC-His and LCC-PelB showed highest specific activity during the first 24 h, while after 48 h, the values decreased to about one third (See Figure 4.6 B). Additionally, the specific activity suggests the optimal enzyme loading to be 1 mg of enzyme per gram pf PET for both, and is therefore consistent with the observations of Arnal et al. (2023). Wu et al. (2023) achieved a specific activity of 6.97 $mg_{TPAeq}h^{-1}mg_{enzyme}^{-1}$ with a concentration of 2 mg LCC_{ICCG} per gram PET. At the same concentration, LCC-His and

LCC-PelB demonstrated slightly higher activities with 8.30 and 7.18 $mg_{TPAeq}h^{-1}mg_{enzyme}^{-1}$, respectively, likely due to their experiment being conducted at 65°C unlike at 72°C as in this project. The lower specific activity of LCC-PelB compared to LCC-His might be attributable to the presence of LCC_{ICCG}-His6-PelB in the eluate of LCC-PelB (See 4.1.5), for which it has not yet been clarified if the attached PelB influences the activity.

The observed patterns for the weight loss of PET was also apparent in the amount of TPA produced (See Figure 4.6 C). On the other hand, the amount of MHET generated after 24 h was in some instances up to twice as much as after 48 h (See Figure 4.6 D). This observation aligns with the anticipated degradation process, as the ongoing reaction converts MHET to the final monomers TPA and EG. However, as the amount of MHET decreased after 48 h, no corresponding increase in TPA was observed. A repetition of the experiment with a higher of replicates, as mentioned above, is therefore strongly recommended, with particular attention to the depolymerization after 24 h.

If summing, for example the amount of TPA and MHET generated after 24 h of incubation with 1 mg of LCC-His per gram of PET, this yields approx. 4.6 mg. However, with a weight loss of 40 % and an average of 15 mg of amorphous PET film added per reaction, a monomer production of around 6 mg would be expected. This discrepancy can be explained by two factors. On one hand, the final monomer EG was not detected by this HPLC measurement, assuming that TPA and EG would be present in equimolar concentrations, this could result in 0.62 mg of produced EG. Additionally, insoluble long-chain degradation products, as well as precipitated TPA and MHET were filtered out prior to HPLC analysis. A more comprehensive analysis of the degradation products and their quantities could be achieved via quantitative NMR.

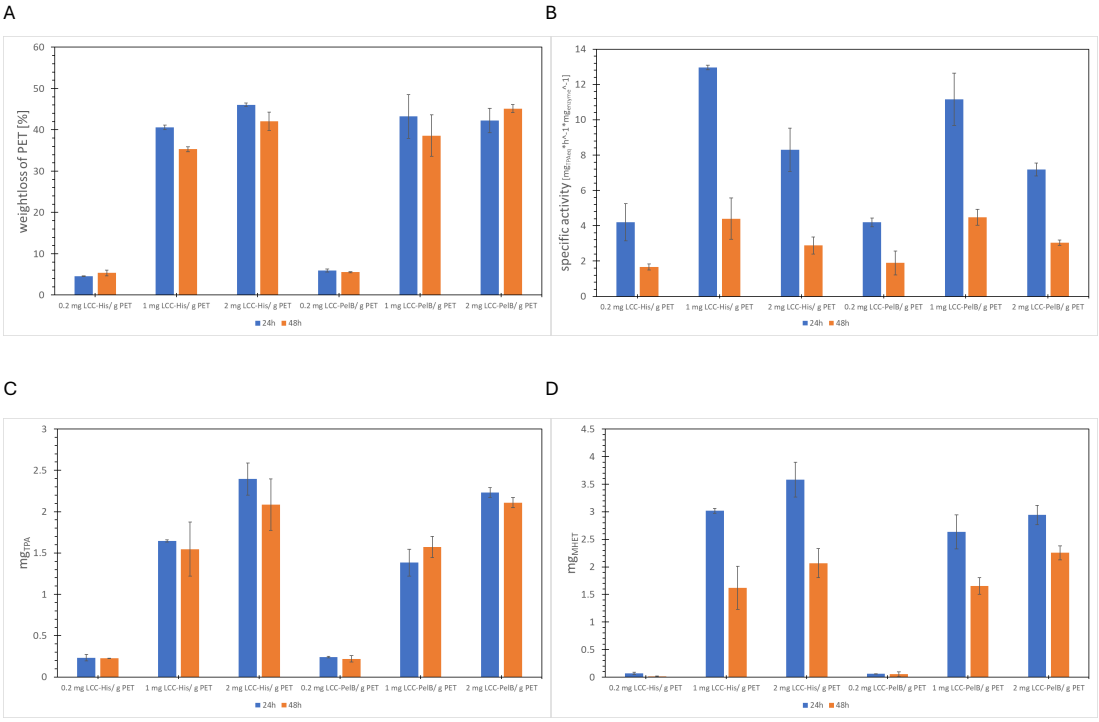

Figure 4.6. (A)Weight loss, (B) specific activity, (C) amount of TPA [mg] and (D) MHET [mg] produced after PET degradation with purified LCC_{ICCG} expressed with no SP (LCC-His) and with PelB (LCC-PelB) after 24 and 48 h. Reactions were performed at 72°C. Calculated values and standard deviation are based on two independent replicates. Calculations were performed as described in 4.1.4.

As mentioned above, it would be beneficial to conduct future experiments in a larger scale in a bioreactor under controlled conditions, especially with regard to pH control and the potential addition of NaOH to neutralize produced acids and enhance their solubility. For example, Arnal et al. (2023) achieved approx. 98 % conversion with 1 mg of LCC_{ICCG} per gram of PET, while Tournier et al. (2020) managed to degrade approx. 80 % of post-consumer PET waste with 1 mg of LCC_{ICCG} after 24 h at 72°C.

To further enhance PET conversion rates, additional strategies could be considered for subsequent investigations, such as the addition of a hydrophobic linker to increase enzyme-substrate interaction. For instance, Dai et al (2021) demonstrated that the fusion of a cellulose-binding domain to *Is*PETase increase depolymerization rates by 44.5 % at 40°C. Similar, Liu et al. (2017) investigated the use of various PET-binding domains e.g. carbohydrate-binding domains, hydrophobins, on cutinase derived from *Thermobifida fusca*, resulting in 22.7-fold increase in conversion at 70°C.

Finally, after processing of the data, it was discovered that the given sequence of LCC-PelB provided in pET26b-LCC_{ICCG}-His6-PelB differed from the cloned sequence of LCC-His from pEt21b+-LCC_{ICCG}-His6. A sequence alignment revealed that the enzyme expressed with pEt21b+-LCC_{ICCG}-His6 was not the expected variant LCC_{ICCG}, but the wild type missing the four mutations (F243I/D238C/S283C/Y127G) (See Appendix 6.9). Since LCC possesses a lower thermostability compared to ICCG, a factor that was highlighted by Tournier et al. (2020) to limit its implementation, this could explain why no further PET conversion occurred after 24 h. However, this does not explain why a similar phenomenon occurred for LCC-PelB. To verify, the transformed plasmid pET26b-LCC_{ICCG}-His6-PelB should be extracted for sequencing.

4.2 Secretory Expression of PET Hydrolases in *B. subtilis* RIK 1285

For the second approach, a screening system developed by Takara Bio Inc. was utilized to assess the secretion efficiency of the PET hydrolases in the host organism *B, subtilis* using the endogenous Sec-mechanism. As *B. subtilis* is known to secrete homologous proteins in concentrations up to 25 g/L, this expression host has the potential to outperform yields currently achieved by the secretion via *E. coli*. This screening system was introduced after Brockmeier et al. (2006) reported that the choice of SP significantly affects the secretion level of the recombinant protein, and therefore, identification of an optimal SP for every secretion target is needed. This system enables the identification of suitable SP for the secretory expression from a library consisting of 173 types of *B. subtilis*-derived Sec-type SPs. The provided shuttle vector pBE-S DNA allows the construction and propagation in *E. coli* due to its pUC-derived origin of replication (ColE1 ori) and an ampicillin-resistant gene (AmpR), and subsequently the expression in *B. subtilis* because of its pUB110-derived origin of replication (pUB ori) and a kanamycin-resistant gene (KanR) (See Figure 4.7 A). Initially, the target gene is inserted in the MCS, ensuring the inclusion of a C-terminal His-tag. Additionally, the plasmid contains the *B. subtilis*-derived subtilisin promoter (*aprE* promoter) and the respective *aprE* SP, which will be replaced by the SP library. After transformation in *B. subtilis* RIK 1285, the extracellular expression of the target protein and activity was evaluated and the most efficient SP identified.

4.2.1 PCR Amplification and Insertion of Target Genes into pBE-S DNA

The plasmids pET32a+-LCC_{ICCG}-His6-bac and pET28a+-FastPETase-His6-bac were ordered from Gene Universal containing the for *B. subtilis* codon optimized gene for LCC_{ICCG} or FastPETase (See Appendix 6.10). The genes were amplified via PCR using the primers LCC-FW-NdeI and LCC-RV-XbaI or FastPETase-FW-NdeI and FastPETase-RV-XbaI (3.3), respectively. Afterwards, the amplicons as well as the provided vector pBE-S DNA were digested with *Nde*I and *Xba*I, ligated, transformed into *E. coli* BL21 (DE3) and plated on LB selection plates (50 µg/mL ampicillin). One colony was selected each for plasmid preparation and subjected to PCR using the primers pBE-S-FW and pBE-S-RV to verify of the presence of the genes LCC_{ICCG}-bac and FastPETase-bac in pBE-S DNA (See Figure 4.7 B).

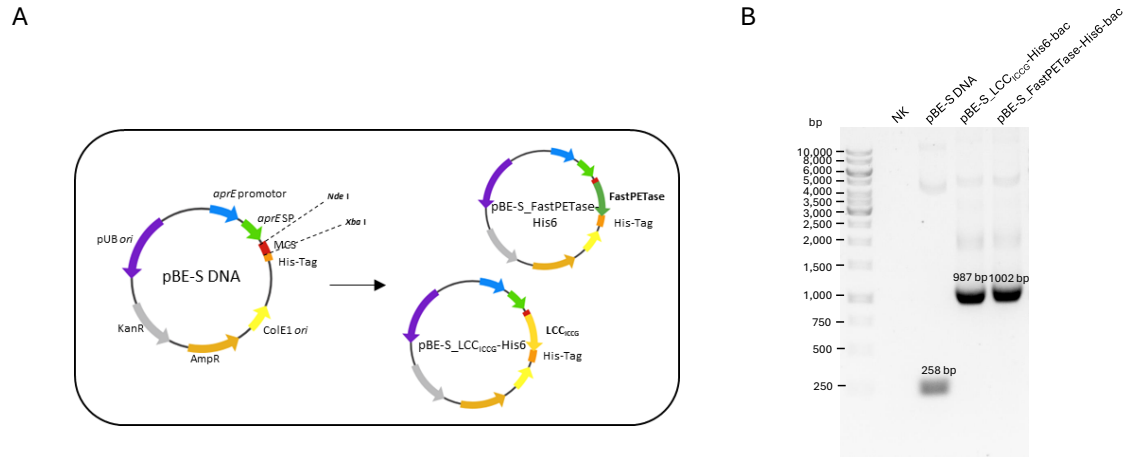

Figure 4.7. (A) Visualisation of the shuttle vector pBE-S DNA and the insertion of the target genes LCC_{ICCG}-bac and FastPETase-bac and (B) Verification of the insertion of the target genes via PCR amplification using the primers pBE-S-FW and pBE-S-RV. The expected length of the amplicons are indicated above the respective band.

4.2.2 Insertion of SP Mix via In-Fusion Cloning

To introduce the DNA library of 173 different Sp in place of the *apreE* SP, both pBE-S-LCC_{ICCG}-His6-bac and pBE-S-FastPETase-His6-bac were linearized using the RE *Mlu*I and *Eco*52 I. The different SP were inserted via In-Fusion Cloning and subsequently transformed into *E. coli* HST08 Stellar. In order to generate a sufficient plasmid library, it was recommended to obtain at least 2000 colonies, which was confirmed for both target genes. By plating each 500 µL of cell suspension, a colony number of approx. 3200 could be obtained for the plasmids carrying LCC_{ICCG}-bac and a count of approx. 2400 colonies for the plasmids carrying FastPETase-bac (See Figure 4.8).

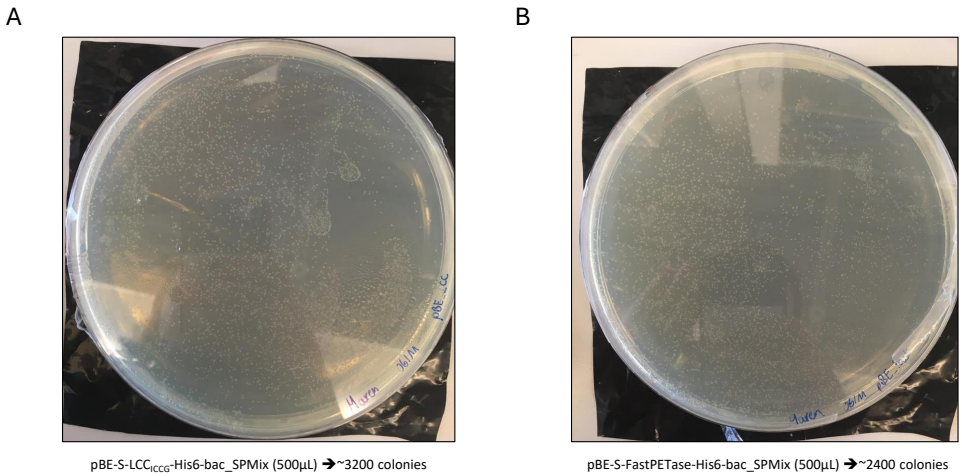

Figure 4.8. Cell count of colonies resulting after the insertion of SP Mix into (A) pBE-S-LCC$_{ICCG}$-His6-bac and (B) pBE-S-FastPETase-His6-bac.

4.2.3 Preparation of Plasmid Library and Transformation into *B. subtilis* RIK 1285

In the course of this project, only the colonies containing the plasmid pBE-S-LCC$_{ICCG}$-His6-bac with the different inserted SP were further processed from this point onwards, due to the workload of the plasmid library preparation and the evaluation of the resulting transformants. The selection of the LCC$_{ICCG}$-His6-bac expressing plasmid allowed the later comparison with the variants expressed in *E. coli* BL21 (DE3). Of the around 3200 colonies of *E. coli* HST08 Stellar, around 8 µg of plasmid DNA were isolated. A total of 3 µg of this plasmid library was used to transform in *B. subtilis* RIK 1285 and plated on LB selection plates (10 µg/mL kanamycin), which resulted in around 400 colonies (See Figure 4.9 A). The cell growth during the preparation of competent *B. subtilis* RIK 1285 was monitored and the time point of transformation can be derived from Figure 4.9 B.

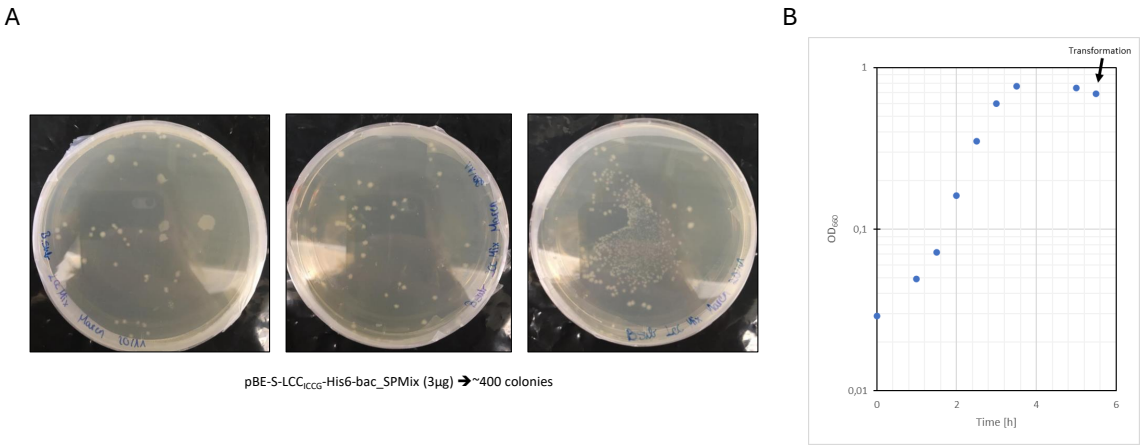

Figure 4.9. (A) Cell count of colonies of *B. subtilis* RIK 1285 after transformation of 3 µg of plasmid library DNA. (B) Cell growth of *B. subtilis* RIK 1285 observed during preparation of competent cells and time point of transformation. The optical density measured at 660 nm was plotted in a logarithmic scale.

4.2.4 Initial Screening of Expression and Activity

In total, 304 colonies were selected and inoculated in 96-Well Microplates in 200 µL LB medium (10 µg/mL kanamycin). After 24 h of incubation, the volumetric activity in the culture supernatant was measured to identify potential candidates (See Figure 4.10 A). The bars colored in green mark clones that showed at least double the activity in the supernatant compared to the baseline activity measured for *B. subtilis* RIK 1285. Based on this initial screening, a total of 16 clones were selected for inoculation in 1 mL expression volume, with 5 clones displaying low activity (B), 5 with medium activity (M) and 6 clones with high activity (S) chosen for comparison. The assessment of their volumetric activity is presented in Figure 4.10 B. Notably, measured activities were up to 10 times higher than compared to the volumetric activity during the first screening. This effect depends most likely on the differences in culture volume. By alternating the volume, cell growth can be influenced, for example, higher cell densities are often reached faster in smaller volumes, leading to nutritional deficiencies and faster cell death, resulting in less protein being produced overall [49].

Clones S15 and S76, which initially exhibited the highest activities, also showed highest extracellular activity in a larger volume. Conversely, S21, as potential strong candidate, displayed a very low activity, likely concluded as false positive in the first screening, while B89 and M23 showed similar activities to other potential candidates (blue), possibly attributed as false negative initially.

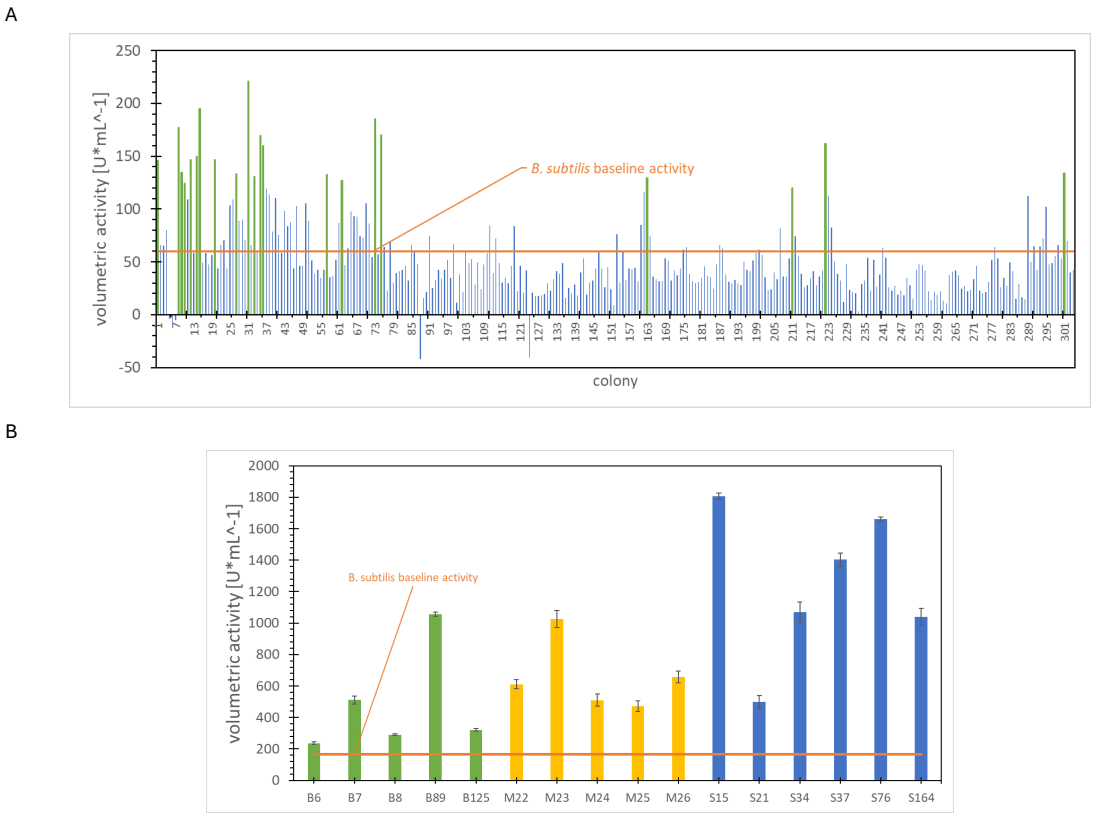

Figure 4.10. Initial screening of the volumetric activity in the culture supernatant assessed for (A) 304 colonies in a total expression volume of 200 µL and (B) selected 16 colonies in a total expression volume of 1 mL. Enzymatic activity in the supernatant was determined using the Esterase Activity Assay (3.6.1). Formulas for the calculation of the volumetric and specific activity can be found in the Appendix 6.5 B.

4.2.5 Identification of the SP

Plasmids were isolated from all 16 clones to identify the SP inserted via sequencing using the primers pBE-S-FW and pBE-LCC-SP-RV (3.3). The obtained sequences were compared with the SP sequences provided by Takara Bio Inc., and the results compiled in Table **??**. Many of the SP prevalent in the isolated plasmids appear to harbor point mutations, i.e. deletion, insertion or substitution of nucleotide bases (red box), which potentially occurred during the insertion of the SP Mix or might simply be sequencing errors. However, since theses clones were categorized as clones showing low extracellular activity, this was not further investigated.

Table 4.1. Identification of the SPs present in the 16 selected clones. The SPs were identified by sequencing the plasmids isolated from all 16 clones. Differences in the identified sequence to the list of SPs provided by Takara Bio Inc. are highlighted by a red box and specified in the right-hand row.

Clone	**Identified SP**	**Sequence** (5'-3')	**Note**
B6	*ydbK*	atgaaacttttaatcg g gaaggtcactttggtttctcttatcc tgatggctgtctttcaattcttcatggcattgatcattaaacgga ttgtcatcag	Point mutation (insertion)
B7	*yxaK*	atggtcaagtcatttcgtatgaaagctttgattgccggagctgcg a tggcggcggctgtttcggcaggcgctgtttctgatgtgcccgctgc caaagtgcttcagccgacagctgcttatgcgg	Point mutation (substitution)
B8	*ydbK*	atgaaacttttaatcggaaggtcactttggtttctcttatc ctgatggctgtctttcaattcttcatggcattgatcattaa acggattgtcatcagtg	-
B89	*ypuA*	atgaagaaaatttggattggaatgctggcagcggcag ttttgctgctgatggttccgaaggtcagtctcgcggatgccg	-
B125	*ywmD*	atgaaaaaattgctggctgccggtatcattggattgttgact gtttccattg a ctccccgtcttttgccg	Point mutation (substitution)
M22	not identified	-	-
M23	*fliL*	atgaaacttttaatcggaaggtcactttggtttctcttatcctga tggctgtctttcaattcttcatggcattgatcattaaacggat tgtcatcagtg	-
M24	*yqgA*	atgaagcaaggraaattttctgtgtttttaattttgctactaatgt taactttggtagttgcacctaaag aaaagcagaggctg	Point mutation (deletion)
M25	*yfkN*	atgagaatacagaaaagacgaacacacgtcgaaa cattctccg tattcttttgcccccaattatgatacttagcctaatcctcccaacac cacccattcatgcag	Point mutation (deletion)
M26	*yrrL*	atgtatatcaatcagcaaaaaaaatcgttttttaataaaaaaagaa tcatactgtcttccattgttgtgctgtttctcatcattggcggggca tttttag	-
S15	*yqgA*	atgaagcaaggaaaattttctgtgtttttaattttgctactaat gttaactttggtagttgcacctaaaggaaaagcagaggct	-
S21	*wprA*	atgaaacgcagaaaattcagctcggttgtggcggcagtgcttatttt tgcactgattttcagccttttttctccgggaaccaaagctgcagcg	-
S34	*abnA*	atgaaaaagaaaaaaacatggaaacgcttcttacacttttcgagtgca gctctggctgcaggtttgatattcacttct gctgc tcccgcagaggcag	12 extra bases

Clone	Identified SP	Sequence (5'-3')	Note
S37	*yqgA*	atgaagcaaggaaaattttctgtgtttttaattttgctactaat gttaactttggtagttgcacctaaaggaaaagcagaggct	-
S76	*yqgA*	atgaagcaaggaaaattttctgtgtttttaattttgctactaat gttaactttggtagttgcacctaaaggaaaagcagaggct	-
S164	*yveB*	atgatctatataatatcaggcagatggctaaccgtatttctaac gtttctagcaatactgctgtctatgaatttag	-

The study published by Brockmeier et al. (2006), on which the protocol for the screening of SP for extracellular protein expression in *B. subtilis* is based on, applied their systematic screening approach on cutinase derived from *Fusarium solani pisi*. During their investigations, the SP *Epr* was identified as the most efficient to export the heterologous cutinase, yielding in 4.67 U/mL in the culture supernatant. In contrast, the SPs identified for LCCICCG-bac, e.g. *abnA* and *yqgA*, resulted only in secretion levels of 1.82 U/mL and 1.64 U/mL for this cutinase. Therefore, it was decided to additionally investigate the use of the SP *Epr*, as well as, third best performing SP *YjfA* (3.84 U/mL) of *Fusarium* cutinase, for their efficiency to secrete LCCICCG-bac.

4.2.6 Comparing Expression, Secretion Efficiency and Activity of potential candidates

Construction of pBE-S-LCC$_{ICCG}$-His6-Epr, pBE-S-LCC$_{ICCG}$-His6-YjfA and pBE-S-LCC$_{ICCG}$-His6-NS

The plasmid pET28a+-LCC$_{ICCG}$-Epr and pET28a+-LCC$_{ICCG}$-YjfA were ordered from Gene Universal containing the for *B. subtilis* codon optimized gene for LCC$_{ICCG}$ and the SP *Epr* or *YjfA*, respectively (See Appendix 6.11). The two plasmids as well as the vector pBE-S DNA were digested with *Mlu*I and *Xba*I, the inserts and the vector were ligated, transformed into *E. coli* BL21 (DE3) and plated on LB selection plates (50 µg/mL ampicillin). Two colonies were selected each for plasmid preparation and sent for sequencing to verify the insertion and successful construction of pBE-S-LCC$_{ICCG}$-His6-Epr and pBE-S-LCC$_{ICCG}$-His6-YjfA.

As LCC$_{ICCG}$ appears to exhibit phospholipase activity, leading rather to leaking of the enzyme to the media than active secretion via an applied secretion system in *E. coli* (See 4.1.3), it was decided to employ the same control for *B. subtilis* by expressing LCCICCG-bac without a SP. However, Gram-positive bacteria confer a different cell wall structure than Gram-negative bacteria, lacking the outer membrane and possessing instead a thick layer of peptidoglycan, which might prevent the leaking [49].

Therefore, the plasmid pBE-S-LCC$_{ICCG}$-His6-NS containing LCCICCG-bac with no N-terminal SP (NS) was additionally constructed. For this purpose, the plasmid pBE-S-LCC$_{ICCG}$-His6 isolated from clone S164 (SP:yveB) was used as a template for PCR amplification using the primers LCC-FW-MluI and LCC-RV-XbaI (3.3). After purification, the amplicon as well as the vector pBE-S DNA was digested with *Mlu*I and *Xba*I, ligated, transformed into *E. coli* BL21 (DE3) and plated on LB selection plates (50 µg/mL ampicillin). Since the primers only amplify the gene of LCCICCG-bac and the cutting site of *Mlu*I is positioned upstream of the

SP, the previously existing SP was thereby eliminated. Two of the resulting transformants were isolated for plasmid preparation and sent for sequencing to confirm the successful cloning of pBE-S-LCC$_{ICCG}$-His6-NS.

After verification via sequencing, the three constructed plasmid were transformed into *B. subtilis* RIK 1285 as described in 4.2.3.

Expression in 100 mL Culture Volume and Esterase Activity Assay on Culture Supernatant

For the expression in a larger culture volume of 100 mL, 5 of the initially screened clones, namely B89, M23, S15, S76 and S164, as well as three transformants containing the previously cloned plasmids pBE-S-LCC$_{ICCG}$-His6-Epr (Epr), pBE-S-LCC$_{ICCG}$-His6-YjfA (YjfA) and pBE-S-LCC$_{ICCG}$-His6-NS (NS) were selected. A prior evaluation showed that extracellular expression level was highest after 48 h (Data not shown). Since pBE-S DNA contains a constitutive promoter for the expression of the inserted gene, it was not possible to compare expression levels before and after induction as performed for the T7-inducible expression system in *E. coli* BL21 (DE3). Therefore, samples for SDS-PAGE were collected from the cell pellet (Pellet) and the supernatant (SN) after 48 h and compared to the baseline protein expression of *B. subtilis* RIK 1285 (See Figure 4.11 C).

Comparing the cell growth (OD_{660}) of the expression cultures after 48 h, it is noticeable that all clones containing the plasmid to express LCC$_{ICCG}$-His6-bac displayed a lower cell density than RIK 1285 (See Figure 4.11 A). Consequently, the protein level measured in the supernatant were also decreased, indicating that the expression of the enzyme constitutes a metabolic burden or a toxic effect, slightly reducing cell growth (See Figure 4.11 B). Lowest OD_{660} was observed for clone S15, nevertheless, its supernatant contained the highest amount of protein apart from RIK 1285, suggesting increased secretion.

The expected MW of LCC$_{ICCG}$-His6-bac was determined to be 28.93 kDa (Expasy [64]). A distinct band at this predicted MW was detected for all the clones, both in the cell pellet and in the supernatant, when compared to RIK 1285. However, all clones display that a large fractions of the expressed LCC$_{ICCG}$-His6-bac seems to accumulate intracellularly, implying that the endogenous Sec-machinery might not be able to efficiently secrete this enzyme. On the other hand, this observation demonstrated that LCC$_{ICCG}$-His6-bac, when expressed within *B. subtilis*, is not able to leak out of the cells by permeabilizing the cells as discovered for *E. coli* BL21 (DE3). Nonetheless, a large proportion of LCC$_{ICCG}$-His6-bac was also identified in the supernatant of all clones. Consistent with previous observations indicating increased secretion by S15, its supernantant appeared to harbor the highest amount of the enzyme. Unfortunately, definite identification of the band associated to LCC$_{ICCG}$-His6-bac by Western Blot analysis was not successful, even when performing the assay with a polyclonal secondary antibody to amplify the reporter signal. On one hand, the concentration of the expressed enzyme could have been so low that the disappeared in the background noise, on the other hand, it might have been masked by a protein running at the same MW in the SDS-PAGE, and therefore, preventing the detection by the antibody. Thus, the next step should be to assure that the antibody is able to recognize the expressed LCC$_{ICCG}$-His6-bac at all by performing the Western Blot analysis on the purified enzyme.

Nevertheless, the measured volumetric and specific activity in the supernatant of all clones confirmed the expression and secretion of LCC_{ICCG}His6-bac (See Figure 4.11 D and E). In the absence of a SP (NS), only a small fraction of the enzyme was secreted to the surrounding media, indicating, as mentioned before, that the cell wall structure of Gram-positive bacteria partially prevents the leaking of the active enzyme as observed for the Gram-negative bacterium *E. coli*. Highest volumetric and specific activity was detected for clone S15, whereas clone S76 displayed a similar volumetric but a lower specific activity, although both were demonstrated to contain the same SP. On the other hand, clone M23 showed lower volumetric activity, agreeing with the low protein content in the supernatant, but exhibited a high specific activity, suggesting that the concentration of LCC_{ICCG}His6-bac among the total protein secreted was higher than for clone S76. Unfortunately, no increased secretion was obtained for the SPs *Epr* and *YjfA*, which were reported to be the best candidates for the cutinase derived form *Fusarium solani pisi* [60], as their mediated level of secretion was similar to the one without SP (NS). Since the cutinase investigated by Brockmeier et al. (2006) originated from a eukaryotic organism, similar SPs did not appear to be applicable for the bacterial LCC_{ICCG}His6-bac, considering as well that it was highlighted in the study that SPs can be unique for every protein.

For subsequent purification of the secreted LCC_{ICCG}His6-bac to evaluate their PET degradation efficiency, the supernatant of clone S15 was selected as the most promising candidate as well as clone S76. Although S76 displayed a lower specific activity than M23, this clone was preferred as the overall higher protein content in the supernatant promised a higher yield.

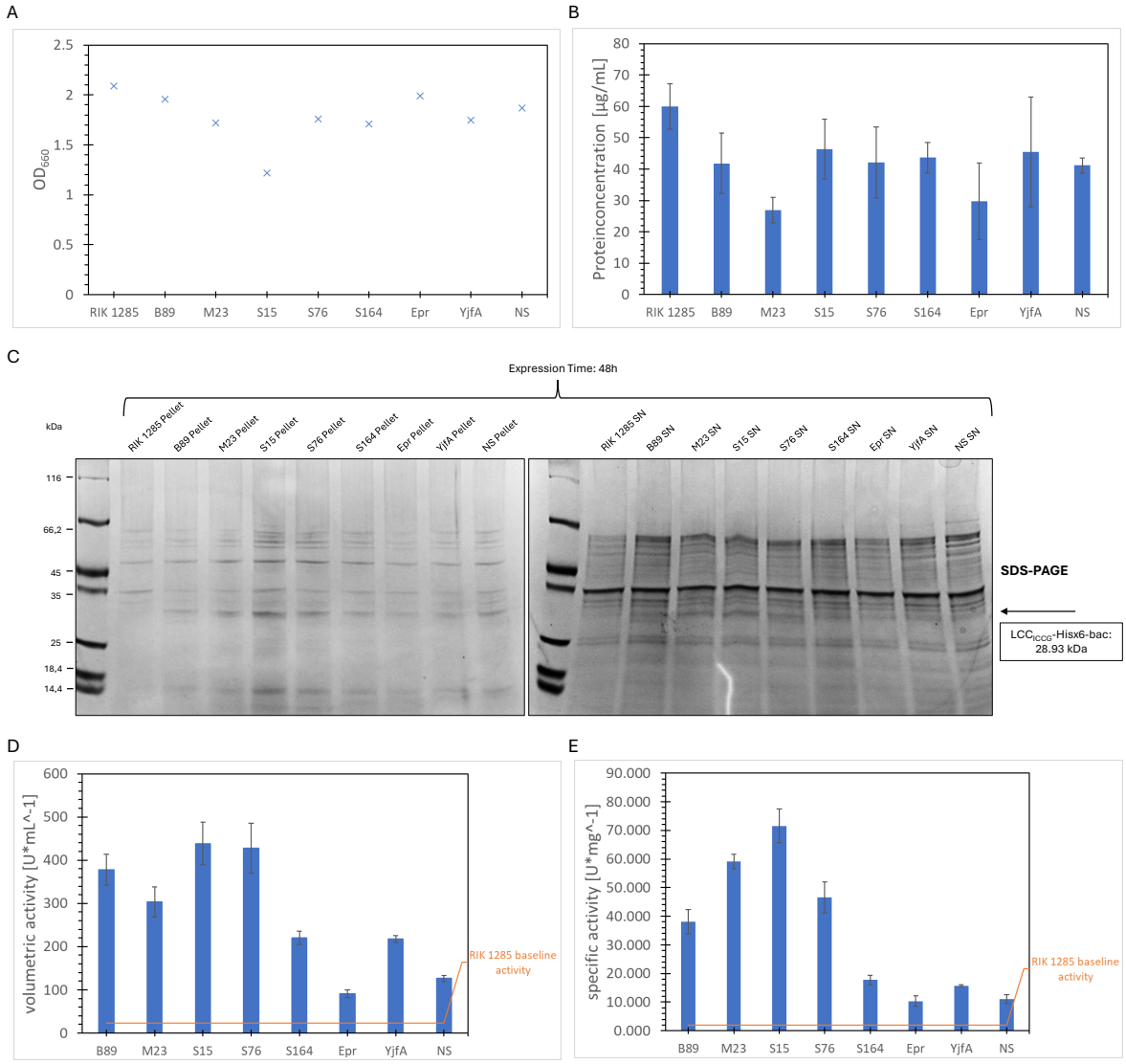

Figure 4.11. Expression of LCC_{ICCG}-His6-bac in 100 mL culture volume and Esterase Activity Assay on culture supernatant of the 8 candidates. (A) Measurement of cell growth in the expression culture after 48 h. **(B)** Protein concentration in the supernatant was determined using the Bradford Assay (3.4.3). For calculations, the slope of the standard curve derived from high protein concentrations (See Appendix 6.4) and the mean absorbance values at 595 nm from three measurements were employed. **(C)** SDS-PAGE of the expression of LCC_{ICCG}-His6-bac analysing the cell pellet (Pellet) and supernatant (SN) after 48 h of incubation. **(D)** Volumetric and **(B)** specific activity in the supernatant. Enzymatic activity in the supernatant was determined using the Esterase Activity Assay (3.6.1). Formulas for the calculation of the volumetric and specific activity can be found in the Appendix 6.5 B.

Purification of LCC_{ICCG}His6-bac Expressed by Clone S15 and S76

The supernatant of clone S15 and S76 were subjected to purification as depicted before in 4.1.5. The purification steps can be followed in Figure 4.12. The eluate of S15 was found to be homogeneous, as it contained primarily the band for LCC_{ICCG}His6-bac at 28.93 kDa. In contrast, the eluate of S76 showed several additional protein bands in addition to the band attributed to LCC_{ICCG}His6-bac, which was generally weaker compared to S15. Given that the amount of secreted LCC_{ICCG}His6-bac in the supernatant of S76 was lower, as previously assumed by the specific activity, it is evident that background contaminates appear more prominent due

to a lower signal to noise ratio. From the supernatant of the initial 100 mL expression culture, a yield of approx. 0.37 mg was obtained for S15 and approx. 0.29 mg for S76 (NanoDrop: ε=38.39 M^{-1} cm^{-1}). In comparison, Brockmeier et al. (2006) yielded 35 mg/L with the SP *Epr* for the cutinase of *Fusarium solani pisi*, which might suggest that the optimal SP for LCC_{ICCG} for the secretion by *B. subtilis* has not yet been identified. However, it should be noted that the expression was carried out with a different plasmid (pBSMuL3) and a different promoter (P_{hpaII}). Thus, in a next step, it should be investigated whether the replacement of the *apreE* promoter by the "strong constitutive HpaII promoter" improves the overall yield [60].

Nevertheless, the question remains as to why both clones displayed a different secretion efficiency and yield in spite of containing the same SP. A sequence comparison of the region upstream of the SP with the sequence obtained with the primer pBE-LCC-SP-RV revealed a mutation close to the promoter region of the isolated plasmid of clone S76. This mutation might have influenced binding and processivity of the RNA polymerase, influencing the level of expressed LCC_{ICCG}His6-bac [69].

Overall, the yield of PET hydrolase obtained via secretory expression in *B. subtilis* RIK 1285 was around 10 times lower than via extracellular overexpression in *E. coli* BL21 (DE3). For subsequent studies, it should also be considered to evaluate the amount of intracellular enzyme to compare the total expression capacity to the level of secretion. Furthermore, for the secretory expression in *B. subtilis* RIK 1285, it should be taken into account that the system has yet not been optimized regarding temperature, agitation and several other factors. Moreover, as afore mentioned, the in *B. subtilis* RIK 1285 expressed LCC_{ICCG}His6-bac is expressed via a constitutive promoter, unlike the IPTG-inducible system in *E. coli*BL21 (DE3) for overexpression. Although there is currently no comparable system established for *B. subtilis*, attempts were performed to introduce the T7-promoter based expression or other studies were reporting high-level extracellular protein production using a dual-promoter system [70, 71]. Also the utilization of another constitutive promoter, such as the "strong constitutive HpaII promoter" applied by Brockmeier et al. (2006), could be considered for implementation in future experiments. In general, the expression of PET hydrolases via the host *B. subtilis* has not been reported in literature thus far, hence further investigation would be required if decided to proceed with this expression host.

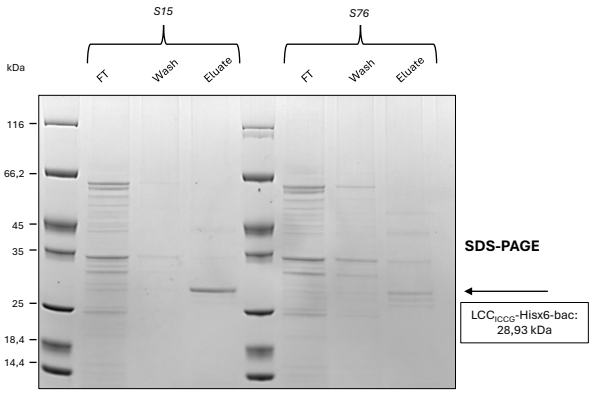

Figure 4.12. Purification of LCC_{ICCG}His6-bac expressed by clone S15 and S76 from the culture supernatant. Supernatant (SN), flow through (FT). The expected MW of LCC_{ICCG}His6-bac is 28.9 kDa.

Catalytic Activity of Purified LCC_{ICCG}His6-bac Expressed by Clone S15 and S76

For the assessment of the catalytic activity of the purified LCC_{ICCG}-His6-bac of S15 and S76 towards amorphous Pet films, the same enzyme loadings were tested as in 4.1.6.

Comparing the weight loss obtained by the different concentrations of purified LCC_{ICCG}-His6-bac from S15 and S76, depolymerization rate observed for S76 were lower (See Figure 4.13 A). This can be attributed to contaminants that were present in the elution fraction of S76 after purification, as these distort the amount of added LCC_{ICCG}-His6-bac to the reaction. The non-homogeneous eluate is likely also accountable for the significant difference that was observed between 1 mg and 2 mg of added enzyme per gram of PET after 24 h. In contrast, for LCC_{ICCG}-His6-bac from S15, a point of saturation was recognized after 1 mg of enzyme per gram of PET, where increasing the enzyme concentration does not further increase PET conversion, as previously described for the PET hydrolases expressed in *E. coli* BL21 (DE3). By adding 1 mg or 2 mg of LCC_{ICCG}-His6-bac obtained from S15 per gram of PET, respectively, a PET conversion of over 50 % was achieved, which was about 10 % higher than for LCC-His expressed in *E. coli* BL21 (DE3). Additionally, there is no significant difference observed between 24 and 48 h of reaction time, as previously noted in 4.1.6. Nonetheless, unlike for LCC-His and LCC-PelB, the depolymerization level after 48 h did not decrease compared to the level after 24 h.

One reason for the higher level of PET depolymerization observed for LCC_{ICCG}-His6-bac obtained from S15 might be the fact, that the enzyme expressed in *B. subtilis* RIK 1285 was confirmed to be the variant ICCG, while LCC-His was discovered to be the wild type of LCC, and for LCC-PelB, further sequencing has to verify the type of enzyme. Since LCC_{ICCG} is known to have a higher thermostability and enhanced substrate binding [40], this would explain higher PET conversion rates. Especially after 48 h, it was previously observed that PET recrystallization kinetics outcompeted the enzyme activities, resulting in the decrease in weight loss after 48 h.

The specific activity calculated based on the released TPAeq confirmed the optimal enzyme loading to be 1 mg of enzyme per gram of PET (See Figure 4.13 B). Here, LCC_{ICCG}-His6-bac from S15 achieved an activity of 20.28 $mg_{TPAeq}h^{-1}mg_{enzyme}^{-1}$ within the first 24 h compared to only 12.49 $mg_{TPAeq}h^{-1}mg_{enzyme}^{-1}$ for an enzyme concentration of 2 mg of enzyme per gram of PET, which is about threefold and twofold higher activity observed by Wu et al. (2023) for LCC_{ICCG} expressed in *E. coli*. However, the activity decreased to 9 and 4.8 $mg_{TPAeq}h^{-1}mg_{enzyme}^{-1}$, respectively, when measured after a period of 48 h. In comparison, LCC-His expressed in *E. coli* BL21 (DE3) reached a specific activity of 12.95 $mg_{TPAeq}h^{-1}mg_{enzyme}^{-1}$ within 24 h at an enzyme loading of 1 mg of enzyme per gram of PET.

The amount of released TPA was consistent with the weight loss (See Figure 4.13 C). In addition, it was observed in the same manner as before, that the amount of MHET produced after 24 h was significantly higher than after 48 h, as it was further degrade to TPA and EG (See Figure 4.13 D). Only the amount of produced TPA and MEHT measured after 48 h of incubation with an enzyme loading of 2 mg per gram of PET were inconsistent with the assessed weight loss of approx. 50 %. The level of produced monomers should be similar to the one measured after 24 h, yet the amount of TPA and MHET was only half. This discrepancy could be due to higher concentration of insoluble long-chain degradation products in the reaction solution that were filtered out before the HPLC analysis.

Overall, the conversion of PET by LCC_{ICCG}-His6-bac from S15 to the soluble monomers, TPA, EG and MHET appeared to be higher compared to the conversion achieved by LCC-His and LCC-PelB from *E. coli* BL21 (DE3). This becomes especially important considering the potential industrial implementation, as only TPA and EG can be recovered at the end of the process, while all other degradation products will be lost, representing a financial loss for the production [43]. For example, summing the amount of TPA and MHET generated after 24 h with 1 mg of LCC_{ICCG}-His6-bac from S15 per gram of PET resulted in 7.3 mg, while with a weigth loss of approx. 53 % of an average of 15 mg PET added per reaction, 7.95 mg of degradation products would be expected. This corresponds to around 92 % of the degradation products being completely converted to TPA and MHET, while only around 77 % was degraded into these monomers by LCC-His (4.6 mg of produced TPA and MHET of 6 mg expected degradation products).

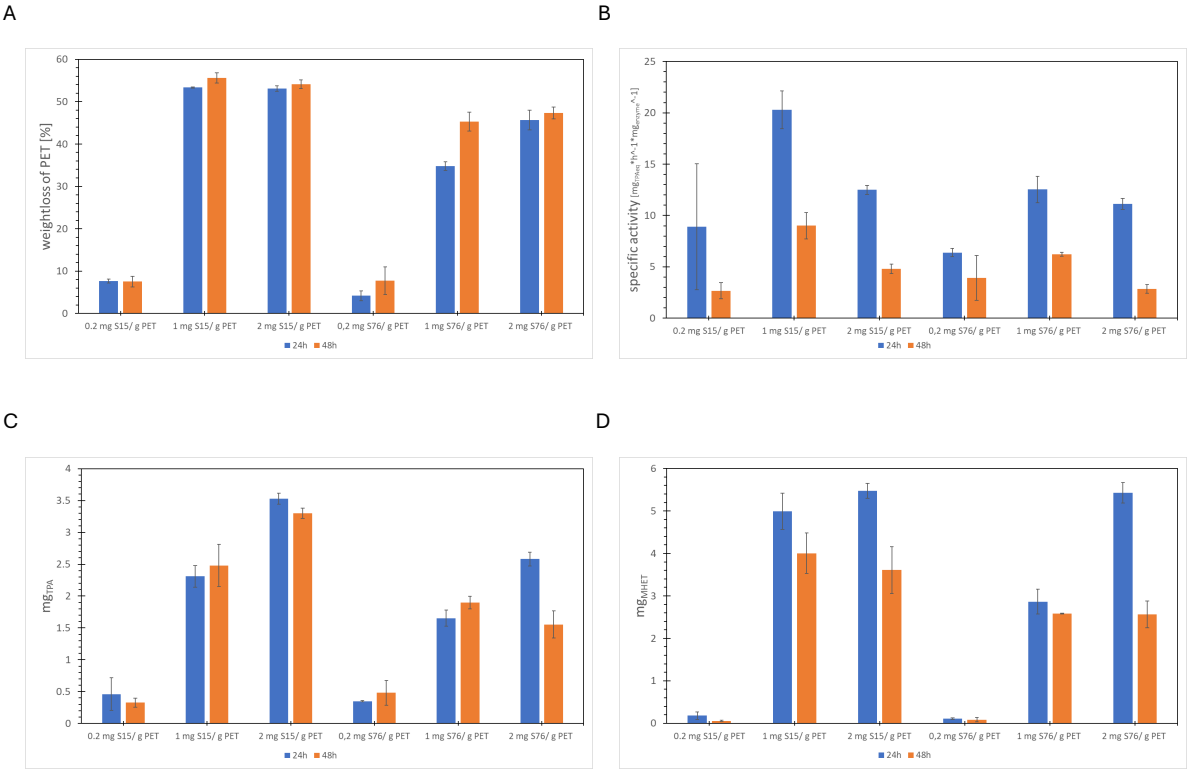

Figure 4.13. (A)Weight loss, (B) specific activity, (C) amount of TPA [mg] and (D) MHET [mg] produced after PET degradation with purified LCC_{ICCG} expressed with no SP (LCC-His) and with PelB (LCC-PelB) after 24 and 48 h. Reactions were performed at 72°C. Calculated values and standard deviation are based on two independent replicates. Calculations were performed as described in 4.1.4.

As Arnal et al. (2023) emphasized that efficiency and output of an enzyme-base PET depolymerization process are dependent one the exclusive formation of TPA and EG, accumulation of intermediate products like MHET must be avoided. Although LCC_{ICCG} is able to convert MHET to TPA and EG, a more complete hydrolsis might be achieved by introducing a chimeric protein with MHETase. Although, Knott et al. (2022) performed their experiments with a MHETase:PETase chimeric protein similar synergistic effects might be observed for a two-enzyme system with LCC_{ICCG}.

Conclusion 5

The main objective of this thesis was to establish a platform for stable secretion of two different PET hydrolases, namely FastPETase and LCC^{ICCG}, to enable enzyme-based depolymerization on a larger scale by its industrial implementation more cost-effective and less labor-intensive.

In the first approach, the efficiency of the T1SS HlyA secretion system was intended to be evaluated in comparison to the already existing SecB-dependant pathway for expression of the PET hydrolases in *E. coli*. However, it was indicated that establishing a secretion system for LCC_{ICCG} might not be necessary, as the enzyme appears to display phospholipase activity, making the cell membrane of *E. coli* BL21 (DE3) more permeable allowing the active enzyme to leak into the surrounding medium. On the contrary, the addition of a SP could even negatively influence the overall yield, as it was shown for the PelB peptide, where a fraction of the expressed enzyme accumulated in the periplasmic space. Although successful PET degradation directly in the supernatant was not demonstrated, this could be achieved by performing the reaction in a larger scale under controlled conditions in a bioreactor.

LCC_{ICCG} expressed without SP (LCC-His), as well as LCC expressed with PelB (LCC-PelB), successfully purified from the culture supernatant, achieving a yield of approx. 3.7 mg per 100 mL expression culture each, equivalent to 37 mg per liter. Compared to the requirements described by Arnal et al. (2023) for operating an industrial unit (20 g/L), the yield obtained is not yet sufficient. Additionally, PET conversion rates observed were lower than those reported in other studies mentioned [40, 41], with highest conversion rates of around 40 % achieved with a concentration of 1 mg of enzyme per gram of PET. However, it should be pointed out that most of these studies conducted their experiments in larger scales under controlled conditions in a bioreactor to counteract the resulting acids.

Finally, LCC-His was revealed to be the wild type and not the high-performance variant ICCG, which was intended to be used in this thesis. For LCC-PelB, confirmation of the sequence is still needed. Expression of FastPETase in *E. coli* BL21 (DE3) was unfortunately not successful within the scope of this thesis, however, suggestions on how this issue could be solved were provided.

In a second approach, an alternative expression organism was selected for the extracellular production of the PET hydrolases. *B. subtilis* is known for its ability to secrete high amounts of homologous protein. To identify the appropriate SP for a specific protein, a screening system was developed by Brockmeier et al. (2006) to characterize all naturally occuring Sec-type SPs for their secretion potential. Several possible candidates were identified for the *B. subtilis*-optimized LCC_{ICCG}, and in the end, the SP *yqgA* was determined to yield highest secretion rates for the expression in *B. subtilis* RIK 1285.

Nevertheless, the yield obtained from the supernatant of a 100 mL expression culture was around 10-fold lower than that achieved via the expression in *E. coli* BL21 (DE3). This raises the question of whether the desired expressability of 20 g/L can ever be reached, even by optimizing the system and conditions of incubation. During PET depolymerization, the LCC_{ICCG}-His6-bac secreted and purified from clone S15 (SP: *yqgA*) achieved approx. 10 % higher PET conversion at the same enzyme loading showed to be best performing for LCC-His and LCC-PelB expressed via *E. coli* BL21 (DE3). It remains to be determined whether this effect was observed due to the high-performance variant ICCG expressed in *B. subtilis* RIK 1285 unlike the wild type expressed in *E. coli* BL21 (DE3) or if the codon optimization has altered the enzyme activity. A repetition of the PET degradation experiment with more replicates could verify the reliability of the data and state if 10 % displays a significant difference.

Appendix 6

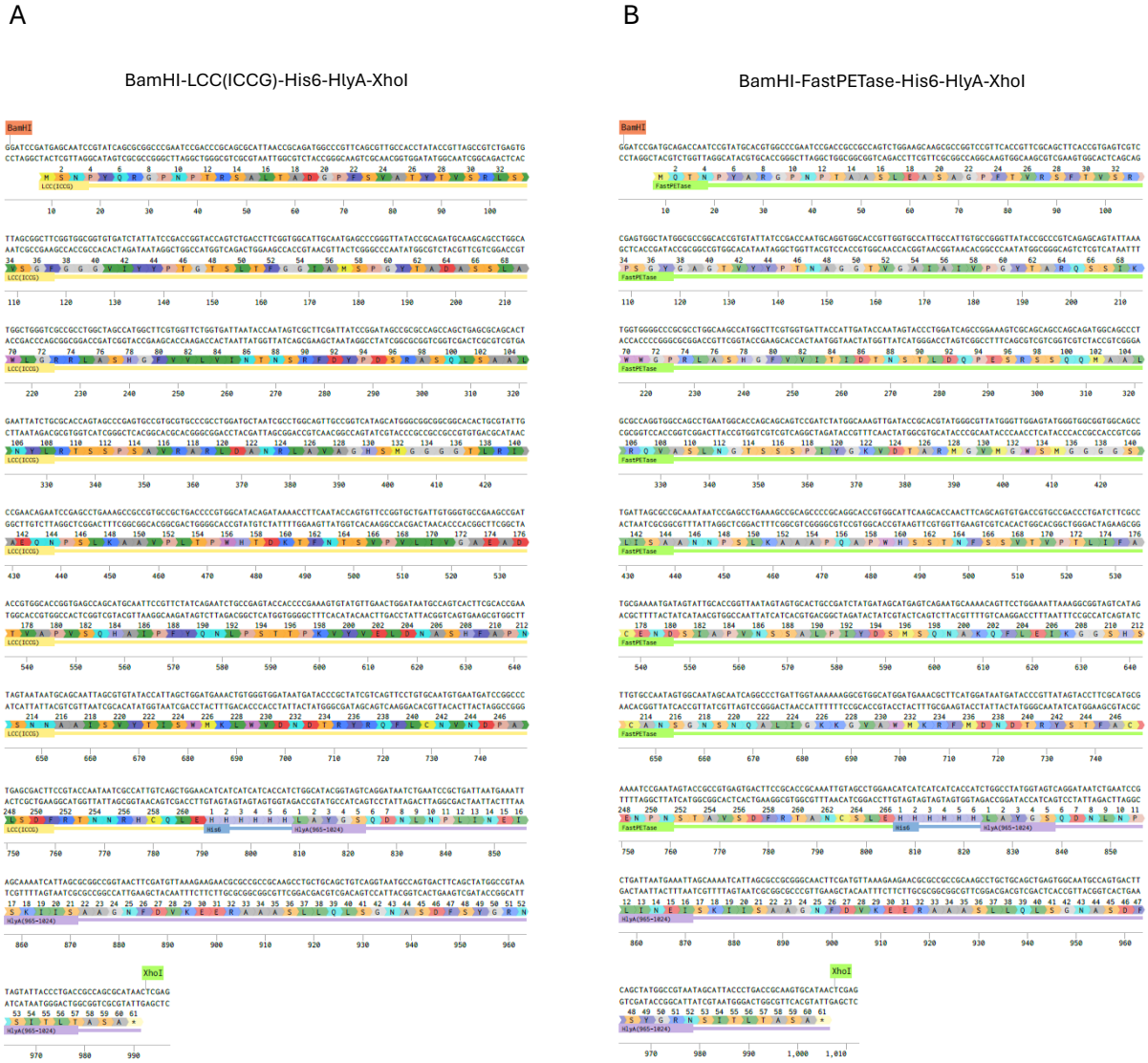

Figure 6.1. Sequence of (A) LCC_{ICCG}-His6-HlyA and (B) FastPETase-His6-HlyA. The sequence was synthesized and cloned into the vector pET21b+ with the RE *BamH*I and *Xho*I by Gene Universal. Visualisation and Annotation were generated with Benchling.

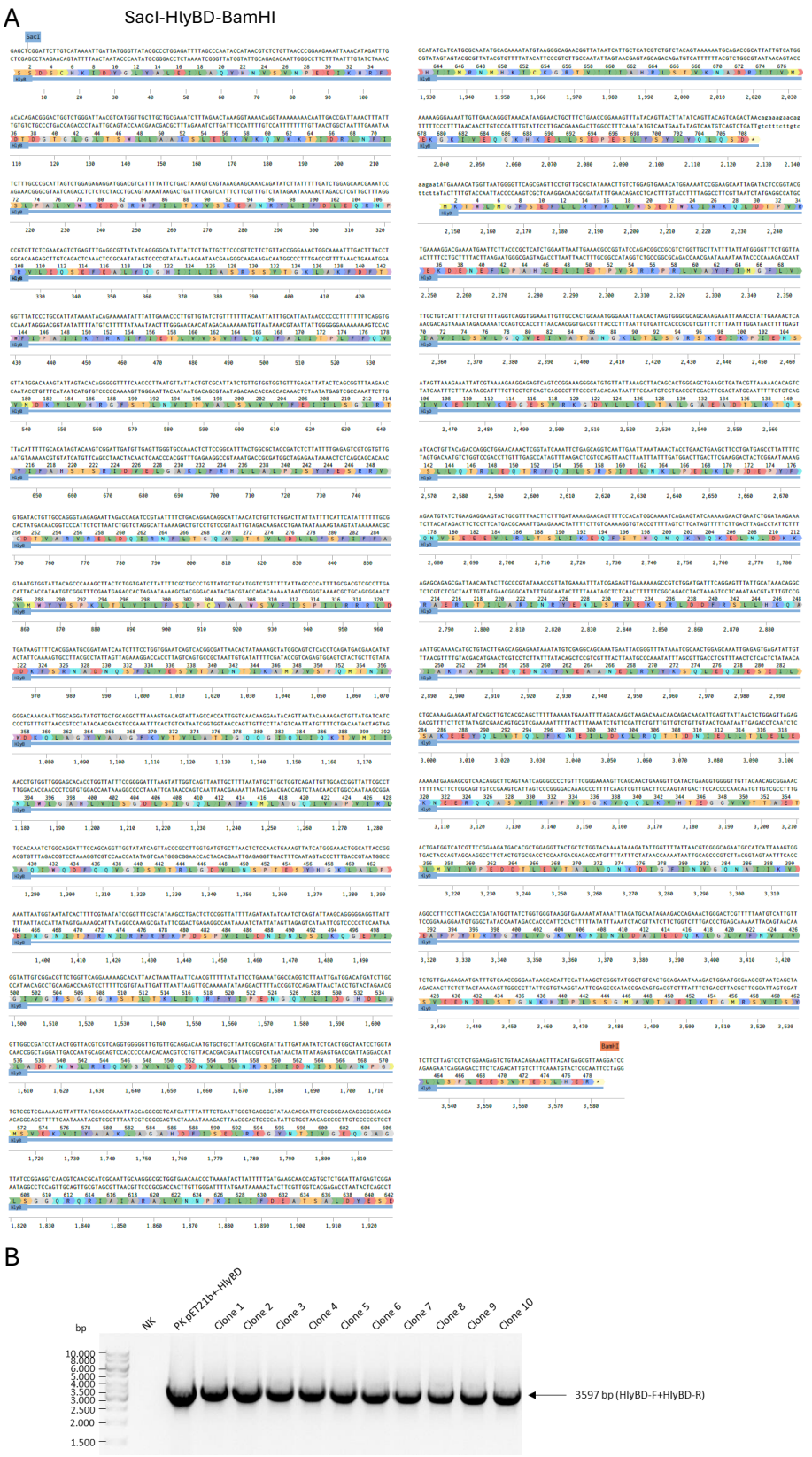

Figure 6.2. (A) Sequence of HlyBD and (B) Colony PCR to identify clones carrying the cloned plasmid pSTV28-HlyBD. (A) The sequence was synthesized and cloned into the vector pET21b+ with the RE *Sac*I and*BamH*I by Gene Universal. Visualisation and Annotation were generated with Benchling.**(B)** Colony PCR was conducted after inserting HlyBD into pSTV28 to identify clones carrying the right plasmid. As PK, pET21b+-HlyBD was added to the reaction as template. The expected length for the amplicon using the primers HlyBD-F and HlyBD-R was 3597 bp.

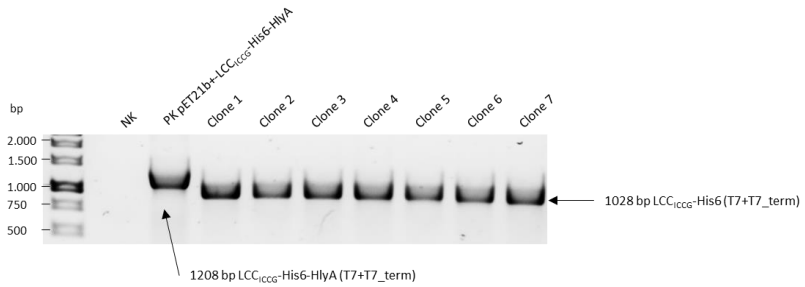

Figure 6.3. Colony PCR to identify clones carrying the cloned plasmid pET21b+-LCC$_{ICCG}$-His6. Colony PCR was conducted after inserting LCC$_{ICCG}$-His6 into pET21b+ to identify clones carrying the right plasmid. The backbone of the plasmid was derived from pET21b+-LCC$_{ICCG}$-His6-HlyA, therefore, possible re-ligation had to be ruled out. The expected length for the LCC$_{ICCG}$-His6 using the primers T7 and T7-term was 1028 bp. If the clones were to carry a re-ligated plasmid with LCC$_{ICCG}$-His6-HlyA, the length of the amplicon would be 1208 bp.

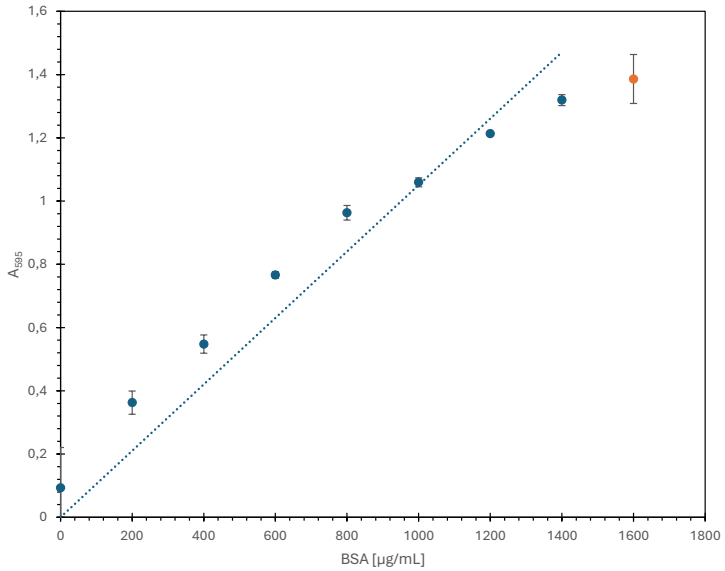

Figure 6.4. Bradford standard curve for high protein concentration (200-1600 µg/mL BSA). Each concentration was measured three times, and error bars represent the respective standard deviation. The linear standard curve was constrained to pass through the origin. The highest concentration (orange) was omitted from the calculation of the curve to obtain a higher coefficient of determination (R^2). y=0.0011x, R^2=0.983

A

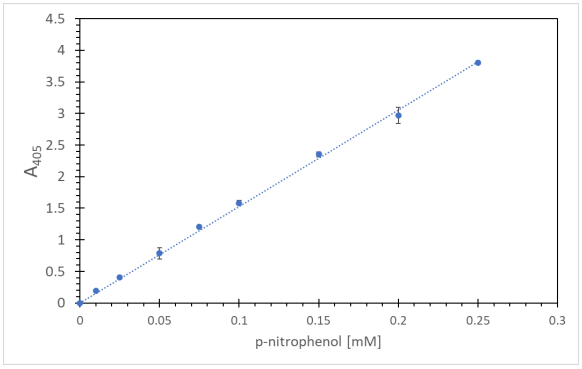

B

$$Volumetric\ activity\ \left[\frac{U}{mL}\right] = \frac{p-nitrophenol\ [\mu mol] * V_{total}[mL] * Df}{V_{enzyme}[mL] * time[min]}$$

$$= \frac{A_{405} * V_{total}[mL] * Df}{slope * V_{enzyme}[mL] * time[min]}$$

$$Specific\ activity\ \left[\frac{U}{mL}\right] = \frac{p-nitrophenol\ [\mu mol]}{m_{enzyme}[mg] * time[min]}$$

$$= \frac{A_{405}}{slope * m_{enzyme}[mg] * time[min]}$$

Figure 6.5. (A)p-Nitrophenol standard curve and (B) calculations for volumetric and specific activity. **(A)** Each concentration was measured three times, and error bars represent the respective standard deviation. The linear standard curve was constrained to pass through the origin. y=15.276x, R^2=0,.994. **(B)** Formulas applied to calculate the volumetric and specific activity in the Esterase Activity Assay using the slope of the standard curve and the measured absorption at 405 nm.

A

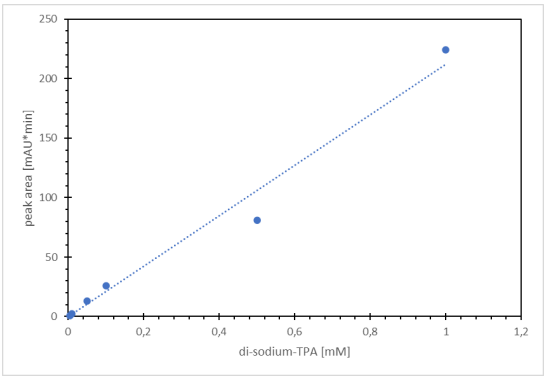

B

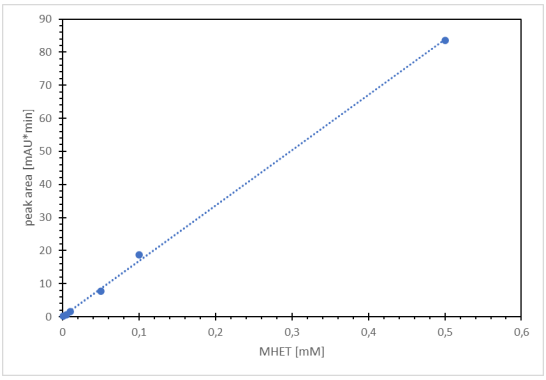

Figure 6.6. (A)Di-sodium-TPA and (B) MHET standard curve for assessment of PET depolymerization via HPLC. The linear standard curves were constrained to pass through the origin.**(A)** y=212.14x, R^2=0.9858. **(B)** y=167.58x, R^2=0.9994.

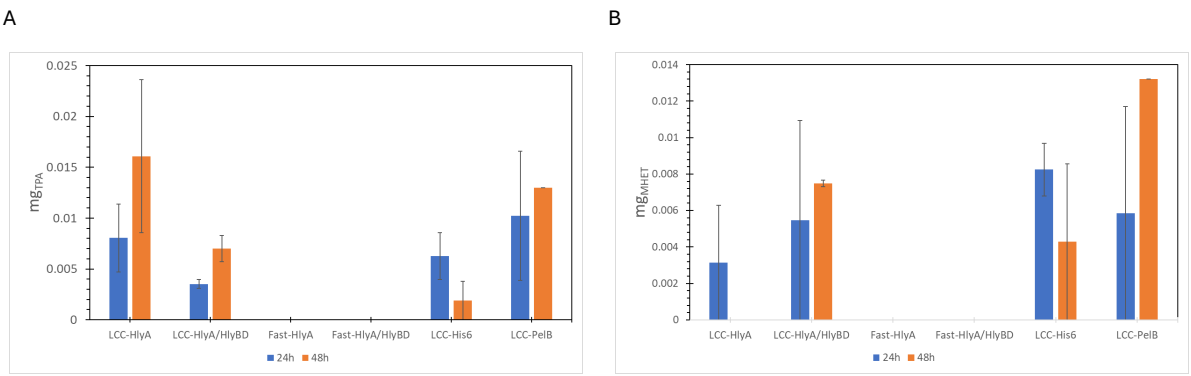

Figure 6.7. (A)Amount of TPA [mg] and (B) MHET detected via HPLC after PET degradation with the culture supernant after 24 and 48 h. Variants of LCC_{ICCG} were incubated at 72°C, variants of FastPETase were incubated at 50°C. Calculated values and standard deviation are based on two independent replicates. Masses were calculated as followed: $mg_{TPA\ or\ MHET}$=peak area [mAU]*dilution factor*$MW_{TPA\ or\ MHET}$*$slope^{-1}$.

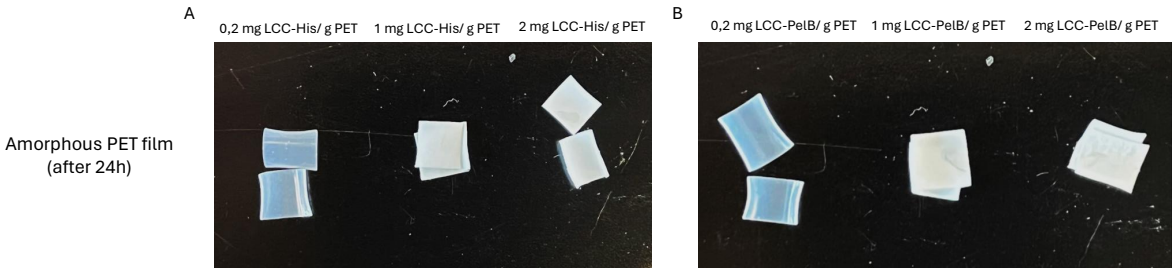

Figure 6.8. Appearance of the amorphous PET film after 24h incubation at 72°C with (A) LCC_{ICCG}-His6 secreted with no SP (LCC-His) and LCC_{ICCG} secreted with PelB (LCC-PelB) with 0.2, 1 or 2 mg of enzyme added per gram of PET

.

```
                1       10        20        30        40        50        60        70        80        90       100       110       120       130
                |--------+---------+---------+---------+---------+---------+---------+---------+---------+---------+---------+---------+---------|
LCC-His6        MSNPYQRGPNPTRSALTADGPFSVATYTVSRLSVSGFGGGVIYYPTGTSLTFGGIAMSPGYTADASSLAWLGRRLASHGFVVLVINTNSRFDYPDSRASQLSAALNYLRTSSPSAVRARLDANRLAVAGH
LCC-PelB        MSNPYQRGPNPTRSALTADGPFSVATYTVSRLSVSGFGGGVIYYPTGTSLTFGGIAMSPGYTADASSLAWLGRRLASHGFVVLVINTNSRFDGPDSRASQLSAALNYLRTSSPSAVRARLDANRLAVAGH
Consensus       MSNPYQRGPNPTRSALTADGPFSVATYTVSRLSVSGFGGGVIYYPTGTSLTFGGIAMSPGYTADASSLAWLGRRLASHGFVVLVINTNSRFDgPDSRASQLSAALNYLRTSSPSAVRARLDANRLAVAGH

                131     140       150       160       170       180       190       200       210       220       230       240       250       260
                |--------+---------+---------+---------+---------+---------+---------+---------+---------+---------+---------+---------+---------|
LCC-His6        SMGGGGTLRIAEQNPSLKAAVPLTPWHTDKTFNTSVPVLIVGAEADTVAPVSQHAIPFYQNLPSTTPKVYVELDNASHFAPNSNNAAISVYTISWMKLWVDNDTRYRQFLCNVNDPALSDFRTNNRHCQL
LCC-PelB        SMGGGGTLRIAEQNPSLKAAVPLTPWHTDKTFNTSVPVLIVGAEADTVAPVSQHAIPFYQNLPSTTPKVYVELCNASHIAPNSNNAAISVYTISWMKLWVDNDTRYRQFLCNVNDPALCDFRTNNRHCQL
Consensus       SMGGGGTLRIAEQNPSLKAAVPLTPWHTDKTFNTSVPVLIVGAEADTVAPVSQHAIPFYQNLPSTTPKVYVELdNASHiAPNSNNAAISVYTISWMKLWVDNDTRYRQFLCNVNDPALcDFRTNNRHCQL

                261 267
                |-----|
LCC-His6        EHHHHHH
LCC-PelB        EHHHHHH
Consensus       EHHHHHH
```

Figure 6.9. Sequence alignment of the AA sequence of the enzymes encoded by pET21b-LCC_{ICCG}-His6 (LCC-His6) or pET26b-LCC_{ICCG}-His6-PelB (LCC-PelB). Translation of the nucleotide sequence to the protein sequence was performed in Benchling and the sequence alignment was carried out in MultiAlign [72]. For the alignment the default parameters were chosen. Differing AA are highlighted in the sequence.

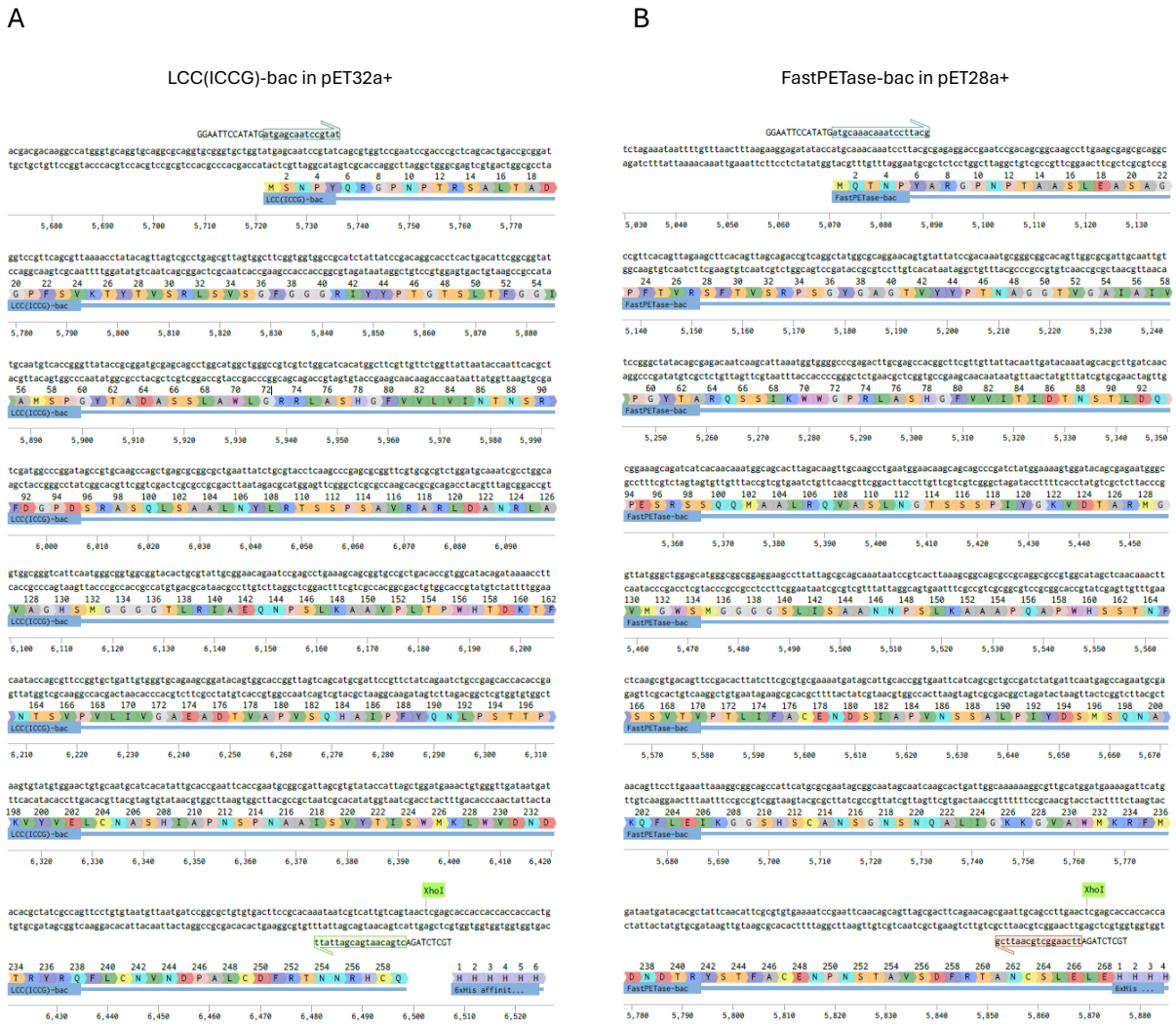

Figure 6.10. Sequence of (A) LCC_{ICCG}-bac in pET32a+ and (B) FastPETase-bac in pET28a+. The sequence was codon optimized for *B. subtilis* and then forwarded to Gene Universal to be synthesized and cloned into the vector pET32a+ or pET28a+, respectively. The primers used for PCR amplification of the genes are highlighted. Visualisation and Annotation were generated with Benchling.

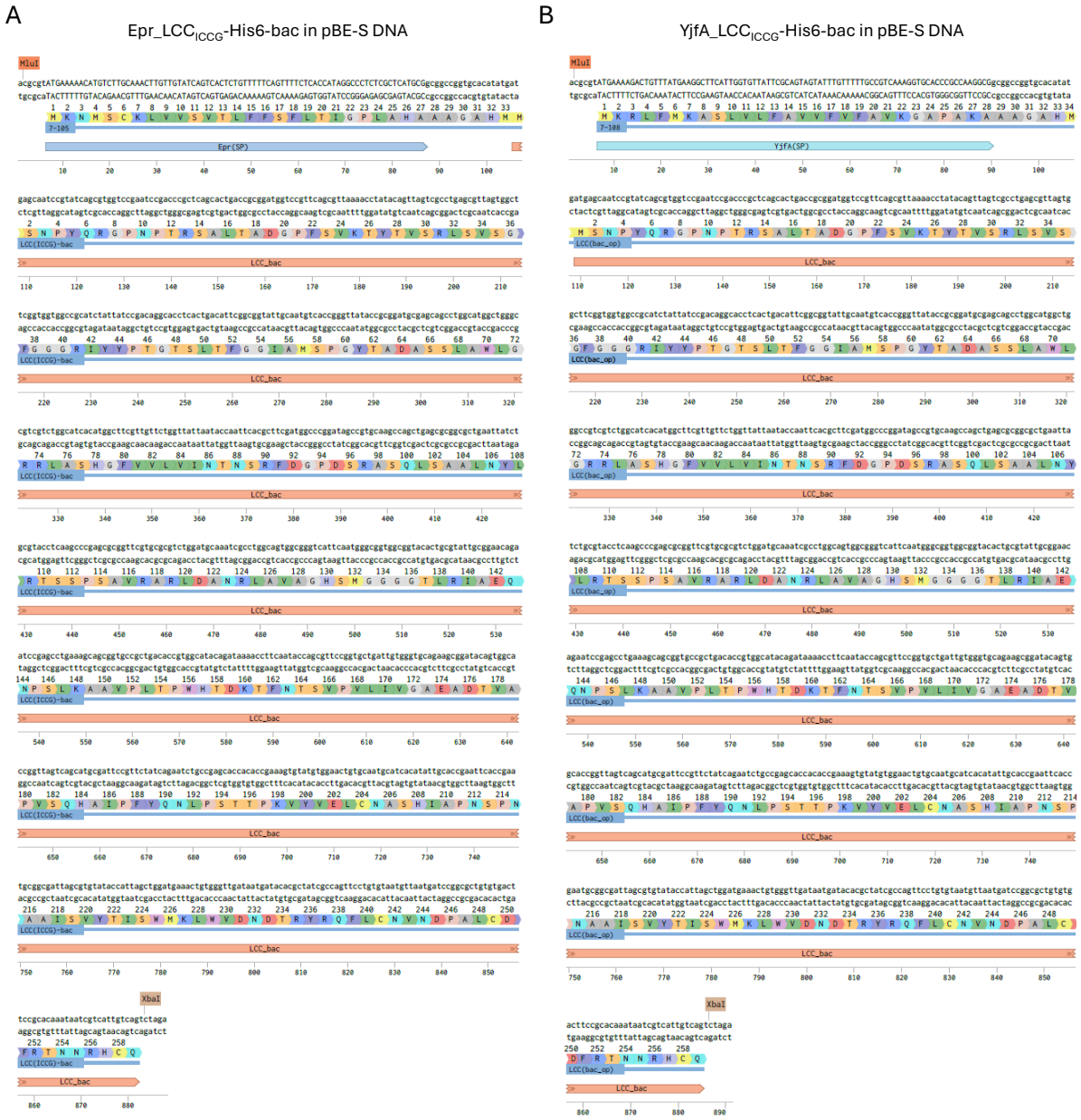

Figure 6.11. Sequence of LCC$_{ICCG}$-His6-bac with the upstream SP (A) Epr and (B) YjfA. The sequence was cloned into the vector pBE-S DNA with the RE *Mlu*I and *Xba*I. Visualisation and Annotation were generated with Benchling.

Bibliography

[1] The circular economy for plastics – a european overview 2022, 2022. URL https://plasticseurope.org/knowledge-hub/the-circular-economy-for-plastics-a-european-overview-2/.

[2] Plastics - the fast facts 2023, 2023. URL https://plasticseurope.org/knowledge-hub/plastics-the-fast-facts-2023/.

[3] The circular economy for plastic, 2024. URL https://plasticseurope.org/knowledge-hub/the-circular-economy-for-plastics-a-european-analysis-2024/.

[4] Sustainable waste management: what the eu is doing, April 2018. URL https://www.europarl.europa.eu/topics/en/article/20180328STO00751/sustainable-waste-management-what-the-eu-is-doing.

[5] Directive (eu) 2018/852 of the european parliament and of the council of 30 may 2018 amending directive 94/62/ec on packaging and packaging waste, 2018. URL https://eur-lex.europa.eu/eli/dir/2018/852/oj.

[6] Krishna Dutt and R. K. Soni. A review on synthesis of value added products from polyethylene terephthalate (pet) waste. *Polymer Science Series B*, 55(7):430–452, July 2013. ISSN 1555-6123. doi: 10.1134/S1560090413070075.

[7] U. S. Government Accountability Office. Science tech spotlight: Biorecycling of plastics | u.s. gao, April 2024. URL https://www.gao.gov/products/gao-23-106261.

[8] New life for waste plastic, 2023. URL https://cinea.ec.europa.eu/news-events/news/new-life-waste-plastic-2023-08-03_en.

[9] Maurizio Crippa and Barbara Morico. *Chapter 12 - PET depolymerization: a novel process for plastic waste chemical recycling*, volume 179 of *Catalysis, Green Chemistry and Sustainable Energy*, page 215–229. Elsevier, January . doi: 10.1016/B978-0-444-64337-7.00012-4. URL https://www.sciencedirect.com/science/article/pii/B9780444643377000124.

[10] Roberto Nisticò. Polyethylene terephthalate (pet) in the packaging industry. *Polymer Testing*, 90:106707, October 2020. ISSN 0142-9418. doi: 10.1016/j.polymertesting.2020.106707.

[11] Anthony J. East. *Polyesters, Thermoplastic*. John Wiley Sons, Ltd, 2006. ISBN 978-0-471-23896-6. doi: 10.1002/0471238961.1615122505011920.a01.pub2. URL https://onlinelibrary.wiley.com/doi/abs/10.1002/0471238961.1615122505011920.a01.pub2.

[12] Firas Awaja and Dumitru Pavel. Recycling of pet. *European Polymer Journal*, 41(7):1453–1477, July 2005. ISSN 0014-3057. doi: 10.1016/j.eurpolymj.2005.02.005.

[13] Li-Chen Hsu. Synthesis of ultrahigh molecular weight poly(ethylene terephthalate). *Journal of Macromolecular Science, Part B*, 1(4):801–813, December 1967. ISSN 0022-2348, 1525-609X. doi: 10.1080/00222346708212364.

[14] K. Ravindranath and R. A. Mashelkar. Polyethylene terephthalate—i. chemistry, thermodynamics and transport properties. *Chemical Engineering Science*, 41(9):2197–2214, January 1986. ISSN 0009-2509. doi: 10.1016/0009-2509(86)85070-9.

[15] Stephen L. Rosen. *Polymers*. John Wiley Sons, Ltd, 2000. ISBN 978-0-471-23896-6. doi: 10.1002/0471238961.1615122518151905.a01. URL https://onlinelibrary.wiley.com/doi/abs/10.1002/0471238961.1615122518151905.a01.

[16] Professor Richard A. Pethrick. *Polymer Science and Technology*. Whittles Publishing Ltd, Dunbeath, UNITED KINGDOM, 2010. ISBN 978-1-84995-023-7. URL http://ebookcentral.proquest.com/lib/aalborguniv-ebooks/detail.action?docID=3417289.

[17] Laurence W. McKeen. *The Effect of Creep and Other Time Related Factors on Plastics and Elastomers*. Elsevier, June 2009. ISBN 978-0-8155-1981-2.

[18] Olagoke Olabisi. *Handbook of Thermoplastics*. January 1997. ISBN 978-0-8247-9797-3. doi: 10.13140/2.1.1399.1365.

[19] Boyang Guo, Sudarsana Reddy Vanga, Ximena Lopez-Lorenzo, Patricia Saenz-Mendez, Sara Rönnblad Ericsson, Yuan Fang, Xinchen Ye, Karen Schriever, Eva Bäckström, Antonino Biundo, Roman A. Zubarev, István Furó, Minna Hakkarainen, and Per-Olof Syrén. Conformational selection in biocatalytic plastic degradation by petase. *ACS Catalysis*, 12(6):3397–3409, March 2022. doi: 10.1021/acscatal.1c05548.

[20] Lars Jerpdal. Processing of self-reinforced poly(ethylene terephthalate) composites for automotive

applications. 2017. URL https://www.semanticscholar.org/paper/Processing-of-self-reinforced-poly(ethylene-for-Jerpdal/337da7aad462839f7b4fc4b17f13d0e8f313a0a4.

[21] Ganesh Kumar A., Anjana K., Hinduja M., Sujitha K., and Dharani G. Review on plastic wastes in marine environment – biodegradation and biotechnological solutions. 150:110733, January 2020. ISSN 0025-326X. doi: 10.1016/j.marpolbul.2019.110733.

[22] Virginija Jankauskaite, Gintaras Macijauskas, and Ramunas Lygaitis. Polyethylene terephthalate waste recycling and application possibilities: a review. *Medziagotyra*, 14:119–127, 06 2008.

[23] Ya-Hue Valerie Soong, Margaret J. Sobkowicz, and Dongming Xie. Recent advances in biological recycling of polyethylene terephthalate (pet) plastic wastes. *Bioengineering*, 9(3):98, February 2022. ISSN 2306-5354. doi: 10.3390/bioengineering9030098.

[24] Mr Mandar Dnyaneshwar Jagtap, Mr Sagar Suryakant Khatavkar, and T Z Quazi. Methods for waste plastic recycling. *International Journal on Recent Technologies in Mechanical and Electrical Engineering*, 2 (6). ISSN 2349-7947.

[25] Daniel Paszun and Tadeusz Spychaj. Chemical recycling of poly(ethylene terephthalate). *Industrial & Engineering Chemistry Research*, 36:1373–1383, 1997. URL https://api.semanticscholar.org/CorpusID:93401555.

[26] Mahsa Babaei, Milad Jalilian, and Kaveh Shahbaz. Chemical recycling of polyethylene terephthalate: A mini-review. *Journal of Environmental Chemical Engineering*, 12(3):112507, June 2024. ISSN 2213-3437. doi: 10.1016/j.jece.2024.112507.

[27] Joyce Mudondo, Hoe-Suk Lee, Yunhee Jeong, Tae Hee Kim, Seungmi Kim, Bong Hyun Sung, See-Hyoung Park, Kyungmoon Park, Hyun Gil Cha, Young Joo Yeon, and Hee Taek Kim. Recent advances in the chemobiological upcycling of polyethylene terephthalate (pet) into value-added chemicals. *Journal of Microbiology and Biotechnology*, 33(1):1–14, January 2023. ISSN 1017-7825. doi: 10.4014/jmb.2208.08048.

[28] John A. Glaser. *Biological Degradation of Polymers in the Environment*. IntechOpen, May 2019. ISBN 978-1-83880-493-0. doi: 10.5772/intechopen.85124. URL https://www.intechopen.com/chapters/66340.

[29] Hayden K. Webb, Jaimys Arnott, Russell J. Crawford, and Elena P. Ivanova. Plastic degradation and its environmental implications with special reference to poly(ethylene terephthalate). *Polymers*, 5(11):1–18, March 2013. ISSN 2073-4360. doi: 10.3390/polym5010001.

[30] Rolf-Joachim Müller, Hedwig Schrader, Jörn Profe, Karolin Dresler, and Wolf-Dieter Deckwer. Enzymatic degradation of poly(ethylene terephthalate): Rapid hydrolyse using a hydrolase from t. fusca. *Macromolecular Rapid Communications*, 26(17):1400–1405, 2005. ISSN 1521-3927. doi: 10.1002/marc.200500410.

[31] David Ollis, Eong Cheah, Miroslaw Cygler, Bauke Dijkstra, Felix Frolow, Sybille Franken, Michal Harel, S. Remington, Israel Silman, Joseph D Schrag, Joel Sussman, Koen Verschueren, and Adrian Goldman. The alpha/beta hydrolase fold. *Protein engineering*, 5, May 1992. doi: 10.1093/protein/5.3.197.

[32] Christian Roth, Ren Wei, Thorsten Oeser, Johannes Then, Christina Föllner, Wolfgang Zimmermann, and Norbert Sträter. Structural and functional studies on a thermostable polyethylene terephthalate degrading hydrolase from thermobifida fusca. *Applied Microbiology and Biotechnology*, 98(18):7815–7823, September 2014. ISSN 1432-0614. doi: 10.1007/s00253-014-5672-0.

[33] Sintawee Sulaiman, Dong-Ju You, Eiko Kanaya, Yuichi Koga, and Shigenori Kanaya. Crystal structure and thermodynamic and kinetic stability of metagenome-derived lc-cutinase. *Biochemistry*, 53(11):1858–1869, March 2014. ISSN 0006-2960. doi: 10.1021/bi401561p.

[34] Seongjoon Joo, In Jin Cho, Hogyun Seo, Hyeoncheol Francis Son, Hye-Young Sagong, Tae Joo Shin, So Young Choi, Sang Yup Lee, and Kyung-Jin Kim. Structural insight into molecular mechanism of poly(ethylene terephthalate) degradation. *Nature Communications*, 9(11):382, January 2018. ISSN 2041-1723. doi: 10.1038/s41467-018-02881-1.

[35] Xu Han, Weidong Liu, Jian-Wen Huang, Jiantao Ma, Yingying Zheng, Tzu-Ping Ko, Limin Xu, Ya-Shan Cheng, Chun-Chi Chen, and Rey-Ting Guo. Structural insight into catalytic mechanism of pet hydrolase. *Nature Communications*, 8(1):2106, December 2017. ISSN 2041-1723. doi: 10.1038/s41467-017-02255-z.

[36] Shosuke Yoshida, Kazumi Hiraga, Toshihiko Takehana, Ikuo Taniguchi, Hironao Yamaji, Yasuhito Maeda, Kiyotsuna Toyohara, Kenji Miyamoto, Yoshiharu Kimura, and Kohei Oda. A bacterium that degrades and assimilates poly(ethylene terephthalate). *Science*, 351(6278):1196–1199, March 2016. doi: 10.1126/science.aad6359.

[37] Ikuo Taniguchi, Shosuke Yoshida, Kazumi Hiraga, Kenji Miyamoto, Yoshiharu Kimura, and Kohei Oda. Biodegradation of pet: Current status and application aspects. *ACS Catalysis*, 9(5):4089–4105, May 2019. doi: 10.1021/acscatal.8b05171.

[38] Hongyuan Lu, Daniel J. Diaz, Natalie J. Czarnecki, Congzhi Zhu, Wantae Kim, Raghav Shroff, Daniel J. Acosta, Bradley R. Alexander, Hannah O. Cole, Yan Zhang, Nathaniel A. Lynd, Andrew D. Ellington, and Hal S. Alper. Machine learning-aided engineering of hydrolases for pet depolymerization. *Nature*, 604 (79077907):662–667, April 2022. ISSN 1476-4687. doi: 10.1038/s41586-022-04599-z.

[39] Brandon C. Knott, Erika Erickson, Mark D. Allen, Japheth E. Gado, Rosie Graham, Fiona L. Kearns, Isabel Pardo, Ece Topuzlu, Jared J. Anderson, Harry P. Austin, Graham Dominick, Christopher W. Johnson, Nicholas A. Rorrer, Caralyn J. Szostkiewicz, Valérie Copié, Christina M. Payne, H. Lee Woodcock, Bryon S. Donohoe, Gregg T. Beckham, and John E. McGeehan. Characterization and engineering of a two-enzyme system for plastics depolymerization. *Proceedings of the National Academy of Sciences*, 117(41):25476–25485, October 2020. doi: 10.1073/pnas.2006753117.

[40] V. Tournier, C. M. Topham, A. Gilles, B. David, C. Folgoas, E. Moya-Leclair, E. Kamionka, M.-L. Desrousseaux, H. Texier, S. Gavalda, M. Cot, E. Guémard, M. Dalibey, J. Nomme, G. Cioci, S. Barbe, M. Chateau, I. André, S. Duquesne, and A. Marty. An engineered pet depolymerase to break down and recycle plastic bottles. *Nature*, 580(7802):216–219, April 2020. ISSN 1476-4687. doi: 10.1038/s41586-020-2149-4.

[41] Grégory Arnal, Julien Anglade, Sabine Gavalda, Vincent Tournier, Nicolas Chabot, Uwe T. Bornscheuer, Gert Weber, and Alain Marty. Assessment of four engineered pet degrading enzymes considering large-scale industrial applications. *ACS Catalysis*, page 13156–13166, September 2023. doi: 10.1021/acscatal.3c02922.

[42] Thore B. Thomsen, Sune Schubert, Cameron J. Hunt, Kim Borch, Kenneth Jensen, Jesper Brask, Peter Westh, and Anne S. Meyer. Rate response of poly(ethylene terephthalate)-hydrolases to substrate crystallinity: Basis for understanding the lag phase. *ChemSusChem*, 16(13):e202300291, 2023. ISSN 1864-564X. doi: 10.1002/cssc.202300291.

[43] Avantika Singh, Nicholas A. Rorrer, Scott R. Nicholson, Erika Erickson, Jason S. DesVeaux, Andre F. T. Avelino, Patrick Lamers, Arpit Bhatt, Yimin Zhang, Greg Avery, Ling Tao, Andrew R. Pickford, Alberta C. Carpenter, John E. McGeehan, and Gregg T. Beckham. Techno-economic, life-cycle, and socioeconomic impact analysis of enzymatic recycling of poly(ethylene terephthalate). *Joule*, 5(9): 2479–2503, September 2021. ISSN 2542-4785, 2542-4351. doi: 10.1016/j.joule.2021.06.015.

[44] Taylor Uekert, Avantika Singh, Jason S. DesVeaux, Tapajyoti Ghosh, Arpit Bhatt, Geetanjali Yadav, Shaik Afzal, Julien Walzberg, Katrina M. Knauer, Scott R. Nicholson, Gregg T. Beckham, and Alberta C. Carpenter. Technical, economic, and environmental comparison of closed-loop recycling technologies for common plastics. *ACS Sustainable Chemistry Engineering*, 11(3):965–978, January 2023. doi: 10.1021/acssuschemeng.2c05497.

[45] Taylor Uekert, Jason S. DesVeaux, Avantika Singh, Scott R. Nicholson, Patrick Lamers, Tapajyoti Ghosh, John E. McGeehan, Alberta C. Carpenter, and Gregg T. Beckham. Life cycle assessment of enzymatic poly(ethylene terephthalate) recycling. *Green Chemistry*, 24(17):6531–6543, August 2022. ISSN 1463-9270. doi: 10.1039/D2GC02162E.

[46] Matthew Theisen and James C. Liao. *Industrial Biotechnology: Escherichia coli as a Host*, page 149–181. John Wiley Sons, Ltd, 2017. ISBN 978-3-527-80779-6. doi: 10.1002/9783527807796.ch5. URL `https://onlinelibrary.wiley.com/doi/abs/10.1002/9783527807796.ch5`.

[47] Zohreh Pourhassan N., Haiyang Cui, Sakshi Khosa, Mehdi D. Davari, Karl-Erich Jaeger, Sander H. J. Smits, Ulrich Schwaneberg, and Lutz Schmitt. Optimized hemolysin type 1 secretion system in escherichia coli by directed evolution of the hly enhancer fragment and including a terminator region. *ChemBioChem*, 23(6):e202100702, 2022. ISSN 1439-7633. doi: 10.1002/cbic.202100702.

[48] F. J. M. Mergulhão, D. K. Summers, and G. A. Monteiro. Recombinant protein secretion in escherichia coli. *Biotechnology Advances*, 23(3):177–202, May 2005. ISSN 0734-9750. doi: 10.1016/j.biotechadv.2004.11.003.

[49] Michael T Madigan, Kelly S Bender, Daniel H Buckley, W. Matthew Sattley, and David A Stahl. *Brock biology of microorganisms*. Pearson Education, global edition. edition, 2018. ISBN 1292235101.

[50] Lixia Shi, Haifeng Liu, Songfeng Gao, Yunxuan Weng, and Leilei Zhu. Enhanced extracellular production of ispetase in escherichia coli via engineering of the pelb signal peptide. *Journal of Agricultural and Food Chemistry*, 69(7):2245–2252, February 2021. ISSN 0021-8561. doi: 10.1021/acs.jafc.0c07469.

[51] Sheng Chen, Zhiguo Liu, Jian Chen, and Jing Wu. Study on improvement of extracellular production of recombinant thermobifida fusca cutinase by escherichia coli. *Applied Biochemistry and Biotechnology*, 165 (2):666–675, September 2011. ISSN 1559-0291. doi: 10.1007/s12010-011-9286-z.

[52] Rachel Binet, Sylvie Létoffé, Jean Marc Ghigo, Philippe Delepelaire, and Cécile Wandersman. Protein secretion by gram-negative bacterial abc exporters – a review1. *Gene*, 192(1):7–11, June 1997. ISSN 0378-1119. doi: 10.1016/S0378-1119(96)00829-3.

[53] Luis A. Fernández and Víctor De Lorenzo. Formation of disulphide bonds during secretion of proteins

through the periplasmic-independent type i pathway. *Molecular Microbiology*, 40(2):332–346, 2001. ISSN 1365-2958. doi: 10.1046/j.1365-2958.2001.02410.x.

[54] Lingqia Su, Sheng Chen, Li Yi, Ronald W. Woodard, Jian Chen, and Jing Wu. Extracellular overexpression of recombinant thermobifida fusca cutinase by alpha-hemolysin secretion system in e. coli bl21(de3). *Microbial Cell Factories*, 11(1):8, January 2012. ISSN 1475-2859. doi: 10.1186/1475-2859-11-8.

[55] I. Barry Holland, Sandra Peherstorfer, Kerstin Kanonenberg, Michael Lenders, Sven Reimann, and Lutz Schmitt. Type i protein secretion—deceptively simple yet with a wide range of mechanistic variability across the family. *EcoSal Plus*, 7(1):10.1128/ecosalplus.ESP–0019–2015, December 2016. doi: 10.1128/ecosalplus.esp-0019-2015.

[56] Hans-Peter Hohmann, Jan M. van Dijl, Laxmi Krishnappa, and Zoltán Prágai. *Host Organisms: Bacillus subtilis*, page 221–297. John Wiley Sons, Ltd, 2017. ISBN 978-3-527-80779-6. doi: 10.1002/9783527807796.ch7. URL `https://onlinelibrary.wiley.com/doi/abs/10.1002/9783527807796.ch7`.

[57] Jolanda Neef, Jan Maarten van Dijl, and Girbe Buist. Recombinant protein secretion by bacillus subtilis and lactococcus lactis: pathways, applications, and innovation potential. *Essays in Biochemistry*, 65(2): 187, July 2021. doi: 10.1042/EBC20200171.

[58] Sunghoon Park and Wolfgang Schumann. Optimization of the secretion pathway for heterologous proteins in bacillus subtilis. *Biotechnology and Bioprocess Engineering*, 20(4):623–633, August 2015. ISSN 1976-3816. doi: 10.1007/s12257-014-0843-5.

[59] Matti Sarvas, Colin R. Harwood, Sierd Bron, and Jan Maarten van Dijl. Post-translocational folding of secretory proteins in gram-positive bacteria. *Biochimica et Biophysica Acta (BBA) - Molecular Cell Research*, 1694(1):311–327, November 2004. ISSN 0167-4889. doi: 10.1016/j.bbamcr.2004.04.009.

[60] Ulf Brockmeier, Michael Caspers, Roland Freudl, Alexander Jockwer, Thomas Noll, and Thorsten Eggert. Systematic screening of all signal peptides from bacillus subtilis: A powerful strategy in optimizing heterologous protein secretion in gram-positive bacteria. *Journal of Molecular Biology*, 362(3):393–402, September 2006. ISSN 0022-2836. doi: 10.1016/j.jmb.2006.07.034.

[61] Elisabeth Gasteiger, Christine Hoogland, Alexandre Gattiker, S'everine Duvaud, Marc R. Wilkins, Ron D. Appel, and Amos Bairoch. *Protein Identification and Analysis Tools on the ExPASy Server*, page 571–607. Humana Press, Totowa, NJ, 2005. ISBN 978-1-58829-343-5. doi: 10.1385/1-59259-890-0:571. URL `http://link.springer.com/10.1385/1-59259-890-0:571`. DOI: 10.1385/1-59259-890-0:571.

[62] Clara L. Kielkopf, William Bauer, and Ina L. Urbatsch. Bradford assay for determining protein concentration. *Cold Spring Harbor Protocols*, 2020(4):102269, April 2020. ISSN 1559-6095. doi: 10.1101/pdb.prot102269.

[63] Bernard R. Glick. Metabolic load and heterologous gene expression. *Biotechnology Advances*, 13(2): 247–261, January 1995. ISSN 0734-9750. doi: 10.1016/0734-9750(95)00004-A.

[64] Elisabeth Gasteiger, Christine Hoogland, Alexandre Gattiker, S'everine Duvaud, Marc R. Wilkins, Ron D. Appel, and Amos Bairoch. *Protein Identification and Analysis Tools on the ExPASy Server*, page 571–607. Humana Press, Totowa, NJ, 2005. ISBN 978-1-58829-343-5. doi: 10.1385/1-59259-890-0:571. URL `http://link.springer.com/10.1385/1-59259-890-0:571`. DOI: 10.1385/1-59259-890-0:571.

[65] Lingqia Su, Ronald W. Woodard, Jian Chen, and Jing Wu. Extracellular location of thermobifida fusca cutinase expressed in escherichia coli bl21(de3) without mediation of a signal peptide. *Applied and Environmental Microbiology*, 79(14):4192–4198, July 2013. ISSN 1098-5336. doi: 10.1128/AEM.00239-13.

[66] Bian Wu, Yinglu Cui, Yanchun Chen, Jinyuan Sun, Tong Zhu, Hua Pang, Chunli Li, and Wenchao Geng. Deep learning-aided redesign of a hydrolase for near 100January 2023. doi: 10.21203/rs.3.rs-2465520/v1. URL `https://www.researchsquare.com/article/rs-2465520/v1`.

[67] Virender Kumar, Alessandro Pellis, Reinhard Wimmer, Vlamdimir Popok, Jesper de Claville Christiansen, and Cristiano Varrone. Efficient depolymerization of poly(ethylene 2,5-furanoate) using polyester hydrolases. *ACS Sustainable Chemistry Engineering*, 2024.

[68] Richard K. Brizendine, Erika Erickson, Stefan J. Haugen, Kelsey J. Ramirez, Joel Miscall, Davinia Salvachúa, Andrew R. Pickford, Margaret J. Sobkowicz, John E. McGeehan, and Gregg T. Beckham. Particle size reduction of poly(ethylene terephthalate) increases the rate of enzymatic depolymerization but does not increase the overall conversion extent. *ACS Sustainable Chemistry Engineering*, 10(28): 9131–9140, July 2022. doi: 10.1021/acssuschemeng.2c01961.

[69] Pieter L. deHaseth, Margaret L. Zupancic, and M. Thomas Record. Rna polymerase-promoter interactions: the comings and goings of rna polymerase. *Journal of Bacteriology*, 180(12):3019–3025, June 1998. ISSN 0021-9193.

[70] Jing Ye, Yunjie Li, Yuqing Bai, Ting Zhang, Wei Jiang, Ting Shi, Zijian Wu, and Yi-Heng P. Job Zhang. A

facile and robust t7-promoter-based high-expression of heterologous proteins in bacillus subtilis. *Bioresources and Bioprocessing*, 9(1):56, May 2022. ISSN 2197-4365. doi: 10.1186/s40643-022-00540-4.

[71] Kang Zhang, Lingqia Su, Xuguo Duan, Lina Liu, and Jing Wu. High-level extracellular protein production in bacillus subtilis using an optimized dual-promoter expression system. *Microbial Cell Factories*, 16(1):32, February 2017. ISSN 1475-2859. doi: 10.1186/s12934-017-0649-1.

[72] F Corpet. Multiple sequence alignment with hierarchical clustering. *Nucleic Acids Research*, 16(22): 10881–10890, November 1988. ISSN 0305-1048.